A LABORATORY STUDY OF SLOPE FLOW

INDUCED BY A SURFACE SALT FLUX

by

Bon J. van Hardenberg

B.Sc.,University of British Columbia, 1984

A THESIS SUBMITTED IN PARTIAL FULFILLMENT OF

THE REQUIREMENTS FOR THE DEGREE OF

MASTER OF SCIENCE

in

THE DEPARTMENT OF OCEANOGRAPHY

We accept this thesis as conforming

to the required standard

THE UNIVERSITY OF BRITISH COLUMBIA

April 1987

32

In presenting this thesis in partial fulfilment of the requirements for an advanced degree at the University of British Columbia, I agree that the Library shall make it freely available for reference and study. I further agree that permission for extensive copying of this thesis for scholarly purposes may be granted by the head of my department or by his or her representatives. It is understood that copying or publication of this thesis for financial gain shall not be allowed without my written permission.

Department of _____ Oceanography _____

The University of British Columbia
1956 Main Mall
Vancouver, Canada
V6T 1Y3

Date _____ 15 April 1987 _____

The salt expulsion caused by the freezing of seawater and the drainage of brine from the ice creates a convectively mixed layer, which extends to the bottom in shallow coastal regions. This buoyancy flux at the surface was simulated in laboratory experiments by percolating salt water through a porous membrane into a tank. Shadowgraph images show that a down-slope flow is induced when the bottom of the tank is set at an angle.

Velocity maxima in the slope flow, measured from the movement of injected dye ranged from 0.09 to 0.66 cm/s. Fluid densities were determined using thermistors and small-volume conductivity micro-cells developed for this purpose. For bottom slope angles between 2.2° and 5.5°, and at computed salt fluxes between $1.82 \ast 10^{-5}$ and $1.63 \ast 10^{-6}$ g/cm²/s, the salinity profiles showed slope flow depths between 7 and 17 mm with a rise in salinity of 0.24 to 0.92 ppt above those in the mixed layer.

Entrainment at a density interface without shear, using this experimental arrangement, agreed closely with predicted results by Bo Pedersen. Using the entrainment model for a turbulent gravity current, entrainment factors computed from the data of the slope flow experiments were up to two orders of magnitude larger than those predicted for flows in a quiescent environment. This is contrary to visual evidence of the experiments or to Arctic field data, which indicate low rates of entrainment. This suggests that a different model is required to explain the interaction between such flows and the turbulent environment.

## 1.1 Arctic subsurface intrusions and slope flow

Typical oceanographic profiles taken during winter of the salinity and temperature under the ice in the Beaufort Sea (see figure 1-1) show a well-mixed surface layer extending to depths of up to 50 meters. This layer is isothermal, near the freezing point, and isohaline due to convective overturning caused by the expulsion of salt at the ice/water interface from the ice that forms as sea water freezes. The subsurface layer below this contains the pycnocline where a large increase in salinity generally is accompanied by a small rise in temperature. Below the thermocline there is gradual mixing with water of Atlantic origin to form the Arctic Deep Water. In many of the profiles, intrusions into this sub-surface layer were found of up to 30 meters in thickness, characterized by temperature minima (see feature 'a' in figure 1-1). This colder water most likely was formed as a convectively mixed surface layer in some other location where water at the surface had a higher salinity or where a faster freezing rate caused a higher salt flux. The colder and saltier water moved to the depth of intrusion where it was found at the profiling station possibly as a slope current or shelf drainage flow. Such slope flows could be the cause of cold water intrusions penetrating out into the Arctic Ocean at depths up to 200 meters (see Perkin and Lewis (1979), Melling and Lewis (1982)).
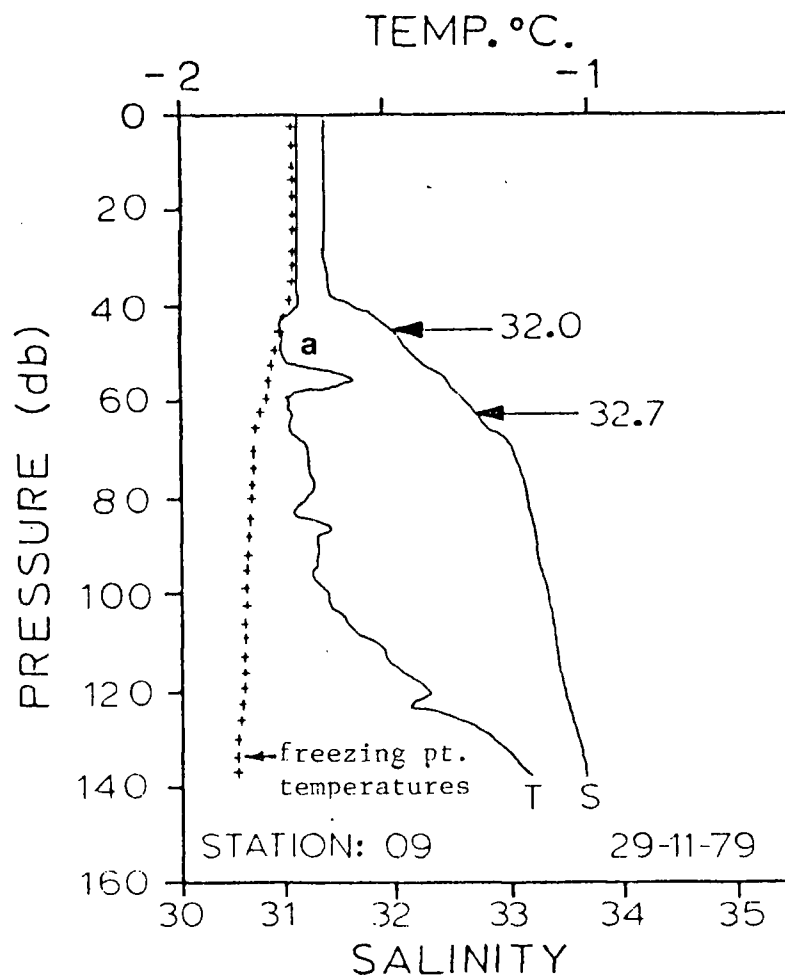
Figure 1-1. Typical Arctic profiles in winter
(Frozen Seas Research Group, IOS)

As sea water freezes, some of the salt is expelled immediately from the ice which forms. Subsequently, more salt drains as brine from a system of dendritic channels that develops in the ice. The influx of salt causes a density increase at the ice/seawater interface and results in convective overturning of the water column below the ice. Laboratory studies by Foster (1969) and by Elliott (1972) looked at haline convection under sea ice. The rejected salt was seen to form a pattern of plumes or streamers with downward velocities ranging from 0.09 to 0.23 cm/s for ice growth rates from 0.3 to 7.8 cm/day. A

2

field study of salt rejection by sea ice during growth is described by Lake and Lewis (1970). In shallow seas, such as parts of the Beaufort Sea in the Canadian Arctic, the convectively mixed layer which is driven by freezing may extend to the bottom. The density in this layer will vary with the amount of salt flowing into it and with the depth into which it is mixed. An uneven salt flux or a bottom slope will create horizontal gradients in the density which in turn can cause a downslope current along the bottom and intrusions at levels below that of normal mixing from surface effects; compensating currents will occur at higher levels.

## 1.2 Laboratory study

A series of laboratory experiments was conducted under the auspices of the Ocean Physics Group at the Institute of Ocean Sciences in Sidney, British Columbia, to examine under controlled conditions and on a small scale, slope flows induced by a surface salt flux over a sloping bottom.

Slope flows were observed in each of the experiments, which were conducted in a plexiglass tank with the bottom set at some small slope angle. The surface salt flux was simulated by slow percolation of salt water through a membrane into the tank, and a simple formulation was developed to obtain estimates of the magnitude of the salt fluxes which generated and maintained the observed slope flows. Shadowgraph images and dye were used to visualize fluid motions in the convectively mixed layer and to determine velocities in the slope flow. A series of micro-cells

were developed to obtain the electrical conductivity of fluid withdrawn from points in the tank. The temperatures of fluid in the micro-cell and in the experimental tank, determined with micro-bead thermistors, were combined with the conductivity to compute the salinity and density of the fluid (appendix A).

Patterns of motions in shadowgraphs show the slope flow and a weaker opposite flow in the mixed layer. Movement of injected dye shows a velocity distribution in the slope flow with a peak of 0.09 to 0.66 cm/s at about 0.5 cm above the bottom. Salinity profiles indicate slope flow depths of 7 to 17 mm in which the salinity rises 0.24 to 0.92 ppt above that in the convectively mixed layer.

Estimates of salt fluxes in these experiments ranged from 1.82e-5 to 1.63e-6 $g/cm^2/s$. The notation (e$\pm$n) is used in the following sections to denote (10 to the power$\pm$n). The computed salt flux estimates were several orders of magnitude larger than those found in Arctic field data, but mixing depths were several orders smaller. The buoyancy velocity scale W*, which can be used to characterize convection, was therefore nearly the same in both cases.

When the slope flow was considered as a turbulent gravity current, entrainment factors calculated by inserting data from this series of slope flow experiments were up to two orders of magnitude larger than those predicted for a quiescent environment. This is also contrary to evidence from the experiments and to Arctic field data which show that such flows maintain their characteristics over great distances from the source.

4

## 2.1 Tank and tray arrangement

A series of laboratory experiments was conducted in a tank made of 12 mm thick plexiglass. The inside dimensions were 87.5 cm long, 23cm wide and 25cm deep (see photo 1 and figure 2-1). The tank was raised at one end to create a sloping bottom and was partly filled with a mixture of fresh and sea water.
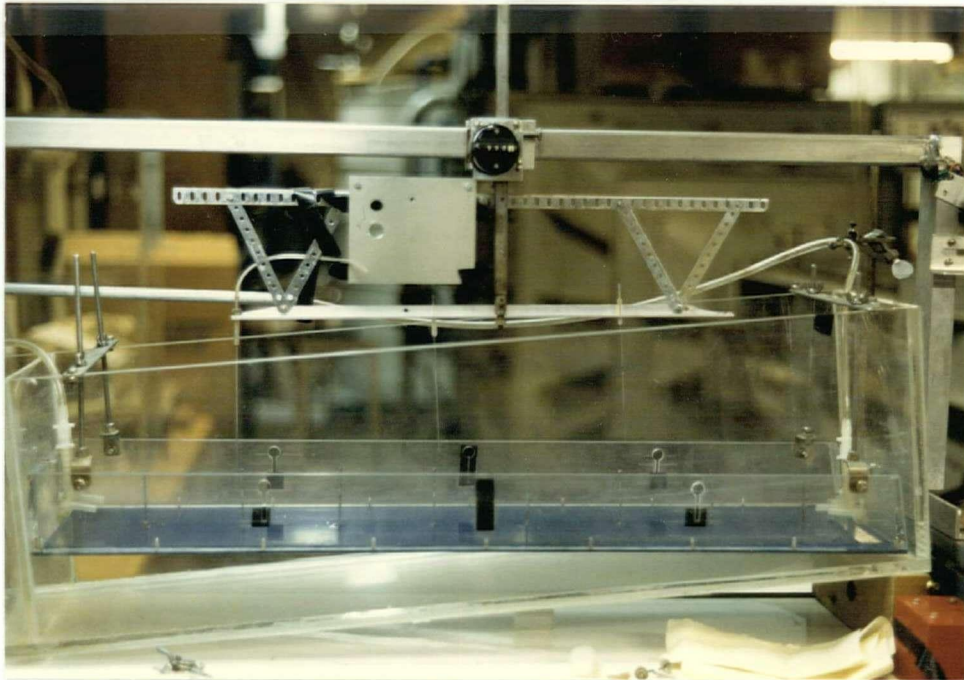


Photo 1. Experimental tank and tray

A tray was suspended level with the surface of the fluid in the tank, and the expulsion of salt from sea ice was simulated by a slow seepage of higher salinity water through the bottom of this tray. The tray bottom consisted of a porous membrane (a Millipore filter membrane, 0.8 micrometer pore size) mounted between two layers of fiberglass circuit boards, with aligned perforations. The tray was filled with sea water to several

millimeters above the height to which levelling slots in the sides were taped shut. In some of the experiments pure sea salt was added to increase the salt flux. When the high salinity fluid percolates through the membrane into the tank this causes an equal return flow of the lighter fluid to the tray. A small pump was used to stir the fluid in the tray, and exchange it with that in a back-up reservoir to help maintain the higher salinity in the tray. The volumes of fluid in tank, tray and reservoir were kept constant during each run and the system is self-levelling.

A series of 6 cm long copper tubes of 1.6 mm inside diameter were mounted through the membrane in the bottom of the tray, at 10 cm intervals along the centre line, starting 7.5 cm from the shallow end of the tank. These access tubes or ports #1 to #8, numbered from the shallow end of the tank, were used to inject dye or to withdraw fluid from various locations and depths in the tank through conductivity micro-cells to determine salinity and density.

Figure 2-1 shows a diagram of the arrangement of the tank, the tray with the sampling tubes and levelling slots, the added reservoir, and the circulation pump used to mix tray fluid and exchange it with that in the reservoir. The micro-cells are shown without the small pumps which return the syphoned fluid to tank and tray to maintain constant levels.
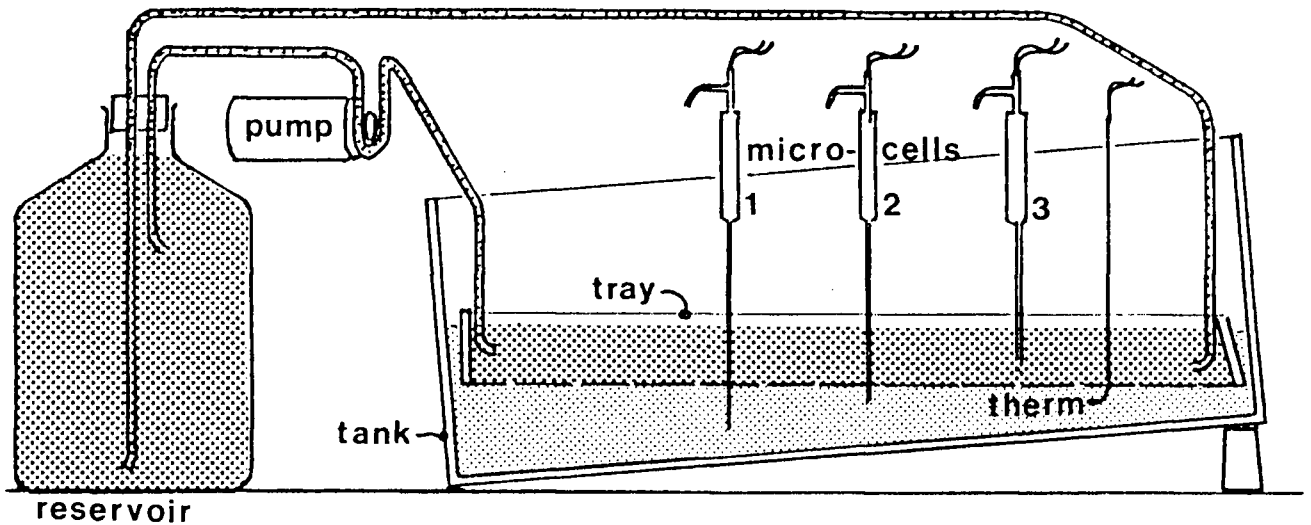
Figure 2-1. Apparatus for slope flow experiments.

## 2.2 Flow visualization

Light from a source placed at a distance behind the tank was focused by cylindrical lenses into a nearly parallel beam (see figure 2-2). This beam was projected through the side of the tank onto a translucent mylar film on the opposite side to form shadowgraph images.
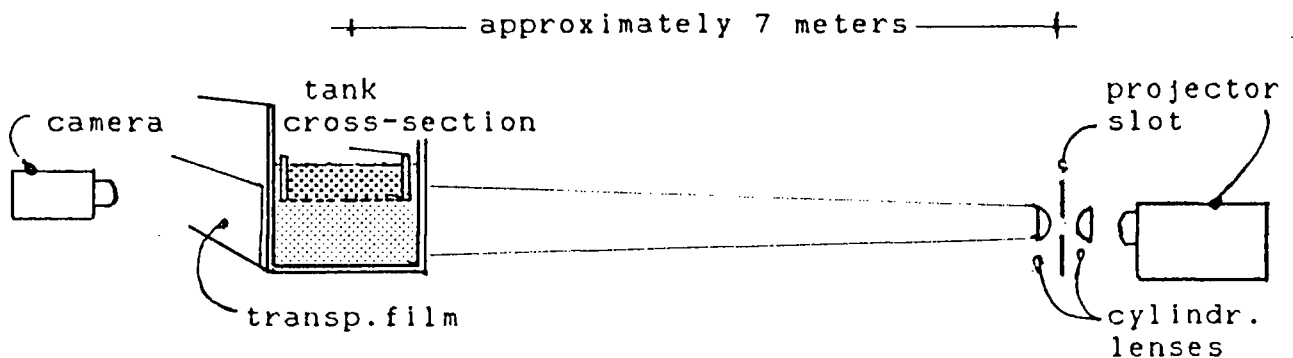


Figure 2-2. Diagram of arrangement for shadowgraphs

7

During the experiments, variations in the refractive index due convective overturning formed patterns of wrinkled lines in the shadowgraph image. The mean circulation pattern created by the bottom slope flow and the compensating flow in the mixed layer were visible as deflections in the line patterns (see photo 2). The image represents the motions of small streamers or parcels of fluid, integrated over the width of the tank and therefore can not show any cross-sectional circulation patterns.
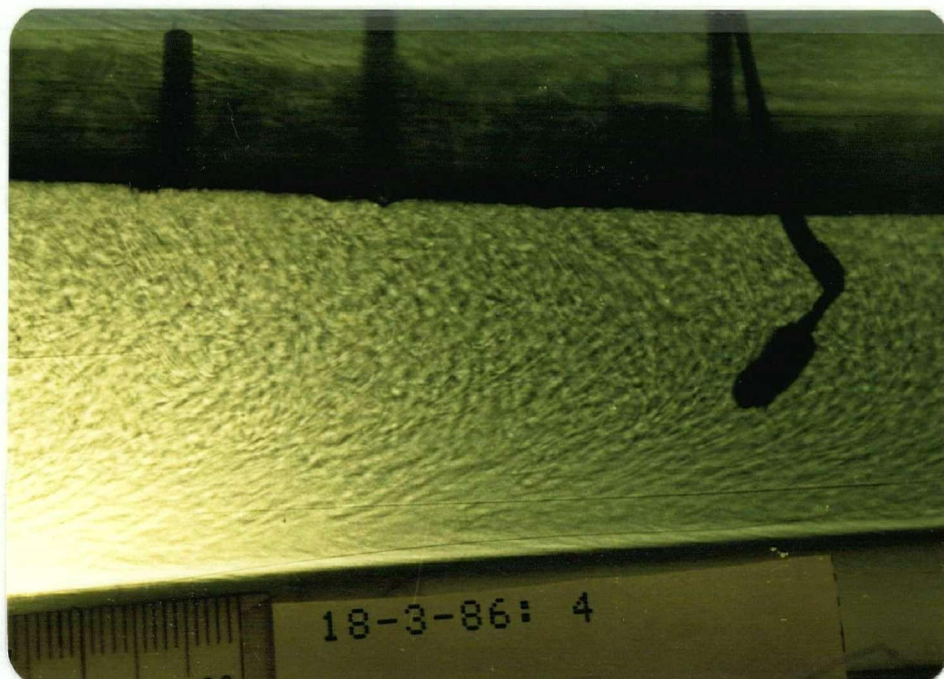


Photo 2. Shadowgraph image of slope flow

The slope flow was also visualized by injecting dye, which was diluted with fluid from the mixed layer in an attempt to match the slope flow density. The dye was injected through one of the sampling tubes along the centerline of the tray. While some of the dye was entrained in the convective motions as it sank through the mixed layer, most of it was carried along as

dye streaks in the slope flow. The flow velocities at different slope angles over a range of salt fluxes were determined from the distance that the dye moved in a known time interval in photo and slide sequences or on video tape footage.

## 2.3 Instrumentation for density determination

Several small-volume conductivity cells were developed for salinity determination and used in combination with thermistors to obtain a quantitative description of fluid densities in the slope flows and in the convectively mixed layer. The data were taken manually or with a datalogger and processed using a desktop computer.

### 2.3.1 Thermistors and micro-cells

To determine the electrical conductivity of fluid taken from different points in the experimental tank, conductivity micro-cells were developed with a small internal volume of about 0.15 ml (figure 2-3). Fluid was sampled by syphoning it from a point in the tank or tray through one of the micro-cells.

The micro-cells consisted of four platinum foil electrode rings (of 3 mm diameter by 5 mm long) separated by segments of glass tubing (of 1.8 mm inside and 3.0 mm outside diameter). Micro-bead thermistors were inserted in the flow at the inlet and outlet of each micro-cell. The average of the temperatures determined from their resistances was combined with the conductivity ratio to calculate the salinity using the polynomials of the Practical Salinity scale (see appendix A1).

The density of the fluid at the intake point in the tank was computed by combining this salinity with the temperature from another thermistor located in the tank using the polynomials of the Unesco equation of state for seawater (appendix A2).

Stable and repeatable readings were obtained with continuous slow syphoning of fluid through the micro-cells. The low rate of withdrawal from a point in the tank did not perceptibly influence the general flow patterns. Dimensions and assembly details of the cells are described in appendix B.
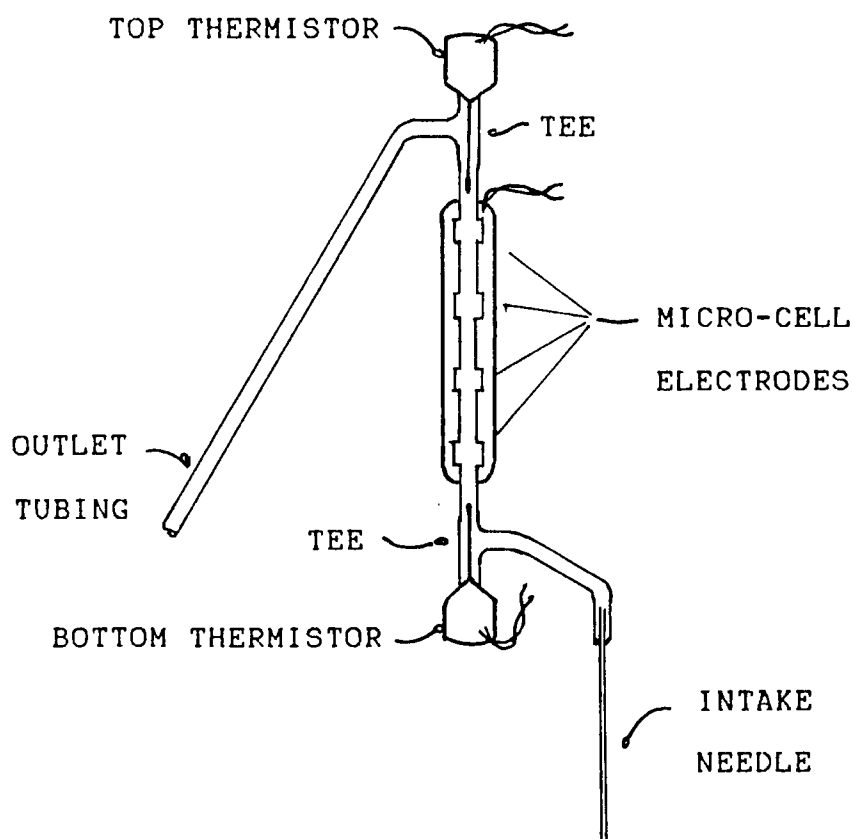


Figure 2-3. Micro-cell with thermistors

One cell was mounted on a vertical traveller which was moved along a track over the tank to one of the sampling tubes spaced along the centerline in the tray. Data points for salinity

10

profiles of fluid in the tank were obtained by lowering the tip
of the intake tube to successive depths. A second cell was used
for simultaneous readings at a fixed depth in the convectively
mixed layer to determine the change in background salinity and
the third cell was used to monitor the slow change in tray
salinity. Fluid was syphoned through the cells at a fixed rate
of 0.05-0.15 ml/s (1 to 3 drops/sec). A small pump with two
pump-heads was used to return fluid from the outlets of diffe-
rent cells to the tray and to the tank to maintain the fixed
fluid levels and volumes used to calculate the salt fluxes, as
shown in figure 2-4.
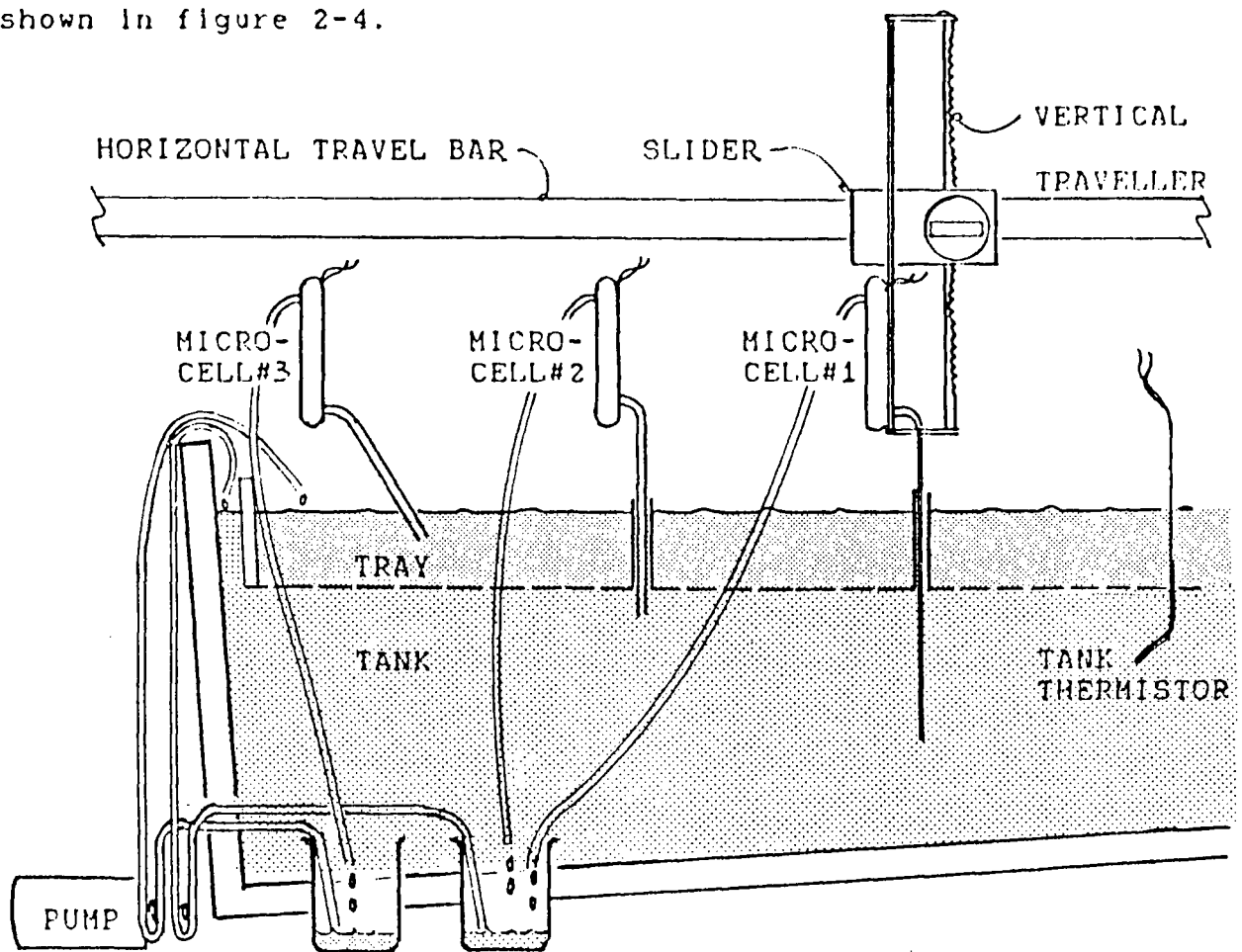


Figure 2-4. Micro-cells in experiments

## 2.3.2 Calibration of cell constants

The electrical conductivity in the micro-cells changes with the salinity of the fluid. An electronic circuit was designed so the output voltage (VC) was a linear function of the micro-cell conductance (1/R) for fluid of a given temperature and salinity. A cell constant (K) was expressed in ohms resistance of the cell at S=35 PSS and T=15 °C. The conductivity ratio (RR) is then computed from the micro-cell output voltage as the product of conductance and cell constant:

(2.1)      $1/R = A + B.VC$          $A = -2.6008e-8$

(2.2)      $RR = K.(A + B.VC)$       $B = -4.5954e-4$

The values of A and B were obtained by least squares linear fit through output voltages for a series of high accuracy standard resistors.

In a number of the experiments an Applied Microsystems C/T datalogger was used to take micro-cell and thermistor readings (see section 2.4). It was found that the different currents and voltages used by the internal conductivity circuit to drive the micro-cells required different values for the constants A and B and for the cell constant K to calculate the conductivity ratio from the datalogger numbers (NC):

(2.3)      $RR = K'.(A'+B'.NC)$      $A' = 5.53084e-5$

                                     $B' = 1.3290e-7$

The cell constants were chosen as those integer values for which the salinity of a fluid sample, calculated from the micro-cell conductivity ratio and temperature, was closest to

the value determined with a Guildline Autosal. This calibration
was frequently repeated to ensure that no shifts had occurred
due to aging or electrode fouling. The average values of the
calibration constant for each of the micro-cells are listed in
table 2.0 below (see appendix B table B.1 for details).

Table 2.0 **Micro-cell calibration constant K**

| Calibration constant K for: | Cell#1 | Cell#2 | Cell#3 |
|---|---|---|---|
| for the AM/CT datalogger: | 1885 | 1793 | 1821 |
| (std. dev. for 18 samples) | (6.3) | (4.2) | (6.7) |
| for separate cond.circuit: | 1803 | 1752 | 1783 |
| (std.dev. for 12 samples) | (5.6) | (3.5) | (6.7) |

## 2.3.3 Time response characteristics

As the salinity changes at the intake to a micro-cell, an
amount of fluid must pass through the intake tubing and the
cell to flush it, before a reading is taken. The time response
to a sudden change in salinity at the intake point was determi-
ned for each of the cells, at flow rates ranging from about 1
to 3 drops per second (or 0.05 to 0.15 ml/s) and for salinity
steps between 0.5 to 5 PSS. To obtain typical response curves
for the micro-cells the results were normalized by plotting the
change in the salinity as a fraction of the total salinity step
against the volume required, which is the product of flow rate
and time. For these syphon flow rates, the volume to flush the
intake tubing and the micro-cell was found to be about 4 ml.
The results are shown in figure 2-5.

MICRO-CELL TIME RESPONSE

Fraction of salinity step

1.0

0.5

syphon flow rates: 1.5-2.8 drops/sec
=0.08-0.14 ml/s
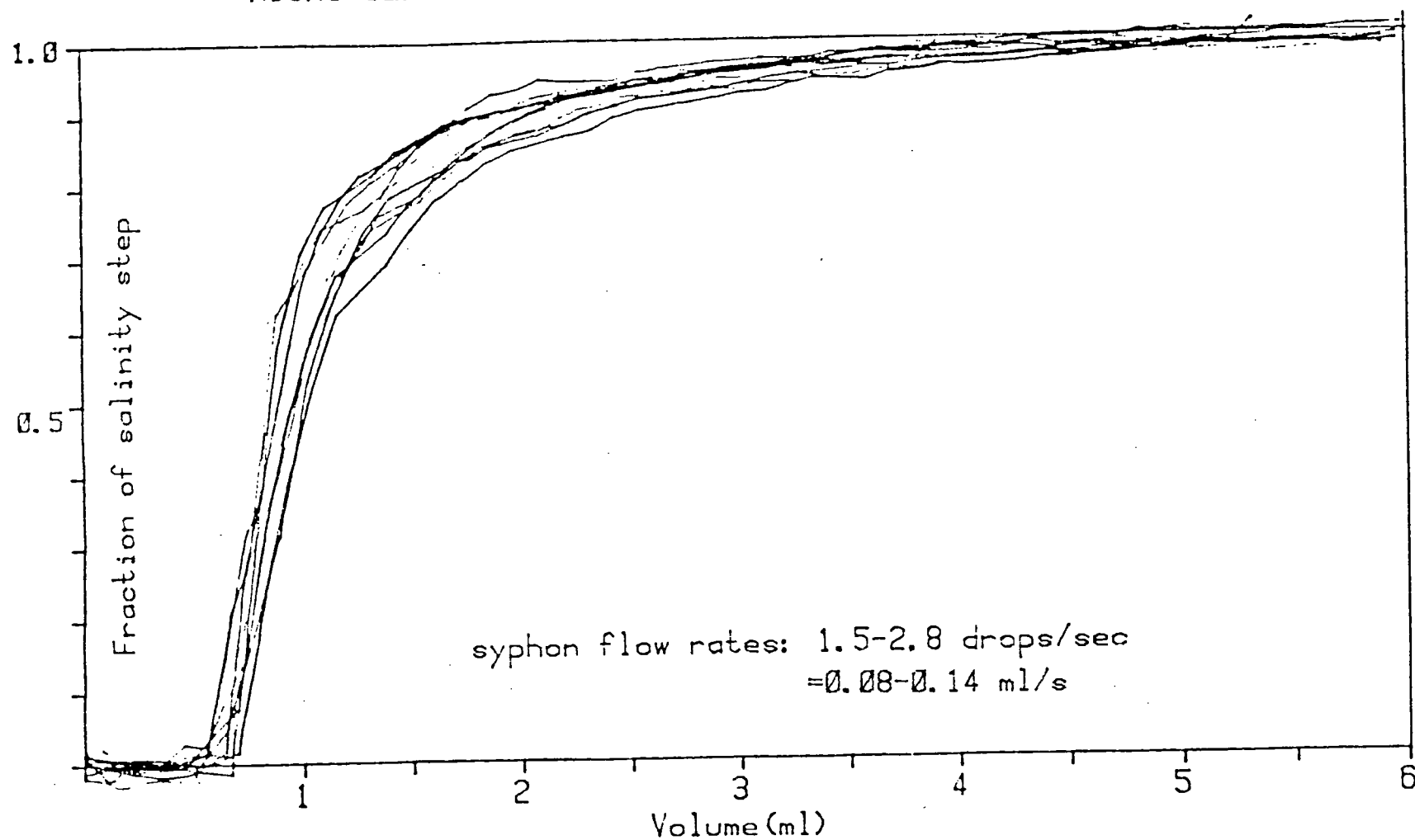
Volume (ml)

Figure 2-5. Volume required to flush the cell

## 2.3.4 Spatial resolution

The fluid syphoned from the intake point to the micro-cell can be considered as a point sink in a flow, and the calculated salinity is an average of fluid drawn from a small region. Some measure of the spatial resolution is then the extent to which a sharp interface appears blurred in a salinity profile.

A two-layer fluid system with a sharp density interface was obtained by partly filling a container with diluted sea water, then slowly piping water of a higher salinity to the bottom and sharpening the interface by syphoning fluid from a point just below it. The interface was visible as a bright line in a shadowgraph. Fluid was then syphoned through the micro-cell at a fixed flow rate of about 2 drops per second and readings were taken after 30 seconds at successive closely spaced depths.

For such two-layer systems with a step in salinity between 0.5 and 5 ppt, salinity profiles plotted from data taken across the interface show a set of distinct steps over a few millimeters of depth (figure 2-6).

A detailed description of the dimensions and assembly of the micro-cells, calibration of the cell constants and electronics, the time response characteristics and the spatial resolution is given in appendix B.
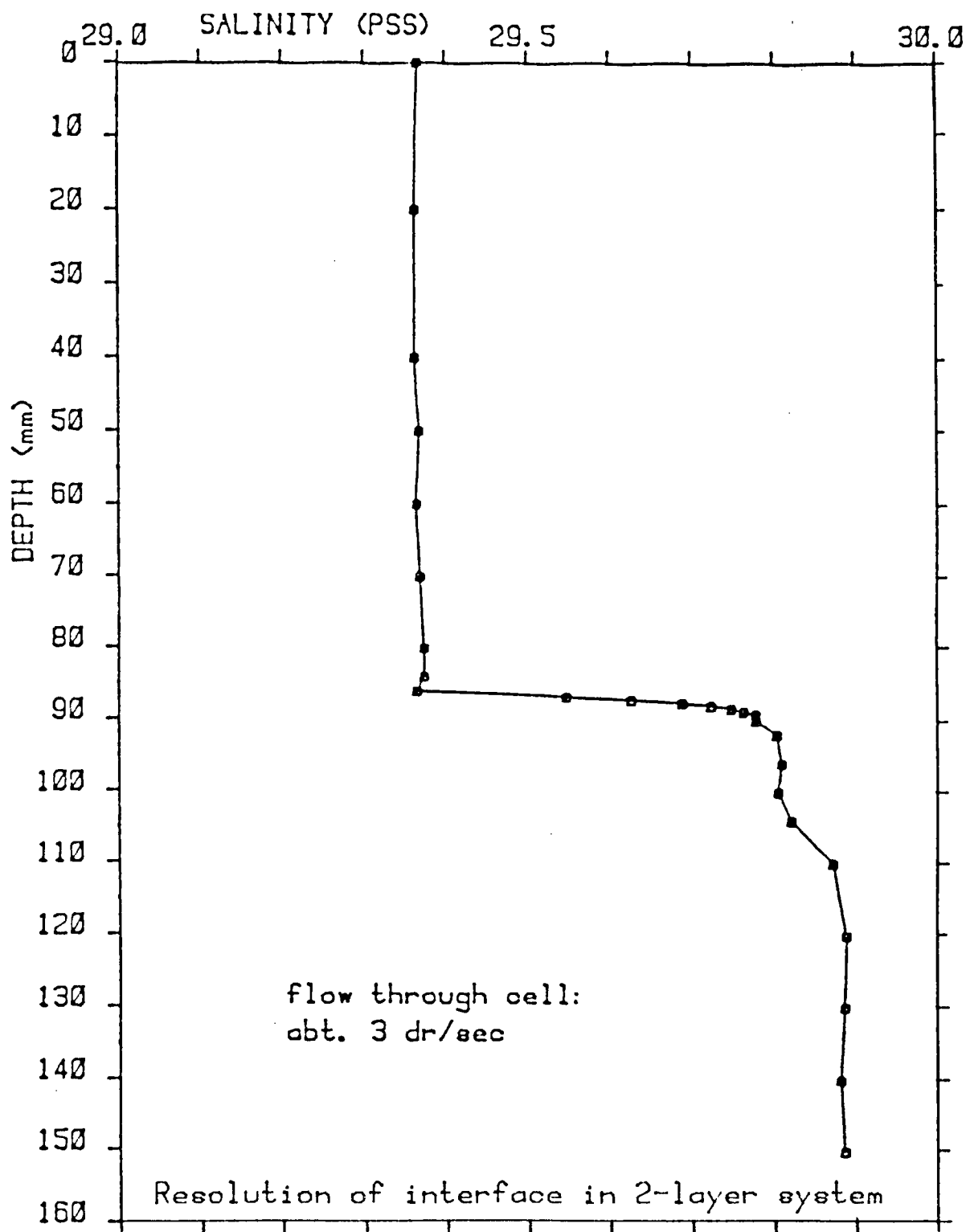
Figure 2-6. Micro-cell spatial resolution

## 2.4 Data acquisition

In the initial tests, a small conductivity circuit was used with a switch to power each micro-cell in turn. The output voltage from this circuit and the resistances of the thermistors were read from a set of digital voltmeters (DVM's). The numbers were entered via the keyboard into an HP-9825 desktop computer, which was programed to apply the calibration relations for the thermistors and micro-cells to the data, print the raw data and computed values, plot selected parameters and store the data on magnetic tape (see figure 2-8).
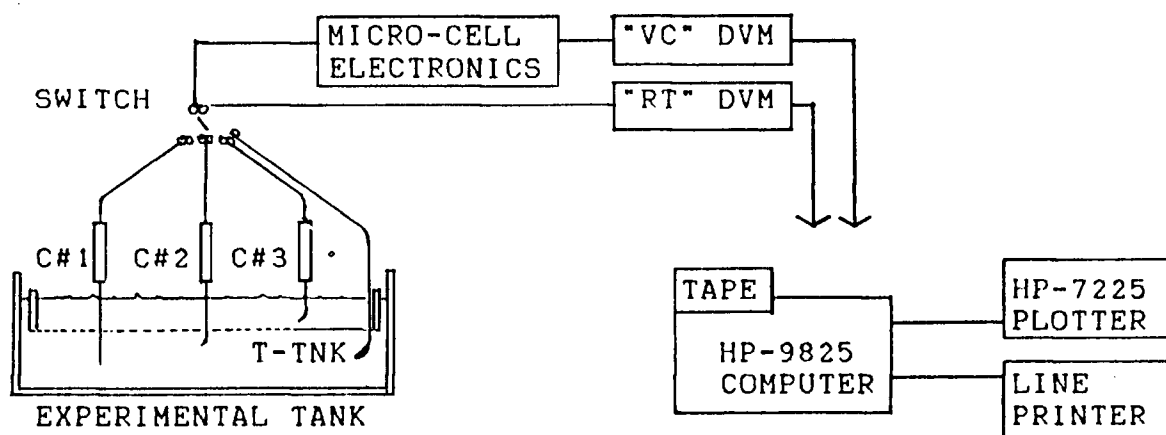


Figure 2-8. Data acquisition - manual input

In most of the experiments, the micro-cells and thermistors were interfaced via an Applied Microsystems (AM/CT) datalogger to the HP-9825. The datalogger internal conductance circuit was modified for use with the micro-cells. The different driving voltage and sensing current used by this circuit required separate micro-cell calibration constants (see section 2.3.2). The AM/CT datalogger could be triggered manually or at a set clock interval to cycle through all sensors and then transmit

17

the data via a serial converter and an RS-232 interface module to the HP-9825 computer (see figure 2-9). The salinity range of the AM/CT datalogger was limited and when the conductivity of the tray fluid was out of range, the separate small circuit was used with the DVM's.
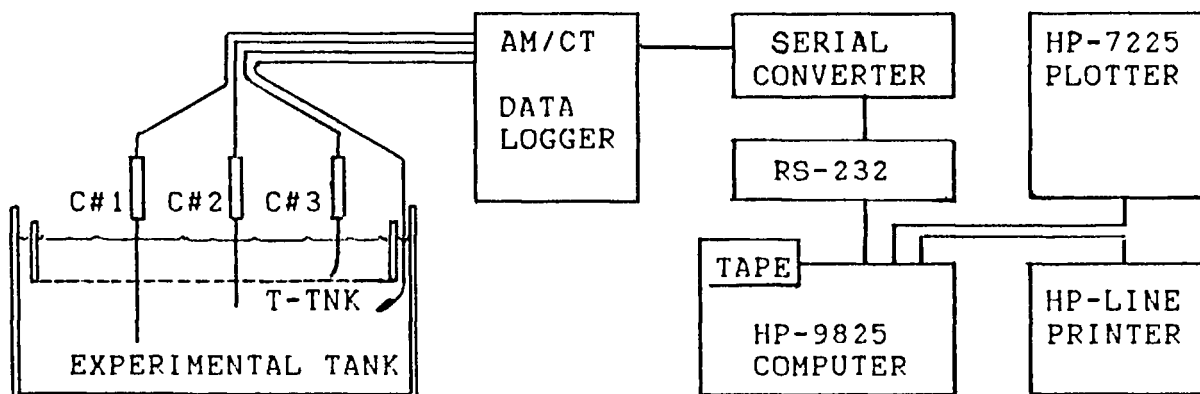


Figure 2-9. Data acquisition: AM/CT datalogger

In the last several experiments an HP-3497A Data Acquisition System was used, combined with a separate conductivity circuit for each micro-cell. This allowed a more rapid sampling rate, automatic averages of multiple readings for each sensor circuit (5 rapid readings were taken of each sensor), and also showed less variability because the cells were continuously powered. Some small shifts were found in data sequences from experiments and later testing revealed that any shift in relative position of the micro-cell outlet tubes could cause a change in apparent conductivity. Data obtained with this arrangement (figure 2-10) provided the most detailed profiles of density distribution in the slope flow.
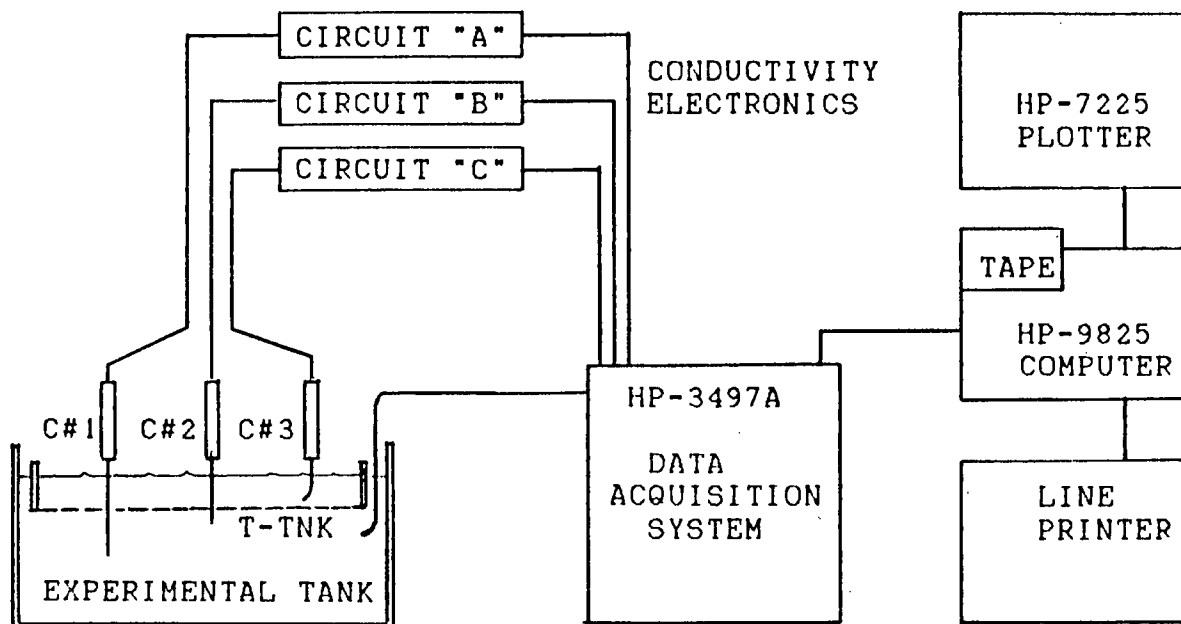
Figure 2-10. Data acquisition: HP-3497A System

The raw data from each sensor circuit and the computed values
of temperatures, conductivity ratio, salinity and density for
each of the cells were printed on a line-printer and saved on
magnetic tape. Depths of the micro-cell intake during profiling
were manually set and noted on the print-out. The salinity time
series points were plotted during each experiment. Profiles of
salinity in the tank were later plotted from these data, as is
described with the experimental results (in section 3).

## 2.5 Experimental procedure

Sea water was mixed with tap water in one tank to create low
salinity fluid for the experimental tank, and salt was added to
sea water in another tank for the high salinity fluid used in
tray and reservoir in some runs. The fluids were pumped to the
experimental tank or to reservoir and tray-filling pail through
a 0.8 micron filter to remove most organic matter and were left

for at least one day to stabilize at ambient room temperature, and to de-gas to avoid the formation of bubbles on the sensor surfaces which would adversely affect readings during the experiment. For the initial wetting of the membrane, the tank was filled to the top with low salinity fluid. The tray was lowered sideways into the tank and gently tapped to remove the air bubbles trapped in the perforated boards. The tray was then lowered horizontally to the desired depth and the tank drained until the fluid was level with the bottom of the tray.

At the beginning of an experimental run, the tray was filled with high salinity fluid while low salinity fluid was added in the edge between tank and tray to keep the fluid levels at the same height. This was done to prevent a rapid initial flux due to pressure caused by a difference in fluid levels in excess of that due to the difference in density between the two fluids.

The start of convection was seen in the shadowgraph image as a slowly and nearly evenly descending curtain of small plumes. Convective overturning produced a mixed layer which extended to the bottom of the tank. A down-slope bottom flow was seen to establish itself shortly after the start of each experiment and was maintained by the salt flux throughout each experiment. Observations were usually taken over a period of 3 to 5 hours, but in one case the slope flow was still seen about 15 hours later. The shadowgraph images and the movement of injected dye were recorded in photo and slide sequences or on video tape to study the flow patterns and to determine slope flow velocities. The experimental results are described in section 3.

## 2.6 Determination of membrane salt flux

The salt flux through the porous membrane is a function of the height of fluid in the tray, the density difference between the fluid in tank and that in the tray and the membrane characteristics. The magnitude of this buoyancy flux determines the turbulence in the convectively mixed layer.

### 2.6.1 Salt- and volume fluxes

Initial estimates of the net salt flux were obtained from the salinity time-series of fluid in the tray and the known volumes of fluid in tray and reservoir. The net salt flux is the rate of change in the total amount of salt in the combined tray and reservoir volume taken per unit of tray area:

$$(2.4) \quad Bn = \frac{d(S2*D2)}{dt} \frac{}{1000} \frac{(V2+Vr)}{A}$$

Bn = net salt flux $(gr/cm^2/s)$

S2 = salinity (gr/kg or ppt)

D2 = density $(gr/cm^3)$

V2 = tray fluid volume $(cm^3)$

Vr = reservoir volume $(cm^3)$

A = membrane area $(cm^2)$

Suffix 2 is used for properties in the tray and 1 for those in the tank. The net salt flux is the rate at which salt flows into the tank through the membrane in the tray bottom, reduced by that in the return flow through the levelling slots in the tray, taken per unit surface area (see figure 2-11). The return flow forms a thin layer at the top of the tray which is only partly mixed into it by the pump which exchanges tray and reservoir fluid. Equation 2.4 will therefore only yield a rough

initial estimate of the net flux due to the incomplete mixing in tray and the slow exchange of tray and reservoir fluid.

The amount of fluid entering the tank through the membrane must equal the return flow from the tank to the tray, and the volume flux $F$ can be expressed in terms of the net salt flux:

$$(2.5) \qquad Bn = F * \frac{(D2*S2 - D1*S1)}{1000} \qquad F = \text{volume flux } (cm^3/cm^2/s)$$

The membrane salt flux $B$ is then the product of volume flux and the amount of salt per unit volume of fluid from the tray:

$$(2.6) \qquad B = F * \frac{(D2*S2)}{1000} \qquad B = \text{salt flux } (gr/cm^2/s)$$

The convection is driven by this membrane salt flux.

## 2.6.2 Salt flux calibration

To calibrate the membrane salt and volume fluxes, a series of experiments was done in which the bottom of the tank was kept horizontal. In these experiments the patterns of lines in shadowgraph images indicated a nearly uniform distribution of convective motions, with end effects of diminished activity near the end walls of the tank. The rate of change in salinity of fluid from a point near the center of the tank was then taken to represent the average change for the whole tank fluid volume. Estimates of the net salt flux were obtained from the rate of change in salinity and density in the tank:

$$(2.7) \qquad Bn = \frac{d}{dt} \frac{(S1*D1)}{1000} * \frac{V1}{A}$$

With the fluid in tank and tray at the same level, the salt
flux through the membrane is driven by the pressure due to the
density difference of fluid columns of equal height in the tray
and in the edge space between tank and tray:

(2.8)   P = (D2-D1)*g*h     with:   P = pressure   (gr/cm/s2)

D = density   (gr/cm3)

h = tray fluid height (cm)

g = gravity = 981 (cm/s2)
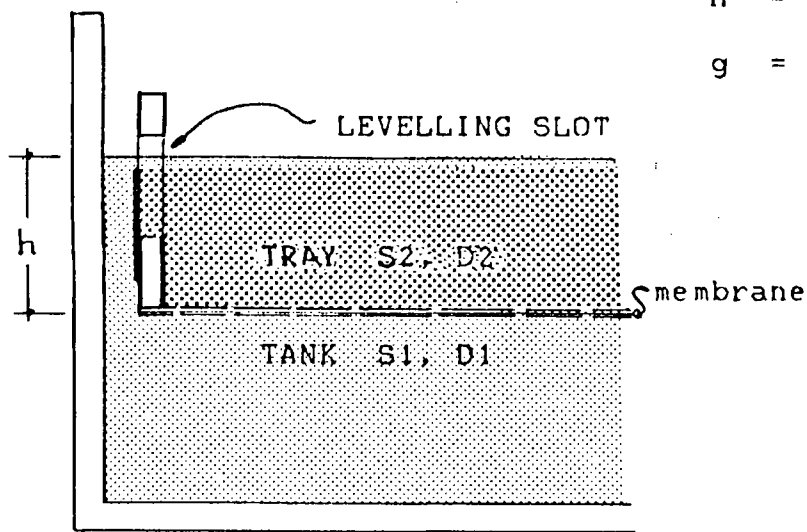


Figure 2-11. **Flux - driving force**

Salinity profiles of fluid in the edge space between tank and
tray (figure 2-12) did show a stable stratification caused by
the increasing salinity of fluid rising from the mixed layer to
return through the levelling slots to the tray, and profiles of
salinity in the tray (figure 2-13) show that this return flow
formed a light layer at the top in the tray. To calculate the
driving pressure, a correction was made by approximating these
stable stratifications with simple 2-layer systems and reducing
the height of the fluid columns by the 2-3 mm of common upper
layer salinity.

The driving pressures and corresponding volume fluxes were calculated from time series data for fluid in the tray and in the tank, using equations 2.6 to 2.8 and these approximations. A calibration curve was fitted through sets of membrane flux data obtained before and after the first slope flow experiment (figure 2-15).

### 2.6.3 Membrane salt flux determination

To estimate the membrane salt flux at the time that a slope flow velocity was measured during an experiment, the salinities of fluid in the tray and in the mixed layer at that time were obtained by linear interpolation, when nearby data points were available from the time-series. Salinities were estimated from a least squares curve fit when only a few tray data points were taken, or when no nearby mixed layer data were available. The driving pressure was then calculated from the corresponding densities, computed from those salinities and the temperature in the tank, using the Unesco Equation of State (appendix A).

The corresponding volume flux was obtained from the calibration graph of membrane flow (figure 2-15) and the membrane salt flux was calculated from equation 2.6.

Several series of flux calibration experiments were done to develop the data acquisition methods. The rate of change in the tank and tray densities was always very similar, but individual numeric results for the volume flux varied, in part due to some clogging of the membrane in successive experiments or to poor readings of fluid depths in tank or tray.
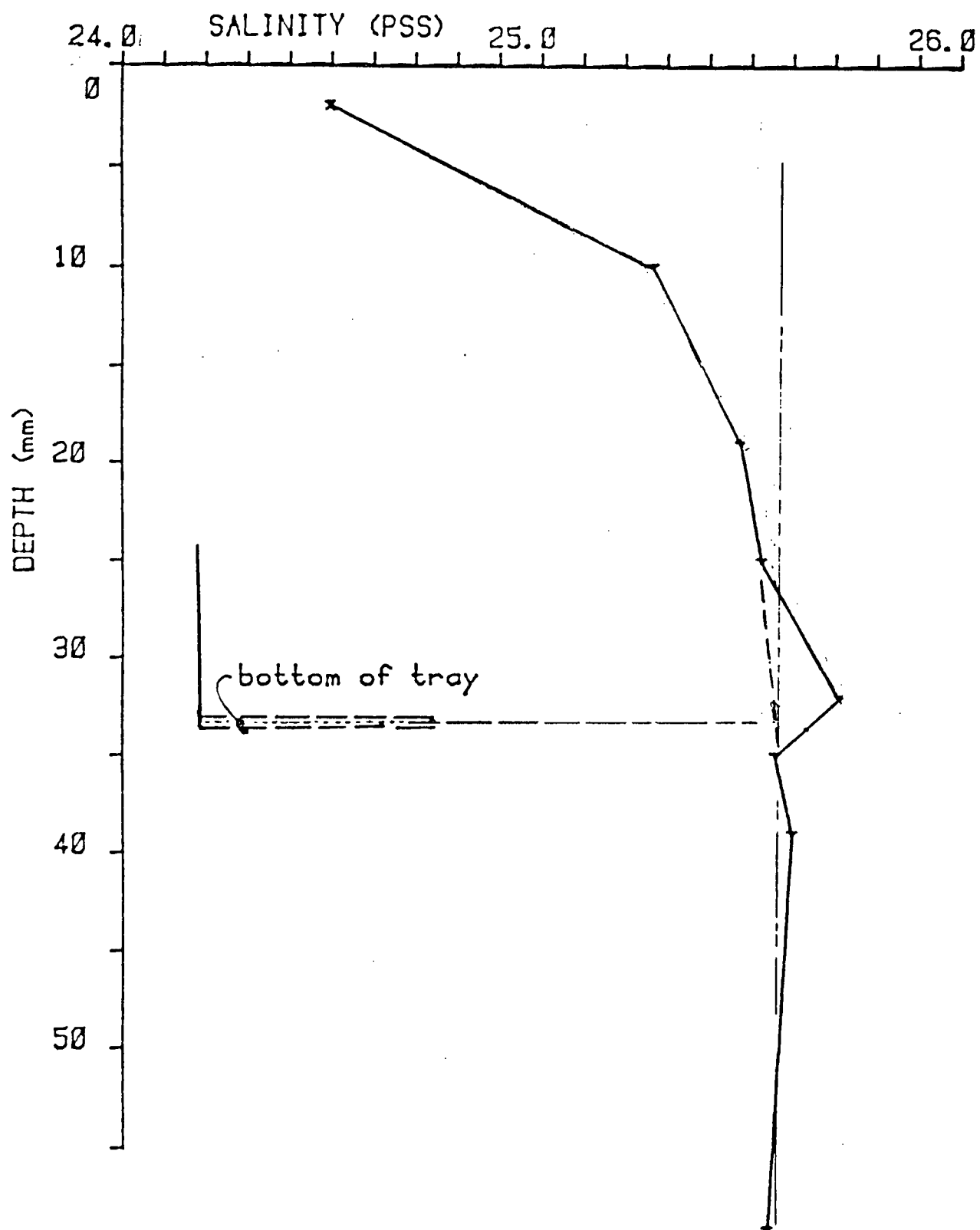
Figure 2-12. Salinity profile in tank/tray edge
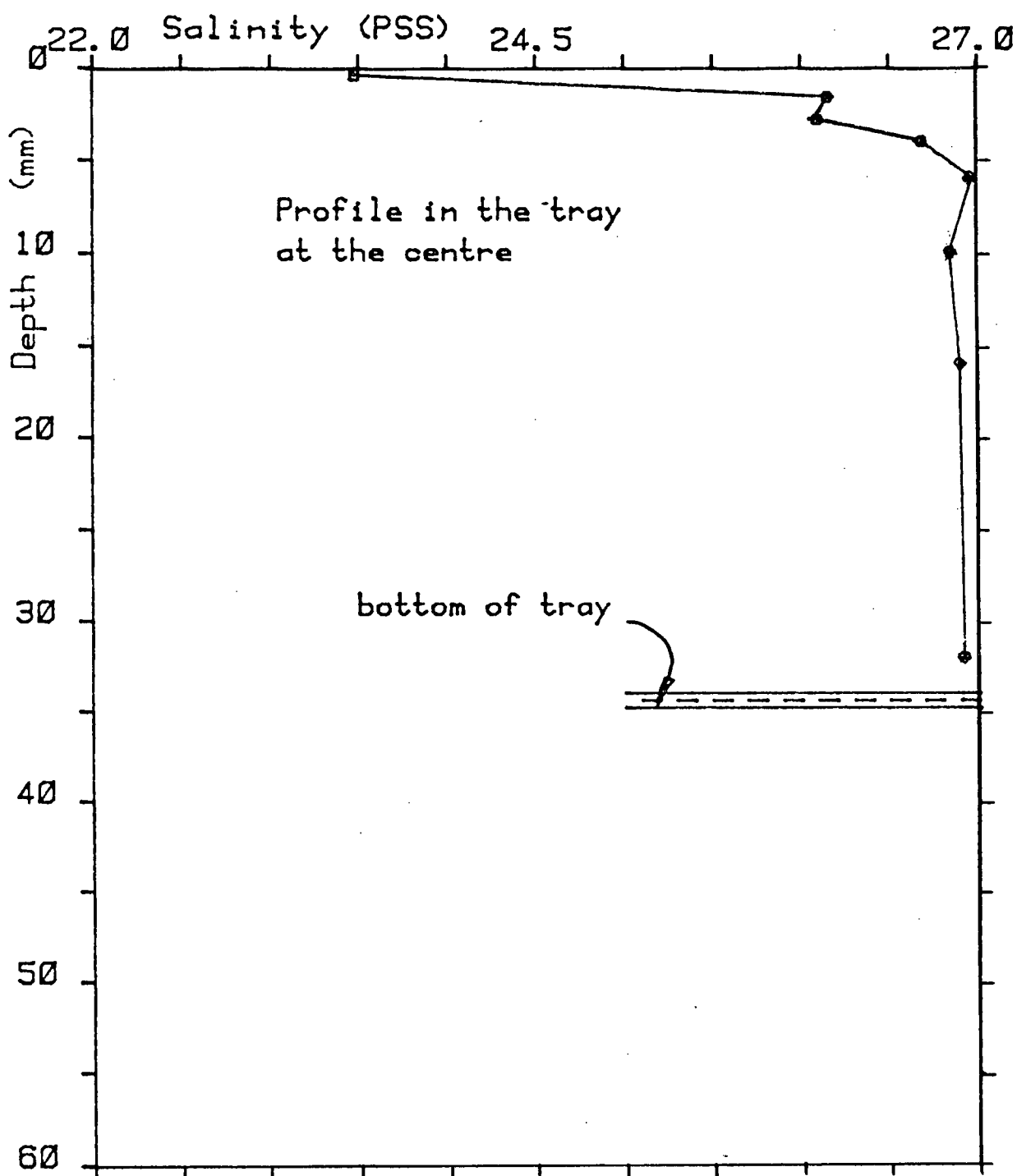
Figure 2-13. Salinity profile in the tray.

Figure 2-15.    MEMBRANE VOLUME-FLUX vs PRESSURE
calibration data for sloperuns
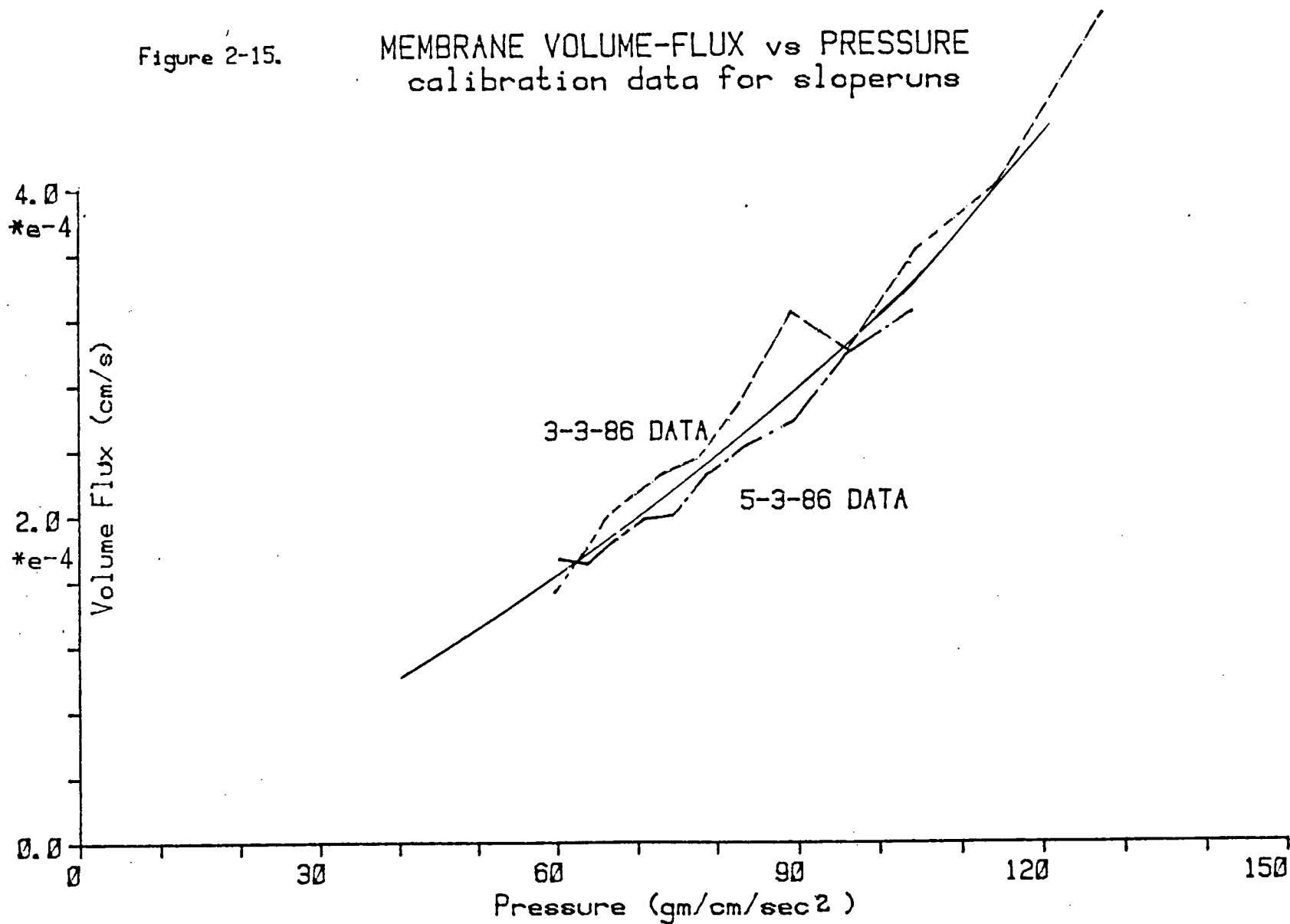
## 2.6.4 Salt flux and entrainment

Several separate experiments were conducted without a bottom slope, over a range of salt fluxes similar to those used in the slope flow experiments, to measure interface entrainment caused by convective turbulence in the absence of shear.

The salt flux into either a 2-layer system or into a linear stratification created an upper well-mixed layer which slowly increased in density due to the salt flux and in depth due to entrainment. The interface was visible in the shadowgraph as a bright line separating the line patterns in the upper layer of convective turbulence from the clear quiescent region below (photo 3). This line slowly moved downward due to entrainment. In the 2-layer system, the line faded as the step in density across the interface became small and the individual convective elements penetrated through it.
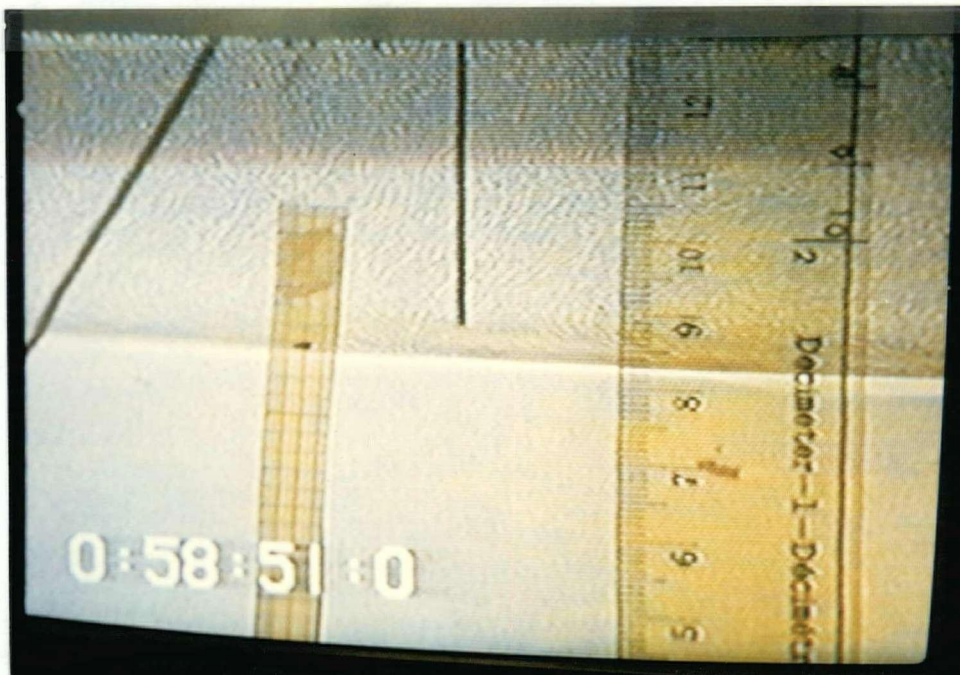


Photo 3. Interface entrainment

28

The entrainment velocity is measured as the deepening of the mixed layer with time:

$$Ve = dY/dt \qquad (2.9)$$

The following diagram defines the dimensions, velocities and densities used to formulate interface entrainment:



Tank and tray        2-layer system        linear stratification
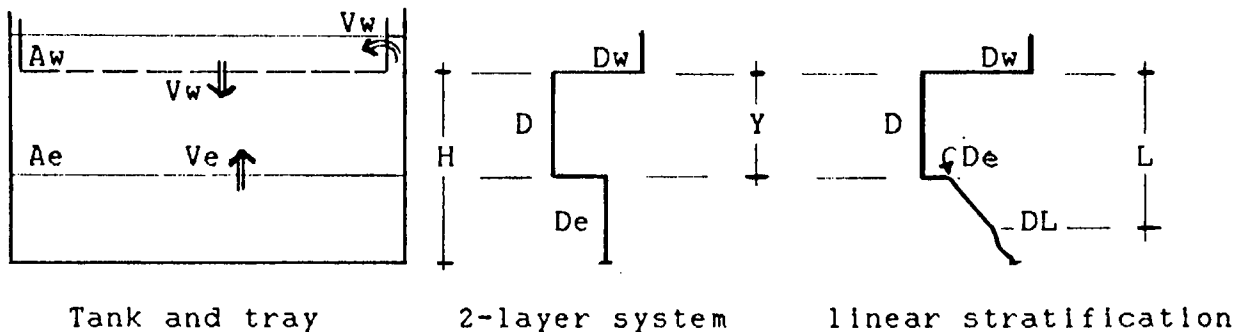
Y  = mixed layer depth          Ve = entrainment velocity

H  = depth of fluid in tank     Vw = membrane volume flux

L  = bottom of linear stratif.  Dw = tray fluid density

Aw = tray membrane area         D  = mixed layer density

Ae = tank interface area        De = density at interface

                                DL = density at depth L

Figure 2-16. Diagram of interface entrainment definitions

The intensity of the convective overturning can be expressed as a vertical velocity scale $W\star$ derived from the mixed layer depth Y and buoyancy flux Q using simple dimensional analysis:

$$W\star = (Y.Q)^{1/3} = \left[ Y.Vw.g.\frac{(Dw-D)}{Dref} \right]^{1/3} \qquad (2.10)$$

$Dref = 1 \ gr/cm^3$

g = gravity acceleration

The ratio of the inertial force to the buoyancy force at the interface describes the relative importance of penetrative convection versus a stabilizing density stratification and has been expressed either as a non-dimensional overall Richardson number **Ri** by Kantha (1978) or as an internal Froude number **Fr** by Bo Pedersen (1980):

$$Fr^2 = 1/Ri = -\frac{W*^2}{g.Y.(D-De)/Dref} \qquad (2.11)$$

The entrainment hypothesis derived by Bo Pedersen predicts that the ratio of flux to entrainment, written as a bulk flux Richardson number **Rf'**, is nearly constant:

$$Rf' = \frac{Ve.(De-D)}{(Dw-D).Vw} \simeq 0.20 \qquad (2.12)$$

In these experiments, conservation of mass requires that the rate at which the salt flux adds mass to the volume in the tank equals the sum of changes in mixed layer and lower layer:

In the 2-layer system, the lower layer density is constant. The mass in the tank is:

$$M = Ae.[Y.D + (H-Y).De] \qquad (2.13)$$

and conservation of mass is described for the 2-layer system by:

$$(Vw.Aw)(Dw-D) = Ae.\frac{d}{dt}\left[Y.D + De.(H-Y)\right]$$

$$\text{or} \qquad Vw = \frac{Ae}{Aw.(Dw-D)}.\left[Ve.(D-De) + Y.\frac{dD}{dt}\right] \qquad (2.14)$$

The entrainment velocity was obtained from video observations of interface depth (figure 2-17). Table 2.1 lists the computed values for the scale velocity and non-dimensional parameters.

# Entrainment by convection
## 2-layer system   5-23-86

Depths from video recording
of shadowgraph image

2nd order curve fit:

$$Y = 41.50 - t*(0.0291 - t*1.31154e-3)$$
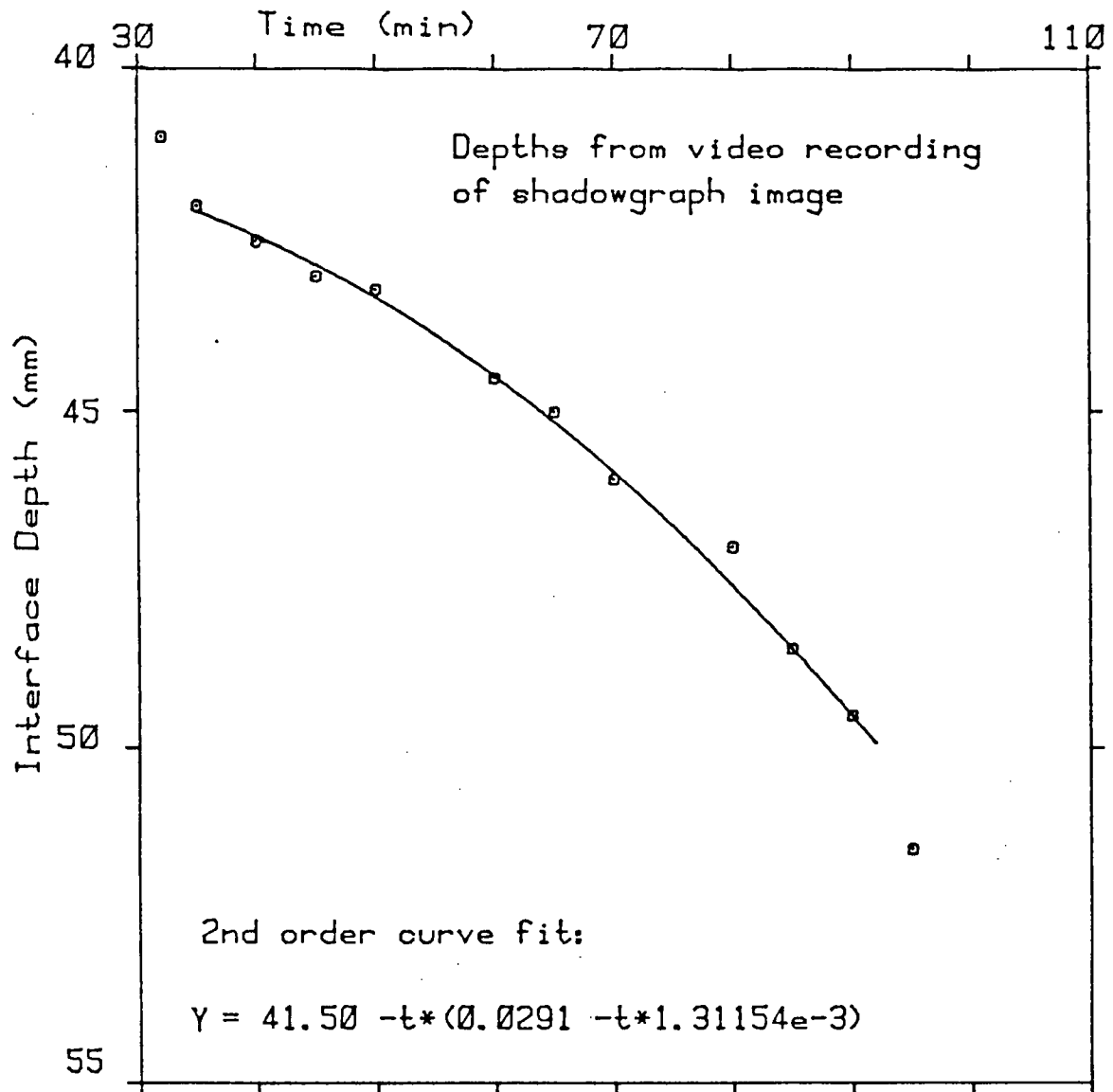
Figure 2-17.  Entrainment at interface
of 2-layer system.

The analysis was done using the data of the 5-23-86 experiment. The ratio of tray to tank area was $Aw/Ae=0.824$, the lower layer density $De=1.00926$ (g/cm³) and the rate of change in the mixed layer density was nearly constant $dD/dt=6.076e-4$ g/cm³/s.

Table 2.1 **Entrainment in 2-layer system**

| t<br>(min) | Ve.e-4<br>(cm/s) | Vw.e-4<br>(cm/s) | W*<br>(cm/s) | Rf' | Ve/W*<br>.e-4 | Fr²<br>.e-3 | Ri |
|---|---|---|---|---|---|---|---|
| 42 | 1.3308 | 1.0528 | 0.157 | 0.222 | 6.01 | 3.834 | 261 |
| 54 | 1.9600 | 1.0618 | 0.196 | 0.223 | 8.80 | 4.495 | 223 |
| 66 | 2.5892 | 1.1035 | 0.217 | 0.227 | 11.42 | 5.265 | 190 |
| 75 | 3.0611 | 1.1631 | 0.214 | 0.232 | 13.19 | 6.170 | 162 |
| 90 | 3.8476 | 1.3334 | 0.169 | 0.246 | 15.65 | 9.275 | 108 |

In the case of a stratification which is linear to a depth L the mass under the tray to that depth is:

$$M = Ae.\left[Y.D + (L-Y).\frac{(DL+De)}{2}\right] \quad (2.15)$$

and conservation of mass for the linearly stratified case is:

$$(Vw.Aw)(Dw-D) = Ae.\frac{d}{dt}\left[Y.D+\frac{(De+DL)}{2}.(H-Y)\right]$$

The time-series plots for interface depth and salinity in the mixed layer (figure 2-18) were combined to show the interface depths at the corresponding mixed layer salinity (figure 2-19). A profile of the initial stratification, plotted in this same graph, shows that the step in salinity across the interface is constant, or:

$$De-D= const \quad so \quad \frac{d(De)}{dt} = \frac{d(D)}{dt}$$

or $\quad Vw = \dfrac{Ae}{Aw(Dw-D)} \cdot \left[ Ve \cdot \dfrac{(2D-De-DL)}{2} + \dfrac{(Y+L)}{2} \cdot \dfrac{dD}{dt} \right]$ $\quad$ (2.16)

A linear least-squares fit to the interface depths from video footage, for points in the nearly linear part of the profile, yielded:

$$Y = 5.30 + (t-24) \times 60 \times 1.128e\text{-}3 \quad \text{(Y in cm, t in min)}$$

and thus a constant entrainment velocity:

$$Ve = 1.128e\text{-}3 \quad \text{(cm/s)}$$

Values for flux, scale velocity and non-dimensional parameters were computed using the above derivations. The results for data from the linear stratification experiment are listed in table 2.2 below.

Table 2.2 **Entrainment in linear stratification**

| t (min) | Vw.e-4 (cm/s) | W∗.e-2 (cm/s) | Rf' | Ve/W∗ | Fr² .e-2 | Ri |
|---|---|---|---|---|---|---|
| 30 | 1.686 | 2.58 | 0.107 | 6.01 | 4.365 | 2.46 |
| 40 | 1.960 | 2.80 | 0.094 | 8.80 | 4.032 | 2.34 |
| 50 | 2.246 | 3.00 | 0.084 | 11.42 | 3.76 | 2.25 |
| 60 | 2.550 | 3.20 | 0.076 | 13.19 | 3.52 | 2.17 |

The computed results of these experiments show good agreement with the hypothesis for entrainment due to free penetrative convection by Bo Pedersen (1980) and agree with data from other sources when plotted in graphs of compiled field and laboratory results by Bo Pedersen and Jurgensen (1984) and by Kantha (1976), as shown in figure 2-20.

# Entrainment by convection
# Linear stratification 5-30-86
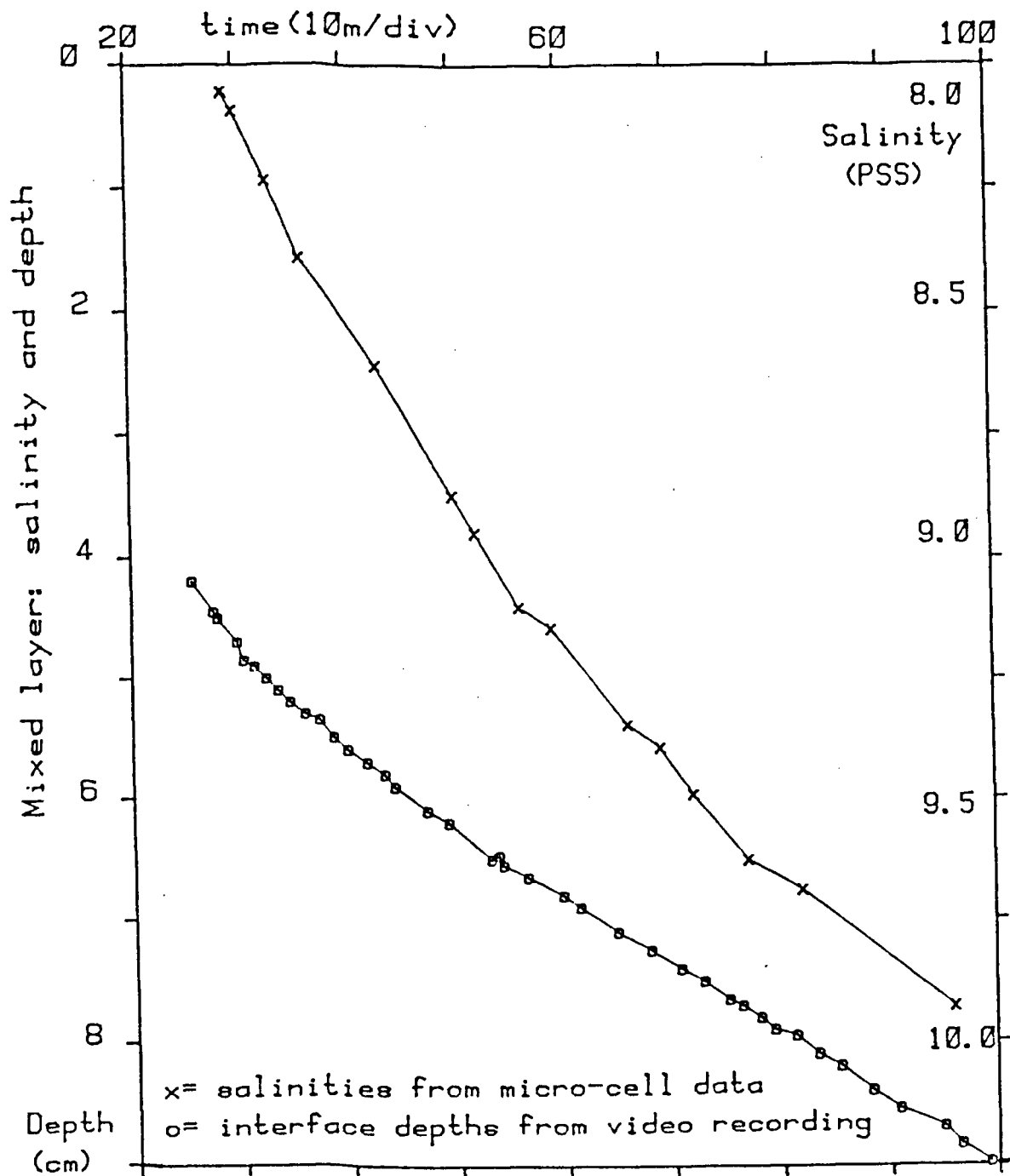


Figure 2-18. Time-series plot of interface depth
and mixed layer salinity.
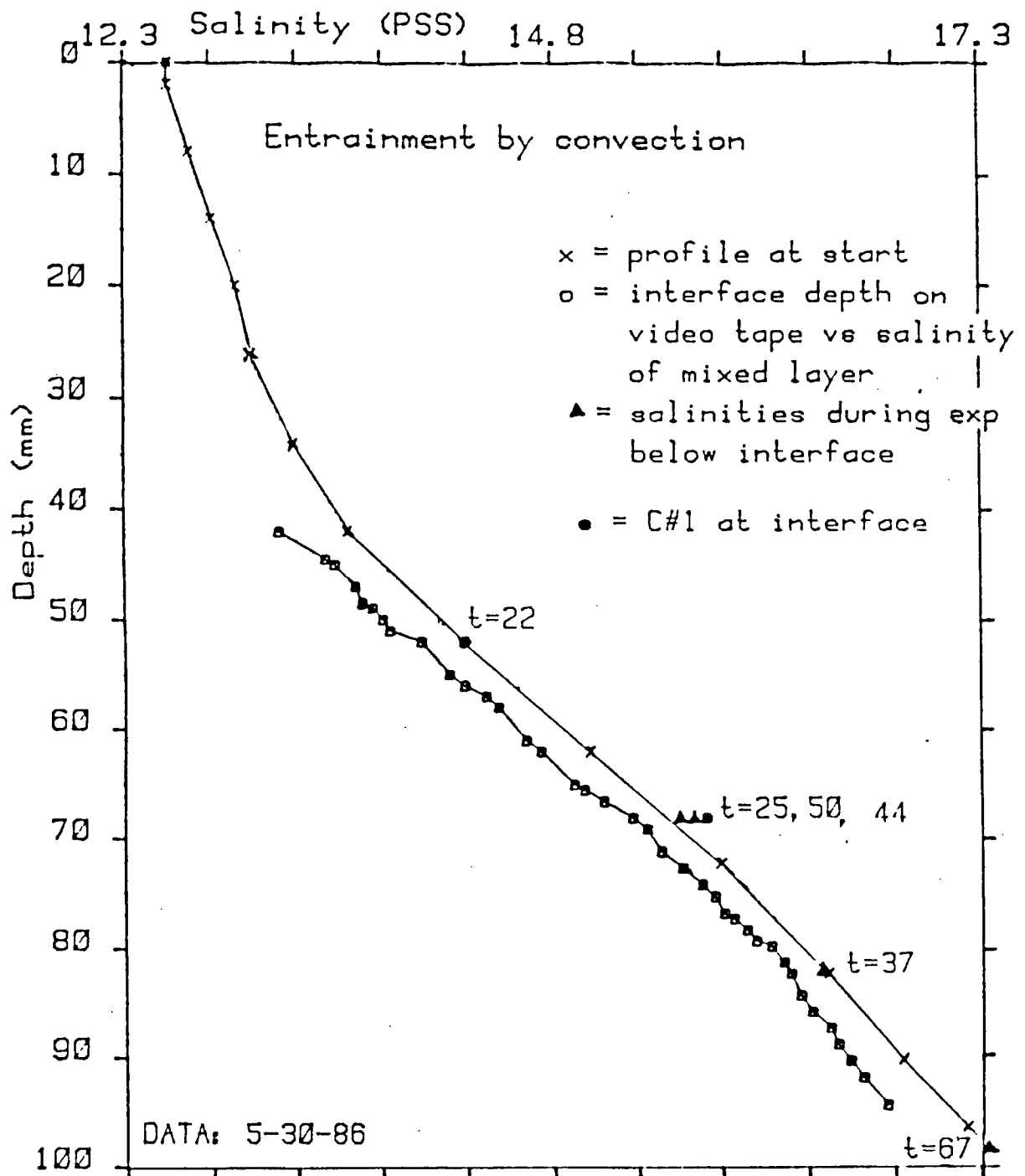
Figure 2-19. Interface depth vs. mixed layer salinity, and initial stratification.

35
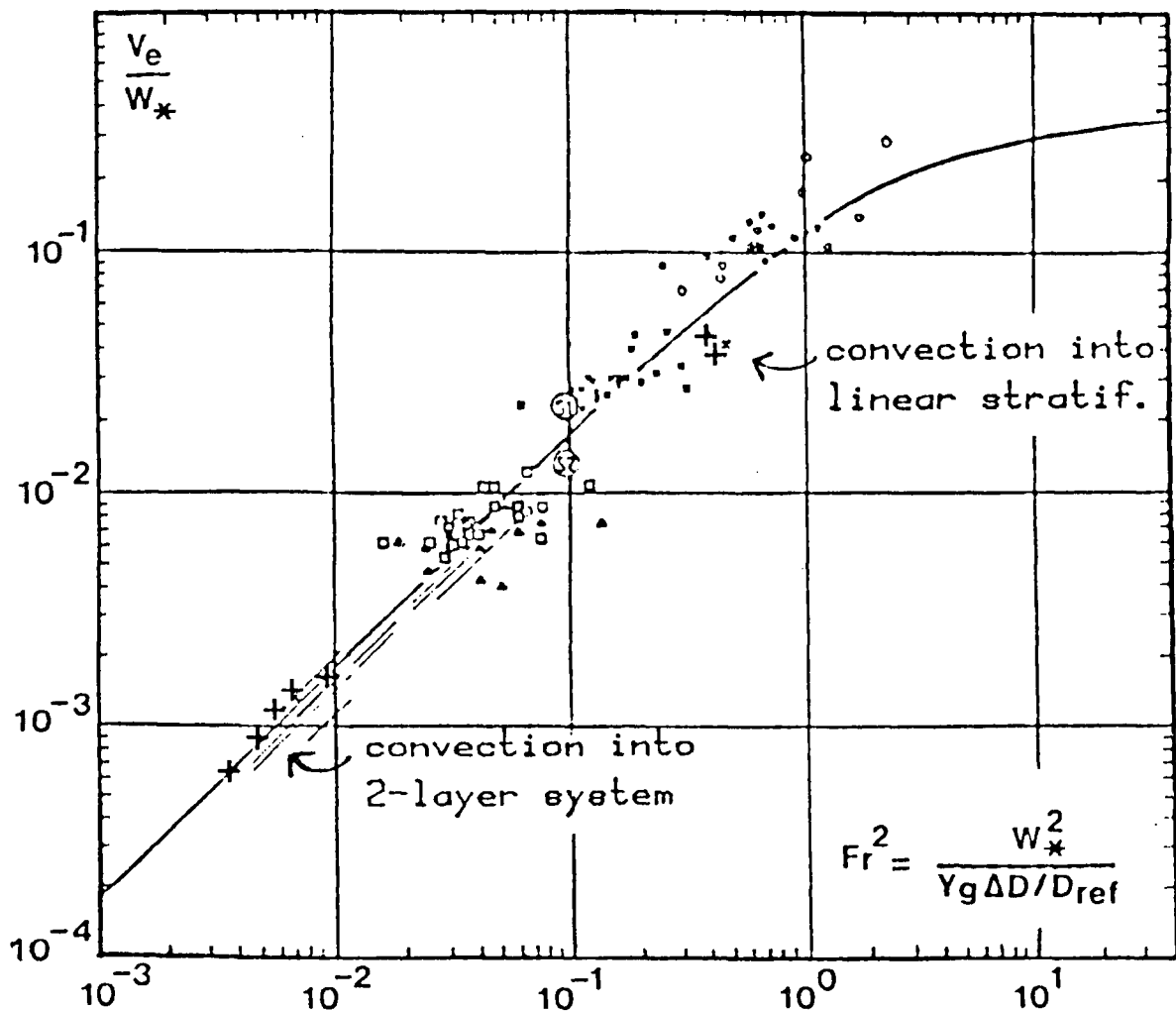
Figure 2-20. Entrainment by penetrative convection

Comparison with Bo Pedersen theory (1980)
and with laboratory and field data by:

// Bo Pedersen and Jürgensen (1984) - laboratory
x,o,□ Heidt (1975) - laboratory experiments
sı,sƨ Willis and Deardorff (1974) - laboratory
▲ Farmer (1975) - solar heating under lake ice
+ BvanH (1986) - laboratory salt flux

## 2.6.5 Arctic saltflux and convection depth

To compare laboratory conditions with those encountered in the field, data from Cambridge Bay in the Canadian Arctic (Gade et al, 1974) were used to derive values for the buoyancy flux, entrainment and Froude number following the above notation.

The data included ice thickness H, mixed layer salinity Sm and observed depth of convection Y between October 1971 and April 1972. The ice salinity Si was estimated as 3.0 ppt and ice density Di as 0.9 g/cm³. The ice growth was obtained by linear interpolation over the time between observations.

The salt flux into the ice is the product of growth, density and salinity in the ice. Using a simplified model, the amount of salt expelled into the mixed layer can then be expressed as a salt flux F :

$$F = (dH/dt).Di.[Sm - Si] \qquad (2.17)$$

The following table shows the field data and the derived values for entrainment velocity Ve= dY/dt, ice growth (dH/dt), salt flux F and buoyancy flux Q= F.g (g=gravity), convective scale velocity Wx= [Y.Q]^{1/3} and corresponding Froude number Fr.
The salt flux from freezing estimated from these field data is several orders of magnitude smaller than those used in the laboratory, however, the large depths of the mixed layer in the field bring the values for the scale velocity Wx close to those in the experiments.

Table 2.3 **Entrainment from Arctic field data**

| Date | days | Mixed layer Depth (m) | Incr (m) | Ve (cm/s .e-4) | Salin (ppt) | Dens (sigma) | Ice Thk (cm) | Incr (cm) | Growth (cm/s .e-5) |
|---|---|---|---|---|---|---|---|---|---|
| 10/12 | | 16.6 | | | | | 0 | | |
| | 17 | <18.5> | 3.1 | 2.11 | | | <11.5> | 23 | 1.566 |
| 10/29 | | 19.7 | | | 26.5 | 21.27 | 23 | | |
| | 37 | <20.35> | 1.3 | 0.407 | <27.15> | <21.30> | <37> | 28 | 0.876 |
| 12/5 | | 21.0 | | | 27.8 | 22.32 | 51 | | |
| | 78 | <24.0> | 6.0 | 0.890 | <28.35> | <22.77> | <95> | 88 | 1.306 |
| 02/21 | | 27.0 | | | 28.9 | 23.21 | 139 | | |
| | 52 | <30.75> | 7.5 | 1.471 | <29.1> | <23.38> | <147.5> | 17 | 0.333 |
| 04/14 | | 34.5 | | | 29.3 | 23.54 | 156 | | |

Values in brackets are linear interpolations between those from the dates of observation.

| Days | Salt Flux (g/cm²/s) .e-7 | Buoyancy Flux (g/cm/s³) .e-4 | W* (cm/s) | Ve/W* | Fr² | Rf$^T$ |
|---|---|---|---|---|---|---|
| 17 | 3.31 | 3.25 | 0.839 | 2.517 | 1.63 | 1.58 |
| 37 | 1.904 | 1.87 | 0.724 | 0.561 | 1.093 | 0.524 |
| 78 | 2.983 | 2.92 | 0.888 | 1.002 | 3.586 | 0.285 |
| 52 | 0.783 | 0.768 | 0.618 | 2.38 | 3.960 | 0.61 |

The computed values for entrainment efficiency Rf' do not agree with the 0.20 predicted by Bo Pedersen but there were few observations, spaced over a period of six months (figure 2-21), and the values for entrainment derived from these field data neglect any advection of salt by tidal flows or by the type of reverse estuarine flow suggested by the slope flow experiments, or any entrainment caused by internal waves.
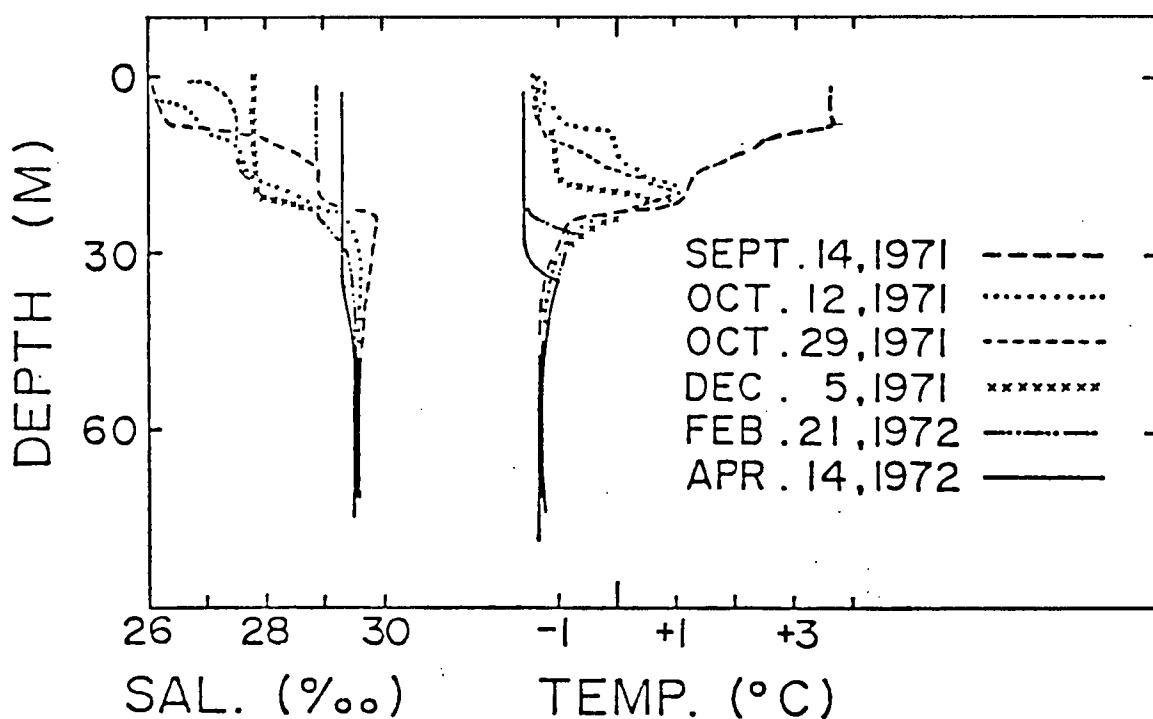
Seasonal changes in water column temperatures and salinities at Cambridge Bay, winter 1971 and 1972.
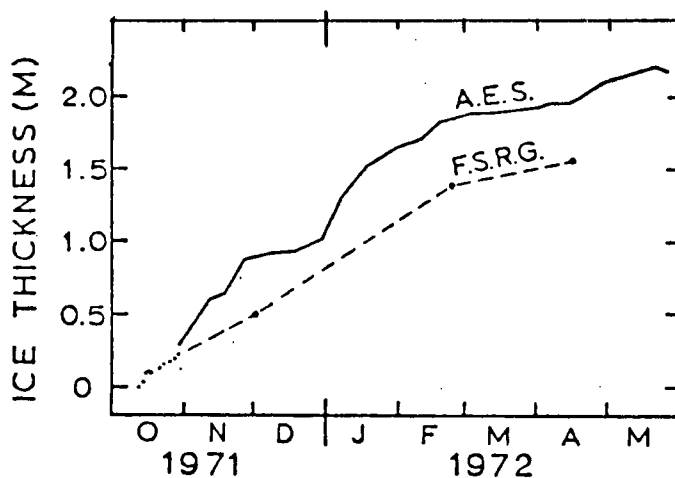


Sea ice thickness at Cambridge Bay according to Atmospheric Environmental Service and Frozen Sea Research Group measurements.

Figure 2-21. Profiles and ice thickness - field data

Slope flows were induced in a series of experiments conducted with different bottom slope angles, set between 2.2° and 5.5°. Salt flux estimates computed from micro-cell data taken during the experiments ranged from 1.82e-5 to 1.63e-6 gr/cm²/s. A slope flow was observed in each of the experiments.

## 3.1 Slope angles, starting salinities and salt fluxes

The bottom slope angle of the tank was fixed before the start of each experiment. The salt flux range through the membrane during the experiment is determined by the height of fluid in the tray and by the difference in the initial salinities of the fluids in tank and tray. Sea water was used in the tray and reservoir for the lower salt fluxes, where conductivities were within range of the AM/CT Datalogger circuit. For the higher salt fluxes, pure sea salt was mixed into the sea water for tray and reservoir to obtain salinity differences of 40-60 ppt between the fluids in tank and tray. In these cases the tray salinities were monitored with a separate conductivity circuit and a digital voltmeter.

Table 3.1 lists the bottom slope angle, the depths of fluids in and under the tray, the starting salinities for each of the slope flow experiments, and the range of computed membrane salt fluxes.

Table 3.1   Starting Conditions for Slope Flow Experiments

| Exp # | Angle (degr) | Tray-h (mm) | Tank-depth Max(mm) | Min | Salinity(ppt) Tray | Tank | Salt fluxes (g/cm²/s*e-6) |
|---|---|---|---|---|---|---|---|
| 1 | 3.3 | 34 | 63 | 7 | 59 | 15 | 17.80 -16.94 |
| 2 | 3.8 | 34 | 65 | 7 | 58 | 7 | 18.20 -17.12 |
| 3 | 2.2 | 34 | 51 | 20 | 58 | 8 | 14.18 - 9.46 |
| 4 | 5.2 | 34 | 100 | 20 | 53 | 7 | 21.89 -13.64 |
| 5 | 5.2 | 34 | 100 | 20 | 52 | 13 | 12.67 - 5.51 |
| 6 | 2.3 | 34 | 57 | 20 | 30 | 16 | 2.21 - 1.63 |
| 7 | 5.5 | 34 | 78 | 0 | 28 | 12 | 1.71 |
| 8 | 5.2 | 34 | 99 | 15 | 46 | 9 | |

With the end of the tray resting on the bottom at the shallow end of the tank, the amount of fluid and the depths in the wedge-shaped volume below the tray became very small at small slope angles. In initial tests, neither the shadowgraph nor injected dye did show any distinct contribution to the slope flow near the shallow end. Therefore, the tray was raised so the fluid depth at the shallow end of the tank was 7 mm im the first and second slope flow experiments and 20 mm in nearly all subsequent experiments.

## 3.2 Shadowgraph observations

When the tray was nearly filled with the denser fluid to the selected height, and the fluids in the tray and in the edge space between tank and tray reached almost the same level, salt began to percolate through the membrane in the tray bottom and convection started as a field of small plumes or streamers. It

became visible in the shadowgraph image as a curtain of small wrinkled line segments, slowly and fairly evenly descending at a speed estimated at less than one cm/sec, depending on the magnitude of the salt flux.

A downslope flow was seen to start up shortly after part of this curtain reached the bottom at the shallow end of the tank: the mostly vertical orientation of the line segments in the shadowgraph image began to display a bend towards the shallow end of the tank in the mixed region, and near the bottom became parallel with it. The typical shadowgraph images seen during the experiments (seen in photo 2, page 8) show a deflection of the vertical line patterns from convective overturning by the general flow pattern imposed by the slope flow and associated return flow in the mixed region (see figure 3-1 below).
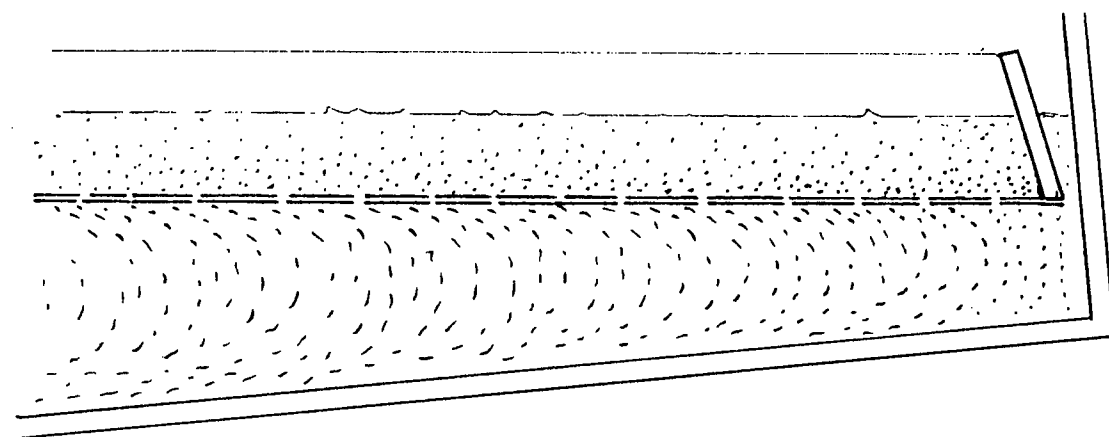


Figure 3-1. Sketch of typical shadowgraph pattern

The slope flow usually was seen to start up very close to the shallow end soon after the saltflux through the membrane became visible, but in several of the experiments it was seen to start initially at 20 to 30 cm from the shallow end of the

tank and to form a counter-rotating cell uphill from there (see figure 3-2). In these cases, the downslope/uphill flow cells did re-establish themselves again after stirring the fluid under the tray to remove flow patterns which might have been introduced by uneven conditions while filling the tray. In some of the experiments, the initial descent of the curtain of lines in the shadowgraph was slightly faster in the area of the tray where the slope flow was seen to start. The starting point of the slope flow gradually moved toward the shallow end, while the uphill flow cell shortened and often disappeared over 8 to 20 minutes. In experiment #6, which had the lowest slope angle (2.3 degrees), the uphill flow cell decreased in length to the last 10 cm at the top of the slope, but persisted throughout the experiment.
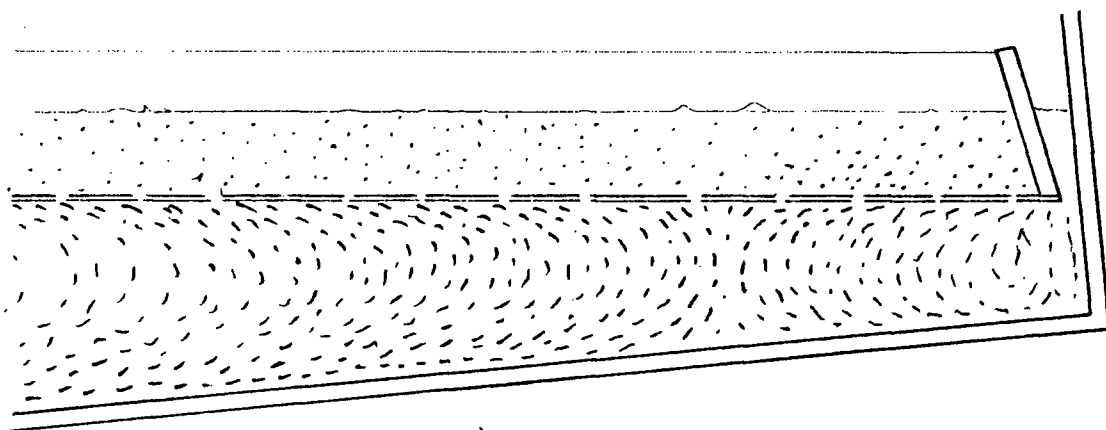


Figure 3-2. Sketch of downslope/uphill flow cells

The slope flow appeared to accelerate from the starting point but then to slown down and reach some equilibrium within about

20 to 30 cm down the slope, beyond which it was not possible to accurately measure any increase or decrease in the flow speed.

As the experiments progressed and the heavier fluid collected at the deep end of the tank, the line patterns associated with convective turbulence did not penetrate into the deeper part of the tank. The slope flow was seen to separate from the bottom at an increasing distance from the end of the slope and move along the interface with the stably stratified fluid at the deep end.

On several occasions, pinhole leaks were seen in the shadow-graph images at some of the points where sampling tubes cut through the membrane in the tray. The leaks showed as small streamers of denser fluid descending slightly faster through the mixed layer than the other motions observed and penetrating into the stably stratified layer which forms in the deeper part of the tank. While these contributed to the salt flux, they are believed to be minor. Some variability in the salinity profile points may have been caused when a streamer from a small leak intermittently was syphoned into a micro-cell during profiling, as was seen to occur in one instance on video footage.

## 3.3 Injected dye

Small amounts of food dye were injected through one of the sampling tubes set along the centerline of the tray. The dye was mixed with some salt water to a density slightly above that of the fluid in the tank. During injection, a line of dye was seen to sink through the convectively mixed layer, in which it

was deflected toward the shallow end of the tank by the overall flow pattern, similar to the lines seen in the shadowgraph. When the dye was more diluted and its density was close to that in the mixed layer, the streaks made during descent through the mixed layer were distorted by the convective motions and moved toward the shallow end of the tank (photo 4).
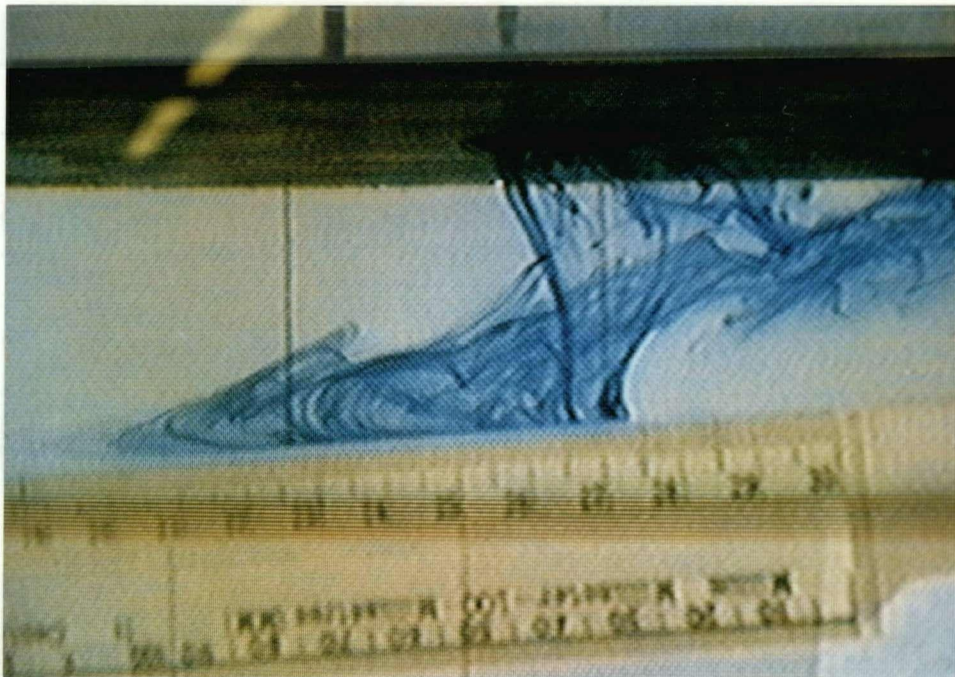


Photo 4. Dye in the mixed layer and slope flow

Where the dye line sank through the bottom flow, vee-shaped features formed, showing a velocity maximum at about 3 to 6 mm above the bottom. These features were carried along much of the length of the tank bottom without noticeable dispersion from mixing, which indicates limited levels of turbulence in the slope flow. The vee-shaped features suggest a shear flow with a depth which would be twice that of the height of maximum velocity if the friction at the interface was equal to that at the bottom. The velocity shear and the penetration of convective

45

turbulence at the upper edge of the slopeflow entrained some of the dye from this edge while bottom friction stretches the lower part of the tongue of dye. (see photo 5).
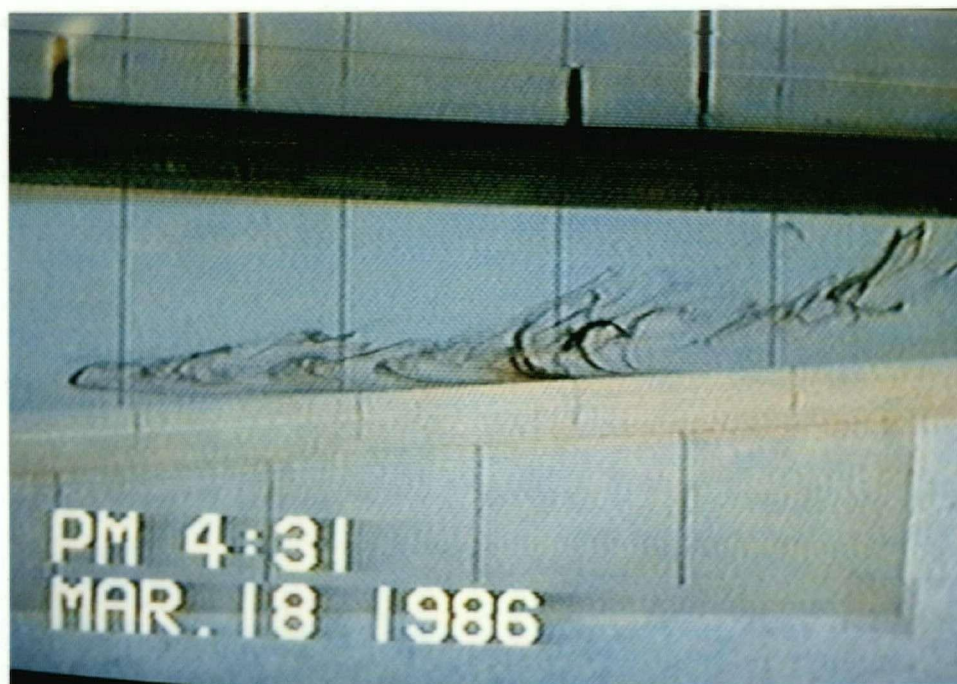


Photo 5. Velocity maxima in dye

The maximum flow velocity was estimated at various times in each experiment from the distance that these dye tongues moved in timed photo or slide sequences, or in video tape footage. Velocities were generally determined from observations made between about 30 to 60 cm from the top of the slope, since the flow in this region appeared steady and not much affected by the conditions at the ends of the tank. The measured flow velocities ranged from 0.09 to 0.52 cm/s and decreased with time during each experiment as the salt flux diminished.

In several of the experiments, dye which was injected in the

edge between tank and tray was slowly raised and carried to the slots into the tray by the return flow from the tank. This flow causes stable stratification in the edge space.   Dye   injected under the tray at the shallow end was seen to be mixed into the last  4 to 6 cm of the tank by the convection but did not  flow down-slope  for the slope angles and salt fluxes used in  these experiments (see photo 6).



Photo 6. Dye at shallow end of tank

At the deep end of the tank the dye from the slope flow was slowly  lifted  and entrained into the mixed  layer. When  the slope  flow  velocities  slowed down in the later  part  of  an experiment,  convective  motions near the deep end of the  tank did appear to penetrate closer to the bottom in the shadowgraph

edge between tank and tray was slowly raised and carried to the slots into the tray by the return flow from the tank. This flow causes stable stratification in the edge space. Dye injected under the tray at the shallow end was seen to be mixed into the last 4 to 6 cm of the tank by the convection but did not flow down-slope for the slope angles and salt fluxes used in these experiments (see photo 6).



Photo 6. Dye at shallow end of tank

At the deep end of the tank the dye from the slope flow was slowly lifted and entrained into the mixed layer. When the slope flow velocities slowed down in the later part of an experiment, convective motions near the deep end of the tank did appear to penetrate closer to the bottom in the shadowgraph

image. In the course of an experiment, the heavier fluid from the slope flow accumulated at the deep end of the tank, where it formed a stably stratified region in which no convective penetration was seen, below a mixed layer of nearly uniform depth. In several of the experiments, the dye in the slope flow was seen to bifurcate where it reached this stable fluid (see arrows in photo 7).
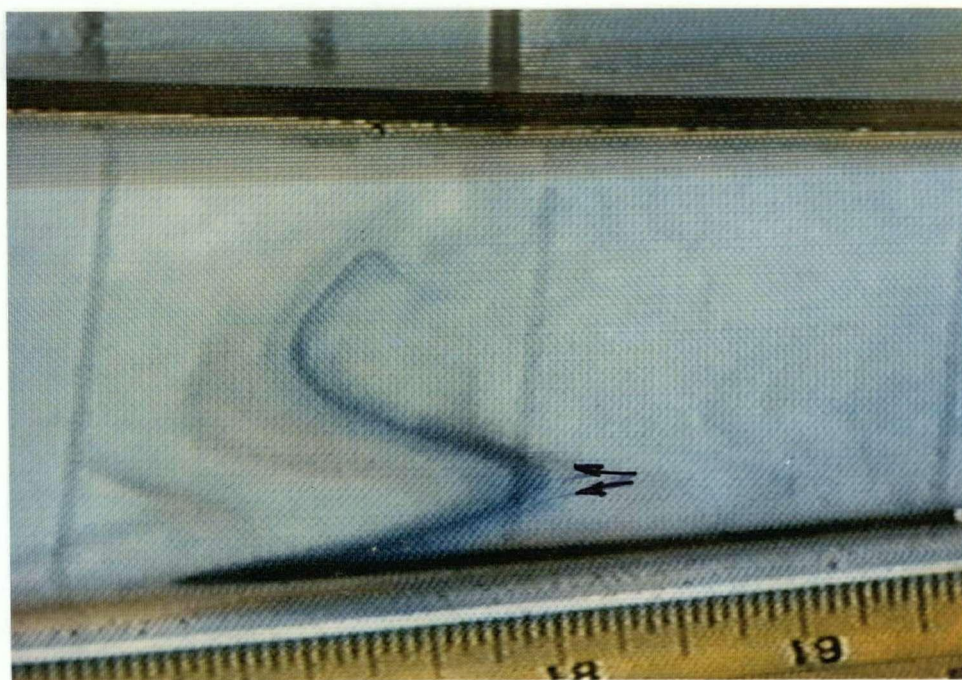


Photo 7. Bifurcation of slope flow

The slope flow lifted off the bottom on reaching the stably stratified lower part of the tank. Dye travelling along the interface was often seen to climb up and over steep waves which were not visible in the shadowgraph (see photo 8). A cloud of dye, injected in the centre of the stratified region, did not move but slowly diffused below the sharp interface with the mixed layer (see photo 9).

48

Photo 8. Waves in dye at lower end of slope
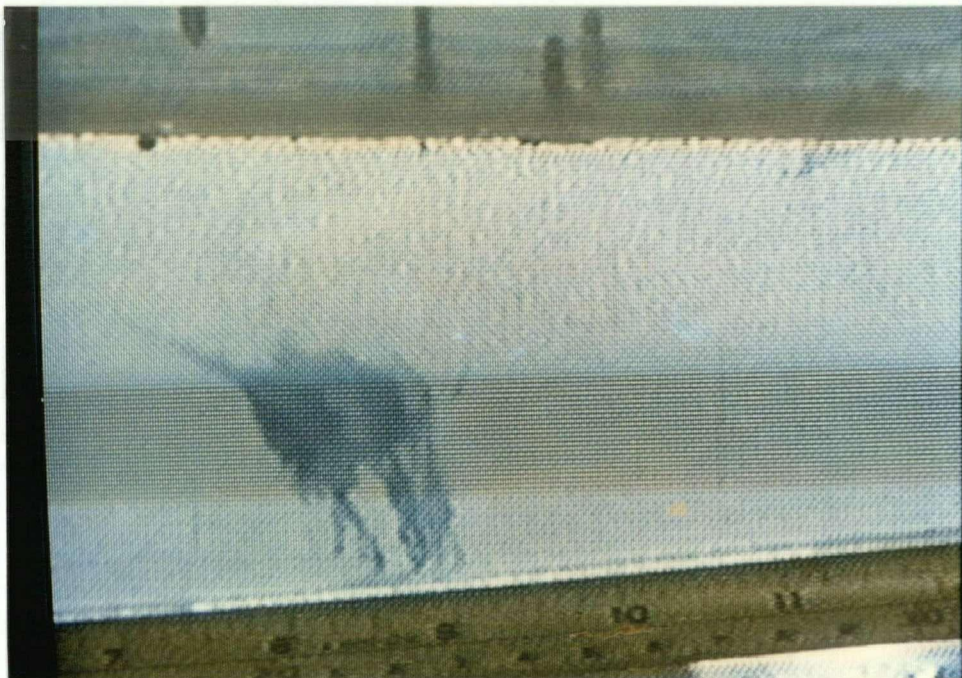


Photo 9. Dye in stably stratified region

Along the part of the slope about 30 cm away from the ends of the tank, there were no perceptible changes in the depth of the slope flow or in the flow velocity, as seen in the dye or shadowgraph images.

Since the volume of fluid in the tank is constant, there must be a return flow above the bottom slope flow for continuity. This was already seen to exist from the deflection of the lines in the shadowgraph image. After dye in the slope flow reached the deep end of the tank, it was seen to rise and be carried in the opposite direction at much slower velocities and in a much less organized manner, while being diffused by convective eddy motions. The flow velocity in the mixed layer increases as the depth in this layer decreases toward the top of the slope.

## 3.4 Salinities and salinity profiles

During the experiments, data were taken from thermistors and micro-cells to determine temperatures, salinities and densities of fluid in the tray and at various locations and depths in the mixed layer and in the slope flow (as described in section 2). Fluid was syphoned through the cells at a constant rate of about 1 ml/s (2 drops per second),and the calibration constants for the micro-cells were usually checked before an experiment.

Due to the salt flux, the salinity in the mixed layer slowly increased in the time needed to take a series of data points. 'Quasi-instantaneous' salinity profiles were obtained by sub-tracting the change in salinity at a fixed point in the mixed layer from actual profile data:

$$S(\text{profile}) = S(\text{actual}) - S(\text{mixed}) + S(t1) \qquad (3.1)$$

in which S(actual) is the salinity calculated from the data at the profile depth, S(mixed) and S(t1) are the salinities in the mixed layer at the same time that the profile data were taken and at the time (t1) that the first profile point was taken.

The adjustment was made either by pointwise subtracting the change in the computed mixed layer salinity, or by subtracting a 'smoothed' value for this change using the slope of a least squares linear fit through the mixed layer salinities for short periods of time (figure 3-3). A line through the time-adjusted profile points in the mixed layer then became vertical (figure 3-4) which indicates that the layer was well mixed (except for points near the underside of the tray where the salt enters the tank). Time-series plots of salinity data taken in the mixed layer indicate that for longer observation times a second order curve gives a better approximation for the change in the mixed layer salinity during an experiment (figure 3-5). The slope flow was seen in the profiles as a 7 to 17 mm thick layer where the salinity rose by 0.24 to 0.92 PSS above the value in the mixed layer. Appendix F gives a brief description of each slope flow experiment with computed results, time-series plots and profiles.

Excessive noise in some of the data was caused by faulty micro-bead thermistors at the micro-cells, and in some cases salinities were re-calculated using the temperature from the good thermistor, offset by half the averaged difference.

51
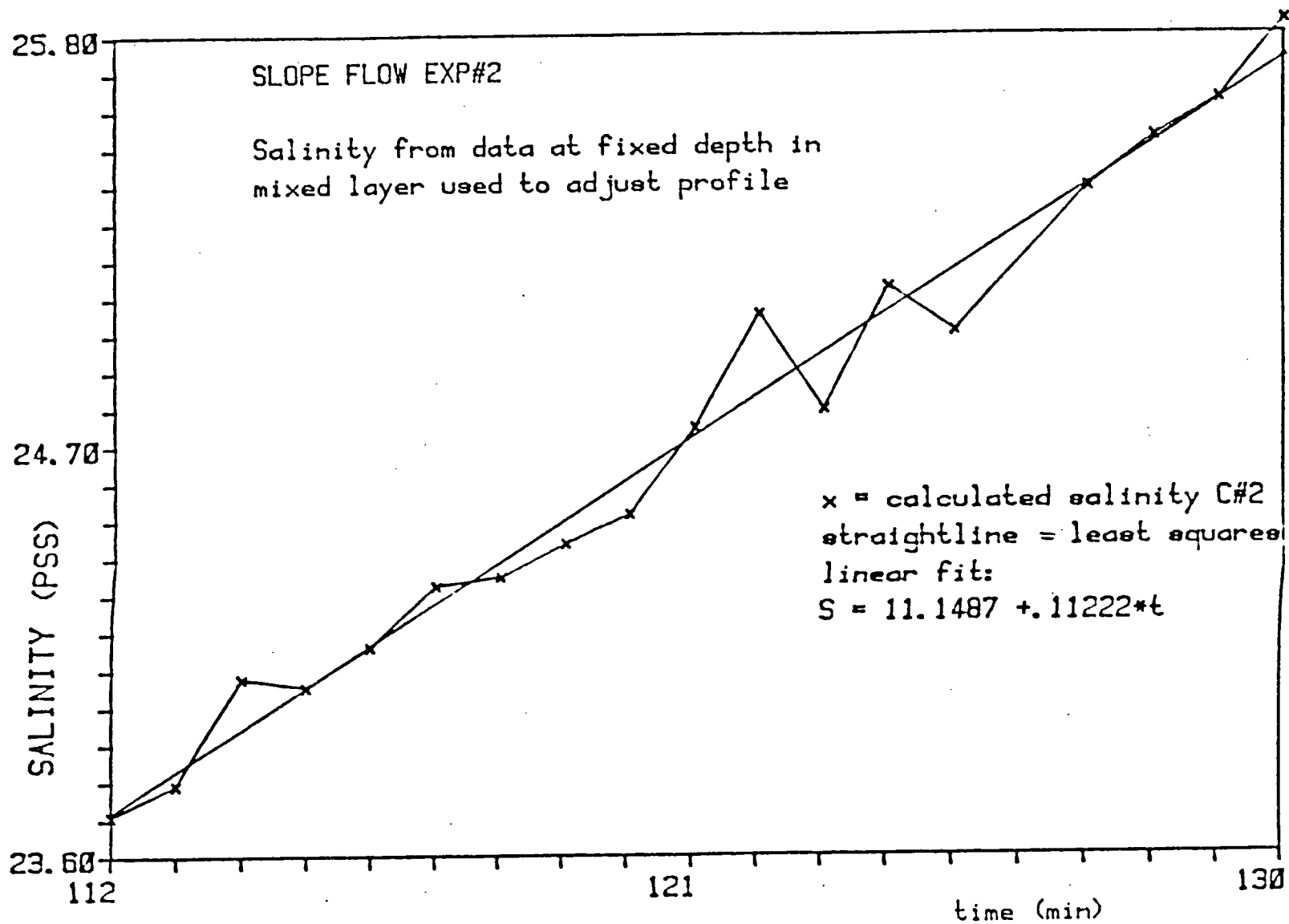
Figure 3-3. Time-series and linear fit

Text within the figure:

SLOPE FLOW EXP#2

Salinity from data at fixed depth in
mixed layer used to adjust profile

x = calculated salinity C#2
straightline = least squares
linear fit:
S = 11.1487 +.11222*t

SALINITY (PSS)

time (min)

52
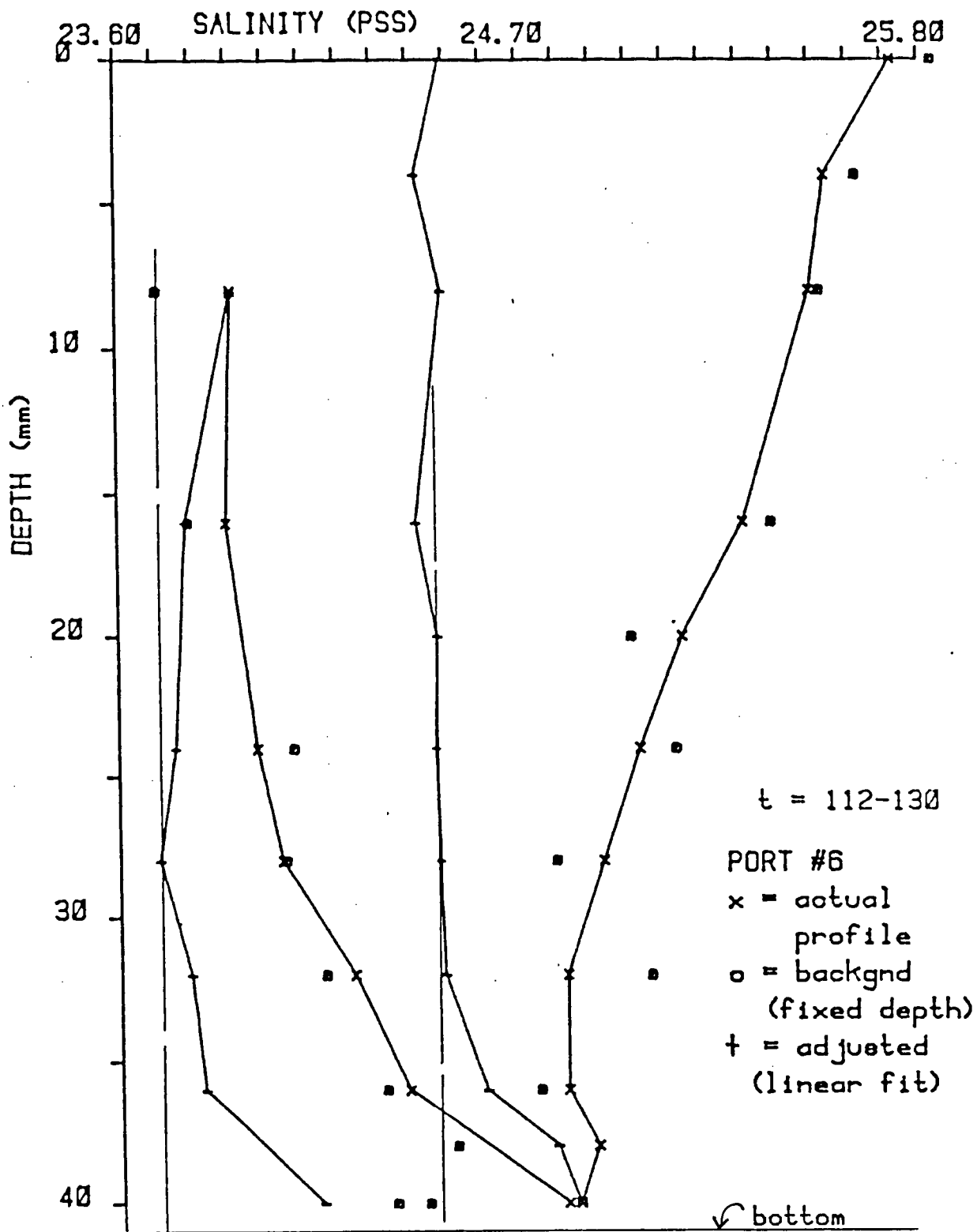
Figure 3-4. Actual and adjusted salinity profiles

Figure 3-5. MICRO-CELL TIME-SERIES
SLOPE FLOW EXP#3

solid line connects data from fixed
depth in mixed layer, dots are data
from various depths (profiles)
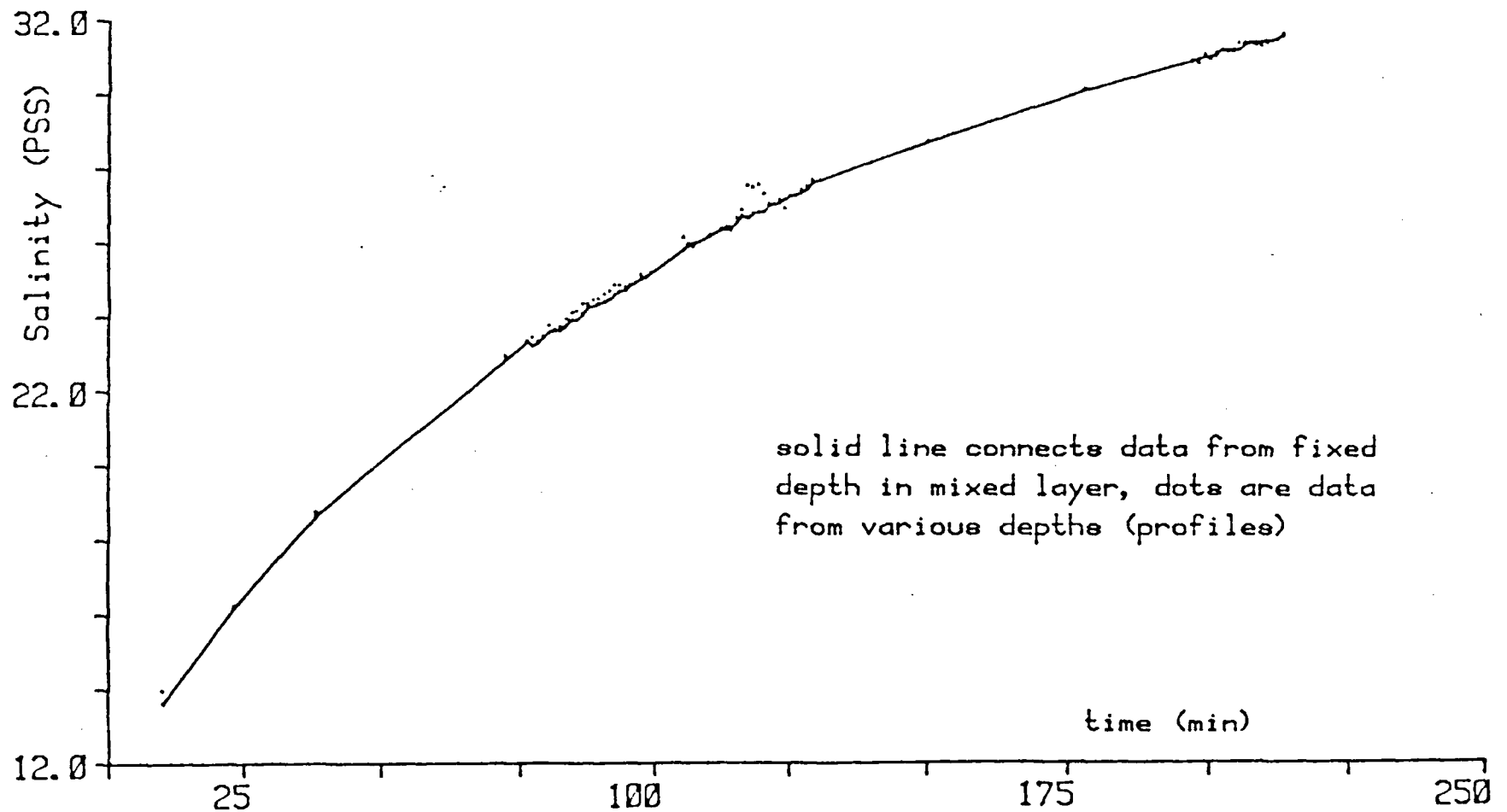
In a separate slope flow experiment, successive profile data were taken by raising the intakes of all three micro-cells to the same height above the bottom, but located near the middle of the tank and 20 cm to either side (figure F-26). The use of the HP-3497A Datalogger System allowed more frequent sampling, and averaging of rapid multiple readings for each sensor. Time series data from this (figure 3-6) and experiment #8 (figure F-27) indicate that the rate of change of salinity with time was the same at different locations along the slope in both mixed layer and slope flow. A curve fit through time-series data from the mixed layer can thus be used to correct for the change in salinity during the time required to collect profile data. When many points were taken, a second order curve was used (figure F-28) to obtain 'quasi-instantaneous' profiles (figures F-30 and F-31) for which the mixed layer salinities at the end would match those at the start. A small but persistent weakening in the salinity gradient was seen near bottom in salinity profiles from locations spaced 20 cm apart down the slope.

As heavy fluid from the slope flow collected in the bottom, a wedge of fluid formed at the deep end in which few convective motions were seen to penetrate in the shadowgraph images. A profile taken at port #7 in experiment #7, when this wedge was about 3 cm thick (figure F-25), shows the stable stratification of fluid at the deep end of the tank. Salinity profiles from data taken in the edge between tank and tray (figure 2-12) also was stably stratified: the return flow, rising from the tank, brought up fluid of increasing salinity from the mixed layer.
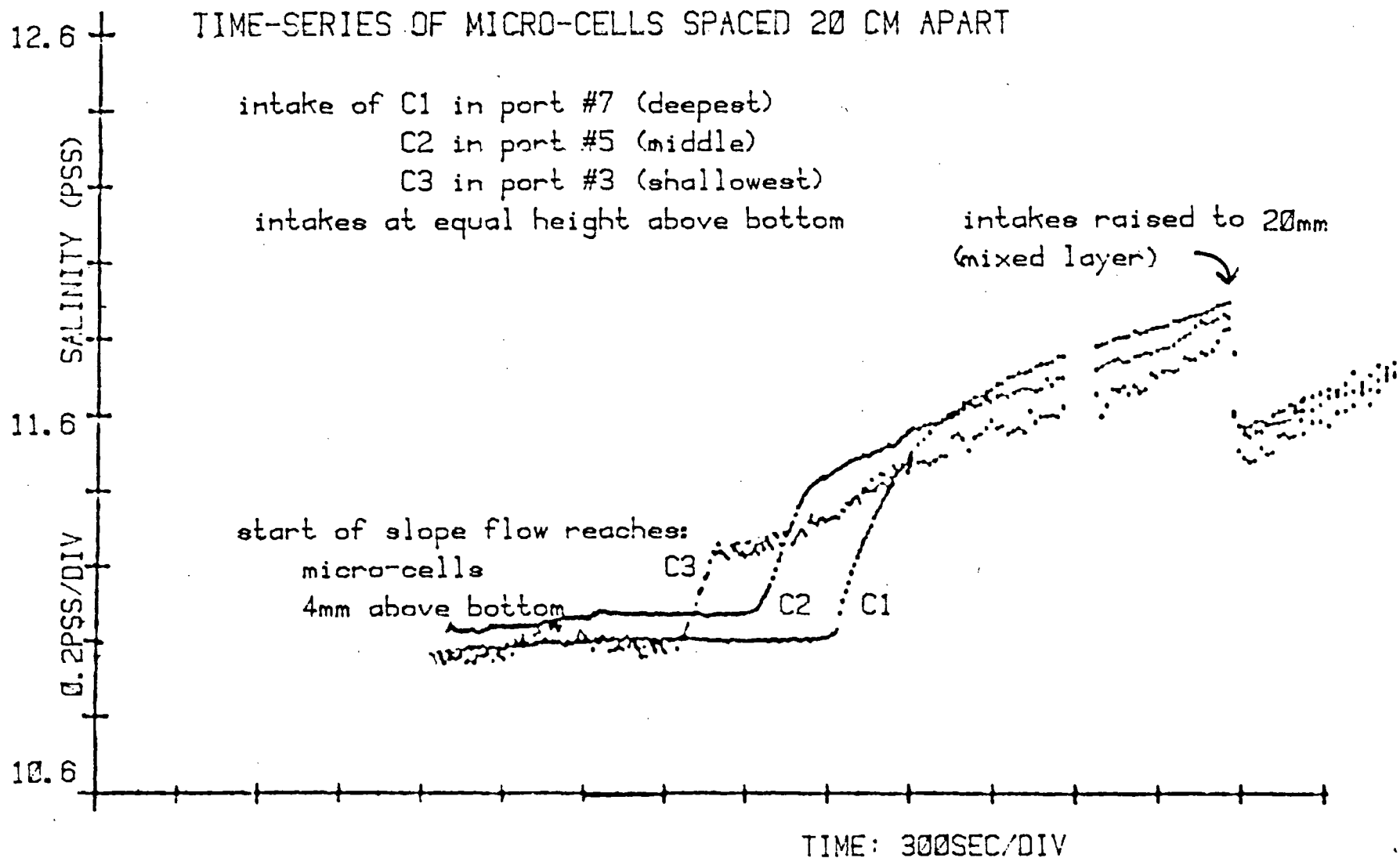
Figure 3-6. Salinity rate of change in mixed layer and bottom flow.

A sequence of micro-cell data taken during experiment #1 near the bottom and 6 mm below the tray in successive sampling ports did not show enough detail to see a distinct distribution in the salinity along the slope or under the tray (figure F-5), but data taken during experiment #4 show a higher salinity over the upper part of the slope, and at the deep end (figure F-17).

## 3.5 Salt fluxes and flow velocities

The time after start, the raw data from thermistors and micro-cells and the calculated values of temperatures, conductivity ratios, salinities and densities (sigma-t) for each set of observations were listed on the line printer. These salinities were plotted as a time-series during each experiment to monitor the overall behaviour of the system.

The salt flux slowly decreased during each experiment as the influx of salt into the tank reduced the difference in salinity between tank and tray fluids. For the times in an experiment at which slope flow velocities were determined, the salt flux was calculated from the time-series data of salinity in the tray and in the mixed layer in the tank, as outlined in section 2.6. The calculated results were tabulated for each experiment and included with the time-series plots and salinity profiles in the description of the individual experiments in appendix F.

Table 3.2 below lists the compiled values from the slope flow experiments of slope angle $\theta$, time t after starting the experiment, slope flow velocity maxima $V_{max}$ measured from photo or slide sequences or from video footage of injected dye, computed

57

salt fluxes for times at which the velocity was determined, slope flow depth h and rise in salinity dS above that in the mixed layer (from profiles), and computed entrainment without (E1) and with (E2) bottom drag Cd (see section 3.6) where:

$$Cd = 4.2e-2/(h.Vmax) \qquad E1 = h.g'sin\theta/V^2 \qquad and \qquad E2 = E1 - Cd$$

Table 3.2 Compiled results of slope flow experiments

| slope # | θ | t (min) | Vmax (cm/s) | saltflx (gr/cm²/s *e-5) | flow depth (mm) | Salinity (PSS) | dS | drag Cd | Entrainment E1 | E2 |
|---|---|---|---|---|---|---|---|---|---|---|
| 1 | 3.3 | 25 | 0.51 | 1.780 | 14-17 | 20.54 | 0.68 | 0.053 | 0.217 | 0.163 |
| | | 30 | 0.46 | 1.694 | | | | | | |
| 2 | 3.8 | 55 | 0.42 | 1.820 | 9-9.5 | 15.69 | 0.57 | 0.108 | 0.183 | 0.075 |
| | | 125 | 0.34 | 1.080 | 9-11 | 25.01 | 0.40 | 0.124 | 0.211 | 0.087 |
| 3 | 2.2 | 60 | 0.26 | 1.418 | 8.5-9 | 21.56 | 0.86 | 0.185 | 0.393 | 0.208 |
| | | 135 | 0.23 | 0.946 | | | | | | |
| 4 | 5.2 | 20 | 0.47 | 0.498 | | | | | | |
| | | 50 | 0.47 | 0.436 | | | | | | |
| | | 102 | 0.40 | 0.373 | 16 | 12.72 | 0.25 | 0.066 | 0.209 | 0.144 |
| | | 138 | 0.35 | 0.332 | | | | | | |
| 5 | 5.2 | 71 | 0.57 | 0.310 | 11-13 | 15.84 | 0.26 | 0.061 | 0.080 | 0.019 |
| | | 200 | 0.28 | 0.167 | | | | | | |
| | | 261 | 0.28 | 0.155 | 7-8 | 26.41 | 0.24 | 0.200 | 0.191 | -0.009 |
| | | 282 | 0.26 | 0.151 | | | | | | |
| 6 | 2.3 | 138 | 0.12 | 0.0897 | | | | | | |
| | | 145 | 0.12 | 0.0796 | | | | | | |
| | | 216 | 0.10 | 0.0673 | | | | | | |
| 7 | 5.5 | 134 | 0.10 | 0.077 | 8-9.4 | 16.87 | 0.24 | 0.483 | 1.844 | 1.361 |
| 8 | 5.1 | | | | 13-17 | 13.10 | 0.34 | | | |

The tabulated velocities have been plotted against both the corresponding angles and salt fluxes to check the dependence of the slope flow velocities on the magnitude of the salt fluxes (figure 3-7) and on the bottom slope angles (figure 3-8). Vertical bars were used in the plots to indicate the range in the measured velocities. The relation between velocity and slope angle is not distinct for the range of angles used in the experiments, but the relation describing the visible rise in slope flow velocity at increasing salt fluxes is further explored in the next section.

The slope flow depths, estimated from the salinity profiles, ranged from 7 to 17 mm. There was no sharp interface between the flow and the convectively mixed layer: in the most detailed profiles the upper part of the bottom flow, where shear and penetrative convection dominate, shows a weak density gradient. The lower part of the slope flow is strongly stratified and dye 'tongues' associated with velocity maxima are carried along with little dispersion. The level of turbulence here is greatly reduced from that in the upper part of the slope flow and in the mixed region, where dye is more rapidly diffused.

Figure 3-7. Slope flow velocity vs. salt flux.

60

numbers are salt fluxes (*e-5)
 bars indicate range in velocities

12. 67

17. 80

16. 94

18. 20

21. 89
18. 72
15. 59

13. 64

10. 80

6. 23
5. 67
5. 51

14. 18
9. 46

1. 95
1. 63

1. 71

0. 70

0. 35

0. 00

velocity (cm/s)

0            2            4            6

Slope angle (degrees)
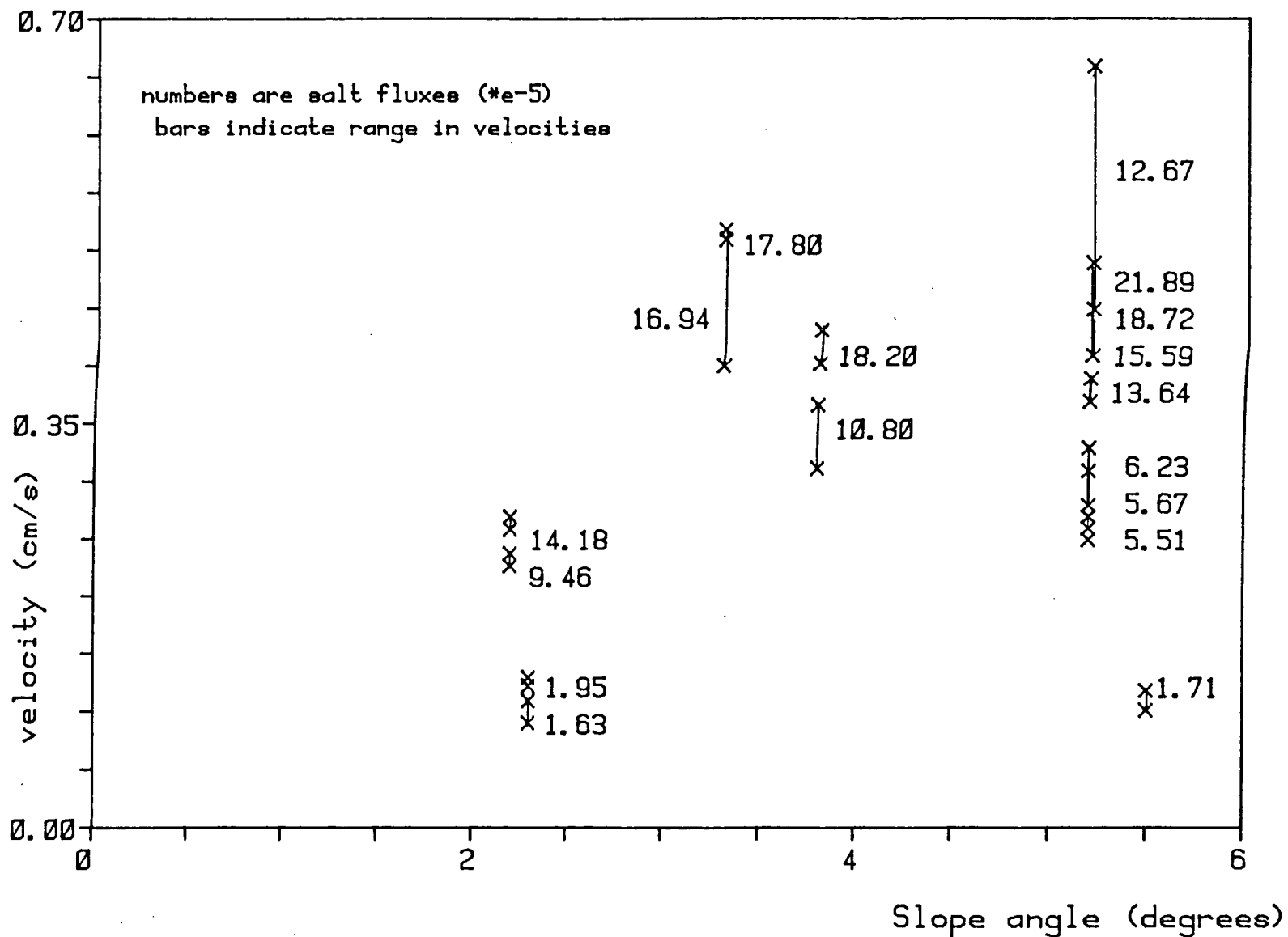
Figure 3-8. Flow velocity vs. slope angle

## 3.6 Interpretation

Density currents and penetrative convection have been studied separately in geophysical fluid flows and in the laboratory by many researchers. In this series of laboratory experiments the two mechanisms are simultaneously involved: the surface salt flux induces a slope flow, which is driven by the component of (reduced) gravity along the slope. The flow is slowed down by friction at the bottom and by shear at the interface which is modified by convective turbulence in the overlying environment. The flow reaches a steady state when the gravitational force is balanced by the friction at the bottom and at the interface:

$$h.g'\sin\theta = \frac{(t_i + t_w)}{Ds} = K.V^2 \qquad (3.1)$$

in which g' is the reduced gravity: $g' = g.\dfrac{Ds-Do}{Dref}$    (3.2)

h = depth of the flow

Ds = density in slope flow

Do = density of environment

g = gravity acceleration

θ = slope angle

$t_i$ = friction at interface

$t_w$ = friction at bottom

K = drag factor

V = averaged flow speed

Ve = entrainment velocity
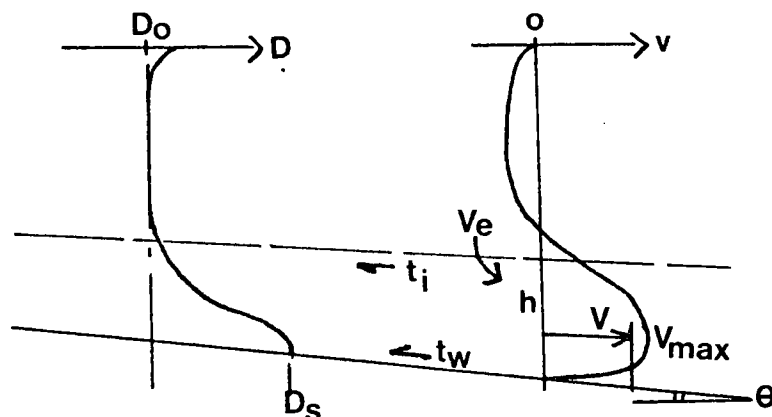


Figure 3-9. Slope flow diagram

Conventional turbulent density plumes have been characterized by an overall Richardson number Ri (Kantha, 1975) which is the inverse of the square of the densimetric Froude number Fr (Bo Pedersen, 1980):

$$Ri = \frac{1}{Fr^2} = \frac{h.g'\cos\theta}{V^2} \qquad (3.3)$$

Such gravity currents grow in depth with distance downstream as fluid from a quiescent environment is 'entrained' into the turbulent flow. This inflow is characterized by an entrainment velocity Ve. The linear spread with distance of free plumes led to the assumption by Morton, Taylor and Turner (1956) that Ve is proportional to the mean flow velocity V. The ratio (Ve/V) is the entrainment factor E. Gravity currents attain a constant mean velocity V and spread linearly with distance along the slope. Ellison and Turner (1959) modified the assumption for gravity currents to include a Richardson dependence of the entrainment factor, and described gravity driven turbulent slope currents in terms of variables integrated over the depth of the flow, specified by flow depth h and mean velocity V which are only dependent on downslope distance x and by the buoyancy flux A= h.V.g'. No assumptions were made about the distribution of properties in a cross section of the flow. The conservation equations could then be reduced to:

mass $\qquad \frac{d(h.V)}{dx} = E.V \qquad (3.4)$

momentum $\qquad \frac{d(h.V^2)}{dx} = h.g'\sin\theta - C_d.V^2 \qquad (3.5)$

buoyancy $\qquad \frac{d(h.V.g')}{dx} = -h.V.N^2(x) \qquad (3.6)$

in which Cd is the coefficient of bottom friction (drag),

$N = (- \frac{g}{@o} . \frac{d@}{dz})^{1/2}$ is the local buoyancy frequency and

@o is the reference density.

In these derivations it was assumed that the Reynolds numbers were high enough that any molecular effects could be ignored. The density differences were considered small enough to neglect inertia terms in the equations of motion (Boussinesq approximation), in which case the entrainment factor (E) only depends on the Richardson number. Algebraic manipulation of equation 3.5 and substitution of eqations 3.4 and 3.3 yields:

$$\frac{d(h.V^2)}{dx} = V. \frac{d(h.V)}{dx} + h.V. \frac{dV}{dx} = E.V^2 = h.g'sin\theta - Cd.V^2$$

or:   $E = \frac{h.g'sin\theta}{V^2} - Cd = Ri.tan\theta - Cd$   (3.7)

For slope currents dominated by turbulent entrainment at the interface, the bottom friction can be ignored and equation 3.7 is reduced to a simple relation:

$$E(Ri) = Ri.tan\theta \qquad (3.8)$$

In the present experiments with low levels of turbulence in the lower part of the observed flows, the bottom friction was estimated from:

$$\tau w = \mu. \frac{dU}{dy} = Cd.@.U^2 \qquad (3.9)$$

in which $\mu/@ = \nu$ is the kinematic viscosity, about 1.4e-2 cm²/s and a first order approximation for dU/dy is the ratio of Vmax to height y of the maximum velocity above the bottom (about 1/3 of the flow depth, based on shadowgraph and dye observations), and thus:

$$Cd = \nu. \frac{1}{y.V} = \frac{4.2e-2}{h.V} \qquad (3.10)$$

The depth averaged velocity V, used in the computation of the entrainment factors, was estimated from velocity profiles for slope flows shown by Löfquist (1960):

$$V = Vmax/1.12 \quad (3.11)$$

Field and laboratory data compiled by Bo Pedersen (1980) from the literature and from his own work indicate that the entrainment factor for sub-critical flows can be approximated by:

$$E = Ve/V = 0.072 \sin\theta \qquad (3.12)$$

The predicted values for entrainment in a quiescent environment from equation 3.12 would range from 2.76e-3 to 6.9e-3 for slope angles between 2.2° and 5.5° used in the present experiments. The entrainment factors calculated from data of the slope flow experiments using equations 3.7 and 3.10 above (table 3.2) were 0.08 to 1.84 without bottom friction (E1). While including the bottom friction (Cd) reduced these values (E2), in nearly every case the computed entrainment factor exceeded that predicted for the quiescent environment by up to two orders of magnitude.

The formulation which describes gravity flows was used here to compare entrainment factors between flows in turbulent and in quiescent environments. The large values for calculated entrainment would indicate that the bottom flows would rapidly loose their density difference. This contradicts the present experimental findings as well as Arctic field data which show that such slope flows maintain their characteristics over great distances, and suggests that a different model is required to account for the interaction between the turbulence and shear.

The intensity of turbulent motions seen in the shadowgraph image appears much higher in the mixed layer than in the bottom slope, which could lead to net entrainment of mass and momentum upward out of the flow. The Richardson numbers calculated from data in table 3.2 using equation 3.3 range from 2.10 to 19.5 and would cause considerable damping of the turbulence at the interface.

In a two-layer system, the velocity and density profiles are idealized by a discrete step at the interface between the slope flow and the environment. In profiles from experimental data the density changed slowly with the depth in the slope flow and the velocity profile extended upward into the mixed layer fluid since some of it is strained along by the friction.

With the instrumentation developed for these experiments more details of the growth or decay of such slope currents might be obtained if a longer slope was used. The change in the shape of salinity profiles taken at different locations along the slope shows the distribution of mass within the slope flow, and can be used to assess the down-slope change in mass when integrated over the depth.

In a series of laboratory experiments, the salt flux due to the freezing of sea water was simulated by a percolation of sea water through a porous membrane into a plexiglass tank below. A two-dimensional bottom slope flow was induced by the convection when the bottom of the tank was set at a small angle.

Low values of salt fluxes, controlled by selected starting conditions, were calibrated from density differences across the membrane. In several interface entrainment experiments with two-layer and linear stratifications, this system confirmed that the constant entrainment efficiency for free penetrative convection as predicted by Bo Pedersen could be extended for these low salt fluxes.

The interface entrainment assumptions were applied to a set of Arctic field data. The small values of computed entrainment did not agree closely with the predicted values, which may be due in part to salt advected into the bay by the reverse estuarine circulation caused by slope flow in the perimeter regions.

Shadowgraph images of the fluid in the experimental tank did show patterns of convective motions in the mixed layer, which were carried along and smoothed out by a bottom slope flow. A weaker flow in the opposite direction was seen superimposed on the convective pattern. Velocity maxima in the slope flow of 0.09 to 0.66 cm/s were measured from the progress of tongue

67

features in injected dye, recorded in sequences of color slides and photographs and on videotape footage.

Salinity profiles of fluid in the mixed layer and in the slope flow were plotted from data obtained from thermistors and from conductivity micro-cells developed for this purpose. These micro-cells have a resolution in calculated salinity of better than 0.05 ppt, require about 4 ml to flush and maintained stable readings over extended periods of use.

The salinity profiles show a region well mixed by convective turbulence, and a rise in salinity in the slope flow of 0.24 to 0.92 ppt above the mixed layer value, for flow depths of 7 to 17 mm and calculated salt fluxes between 1.82e-5 and 1.63e-6 g/cm²/s. The spatial resolution achieved with the micro-cells allows a more detailed look at the density distribution within a slope flow, and with a longer slope it may be possible to model the down-slope behaviour of these bottom currents.

The depth of the slope flow, the density difference between the flow and the mixed layer determined from the profiles, and the velocity maxima measured in the flow, were applied to the model for predicting entrainment of fluid from a quiescent environment by a turbulent gravity current. Entrainment factors computed by inserting data from the slope flow experiments were several orders of magnitude larger than the predicted values for the quiescent environment.

The conclusions from these experiments are:

- Low calibrated salt fluxes to simulate salt expulsion due to freezing were achieved by percolating sea water through a porous membrane. The magnitude was controlled by selecting starting depths and density differences.

- Entrainment experiments across a density interface without shear confirmed that the constant entrainment efficiency predicted by Bo Pedersen applied to these low salt fluxes.

- A surface salt flux over a sloping bottom always produced a slope flow.

- Maxima in the slope flow velocity show an increase for higher salt fluxes (figure 3-5), but for bottom slopes of 2.2° to 5.5° in the experiments, there was no distinct relation between flow velocity and slope angle (figure 3-6).

- High resolution salinity profiles were obtained from data from small-volume conductivity micro-cells, developed for these experiments and used with micro-bead thermistors.

- Entrainment factors calculated by inserting data from the slope flow experiments into a model for turbulent gravity flows were several orders of magnitude larger than those predicted for a quiescent environment, contrary to visual evidence from the experiments or from Arctic field data, which show that such flows under a turbulent environment maintain their characteristics over great distances. This suggests that a different model is required to describe the interaction between the slope flow and the turbulent environment.

69

Benjamin, T.B. 1968. Gravity currents and related phenomena.
    J.Fluid Mech. 31, 209-248


Bo Pedersen, F. 1980. A monograph on turbulent entrainment and
    friction in two-layer stratified flow.  Paper 25,
    Inst.of Hydrodyn., Techn. Univ.of Denmark, 397 pp.


Bo Pedersen, F. and C. Jurgensen, 1984. Laboratory experiments
    on entrainment due to free convection. Prog.Rep.61
    Inst.of Hydrodyn., Techn.Univ.of Denmark, pp.47-54


Deardorff J.W., G.E. Willis and D.K. Lilly, 1969. Laboratory
    investigation of non-steady penetrative convection
    J.Fluid Mech. 35, 7-31


Deardorff J.W. 1980. Progress in understanding entrainment at
    the top of a mixed layer. Am.Meteorol.Soc. 1978
    Workshop on the Planetary Boundary Layer. pp.33-66


Deardorff J.W., G.E. Willis and B.H. Stockton 1980. Laboratory
    studies of the entrainment zone of a convectively
    mixed layer. J.Fluid Mech. 100, 41-64


Elliott, J.A. 1972. Convective motions under sea ice. Frozen
    Seas Research Group, Inst.of Ocean Sci.
    Sidney, B.C. Unpublished, 17 pp.


Ellison, T.H. and Turner, J.S. 1959. Turbulent entrainment in
    stratified flows. J.Fluid Mech. 6, 423-448


Fofonoff, N.P. and R.C. Millard Jr., 1983. Algorithms for com-
    putation of fundamental properties of seawater.
    Unesco Techn. Papers in Marine Sci. 44, 53 pp.


Foster, T.D. 1969. Experiments on haline convection induced by
    the freezing of seawater. J.Geop.Res. 74,6967-6974


Gade, H.G., R.A. Lake, E.L. Lewis and E.R. Walker, 1974
    Oceanography of an Arctic Bay.
    Deep-Sea Res. 21, 547-571

Heidt, F.D. 1977. The growth of the mixed layer in a stratified
        fluid due to penetrative convection.
        Bdy.Layer Met. 12, 439-461


Kato, H. and O.M. Phillips, 1969. On the penetration of a
        turbulent layer into a stratified fluid.
        J.Fluid Mech. 37, 643-655


Kantha L.H. 1975. Turbulent entrainment at the density interface
        of a two-layer stably stratified fluid system.
        Techn.Report 75-1, Johns Hopkins Univ. 162pp.


Kullenberg, G. 1977. Entrainment velocity in natural stratified
        shear flow. Estu.& Coast.Mar.Sci. 5, 329-338


Lake, R.A. and E.L. Lewis 1970. Salt rejection by sea ice
        during growth. J.Geophys.Res. 75, 583-597


Linden, P.F. 1975. The deepening of a mixed layer in a
        stratified fluid. J.Fluid Mech. 71, 385-405


Löfquist, K. 1960. Flow and stress near an interface between
        stratified liquids. Phys.of Fluids 3, 158-175


Long, R.R. 1975. The influence of shear on mixing across
        density interfaces. J.Fluid Mech. 70, 305-329


Meagher, T.B. A.M. Pederson and M.C. Gregg, 1982. A low-noise
        conductivity micro-structure instrument.
        IEEE J.of Ocean.Eng, pp.283-290


Melling, H. and. E.L. Lewis 1982. Shelf drainage flows in the
        Beaufort Sea and their effect on the Arctic
        Ocean pycnocline. Deep-Sea Res. 29, 967-985


Millero, F.J., C.T. Chen, A. Bradshaw and K.Schleicher, 1980.
        A new high-pressure equation of state for seawater.
        Deep-Sea Res. 27A, 255-264


Moore, M.J. and R.R. Long 1971. An experimental investigation
        of turbulent stratified shearing flow.
        J.Fluid Mech. 49, 635-655

Mowbray, D.E. 1967. The use of schlieren and shadowgraph tech-
niques in the study of flow patterns in density
stratified fluids. J.Fluid Mech. **27**, 595-608


Perkin, R.G. and E.L. Lewis 1978. Mixing in an Arctic Fjord.
J.Phys.Ocean. **8**, 873-880


Perkin, R.G. and E.L. Lewis 1978. Salinity: Its definition and
calculation. J.Geop.Res. **83**, 466-478


Perkin, R.G. and E.L. Lewis 1980. The Practical Salinity Scale
1978:Fitting the Data.
IEEE J.of Oceanic Eng. **OE-5**, 9-16


Phillips, O.M. 1972. The entrainment interface.
J.Fluid Mech. **51**, 97-118


Thorpe, S.A. 1973. Turbulence in stratified fluids: a review of
laboratory experiments. Bdy.Layer Met. **4**, 95-119


Turner, J.S. 1968. The influence of molecular diffusivity on
turbulent entrainment across a density interface.
J.Fluid Mech. **33**, 639-656


Turner, J.S. 1973. "Buoyancy effects in fluids"
Cambridge University Press, 367 pp.


Turner, J.S. 1980. "Small scale mixing. In "Evolution of
Physical Oceanography". edited by B.A. Warren
& C. Wunsch, MIT Press, Cambridge. pp.236-262


Walin, G. 1971. Contained non-homogeneous flow under gravity
or how to stratify a fluid in the lab.
J.Fluid Mech. **48**, 647-672


Wyatt, L.R. 1978. The entrainment interface in a stratified
fluid. J.Fluid Mech. **86**, 293-311

SALINITY AND DENSITY COMPUTATION

## A.1 Salinity

The salinity of fluids used in the convection experiments is calculated from electrical conductivity, pressure and temperature using a standard set of polynomials known as the Practical Salinity Scale (Lewis and Perkin, 1980).

If R is the conductivity ratio of the fluid (i.e. the ratio of the conductance at temperature T and pressure P to that at atmospheric pressure and 15 °C) then the salinity S in units of the Practical Salinity Scale is calculated from:

$$Q = 1+P(A1+P(A2+P*A3))/(1+T(B1+T*B2)+R(B3+T*B4))$$

$$U = C0+T(C1+T(C2+T(C3+T*C4)))          W = R/(Q*U)$$

$$Y =W^{1/2}        F=(T-15)/(1+.0162(T-15))$$

$$S=E0+F*F0+Y(E1+F*F1+Y(E2+F*F2+Y(E3+F*F3+Y(E4+F*F4+Y(E5+F*F5)))))$$

in which P is the pressure in bars, T the temperature in °C, S is the salinity in PSS (units are close to the formerly used grams/kilogram or parts-per-thousand), Q, U, W, Y, F are intermediate results, and Ai through Fi are constants with values:

| | | | |
|---|---|---|---|
| A1=2.070e-5 | C0=0.6766097 | E0=0.0080 | F0=0.0005 |
| A2=0.637e-9 | C1=0.0200564 | E1=-0.1692 | F1=-0.0056 |
| A3=3.989e-15 | C2=1.104259e-4 | E2=25.3851 | F2=-0.0066 |
| B1=0.03426 | C3=-6.9698e-7 | E3=14.0941 | F3=-0.0375 |
| B2=4.464e-4 | C4=1.0031e-9 | E4=-7.0261 | F4=0.0636 |
| B3=0.4215 | | E5=2.7081 | F5=-0.0144 |
| B4=-0.003107 | | | |

For laboratory experiments these calculations are simplified since P=0 at atmospheric pressure.

These polynomials are defined for a range of salinities from 2 to 42 parts-per-thousand. Although PSS units are not defined outside this range, a graph of the conductivity ratio over an extended range of salinity and for laboratory temperatures from 17 to 25 °C shows that these polynomials smoothly extend to higher values of S (see figure A-1).

To create higher salt fluxes, pure sea salt was added to sea water. Salinity values of this fluid, obtained with an optical refractometer, from the Guildline Autosal after a 2-to-1 volume dilution and doubling the result, and from the output of the calibrated micro-cell were found to agree within several ppt, indicating that values computed from the above formulas for the Practical Salinity Scale may be used with caution as reasonable estimates.

## A.2 Density

The Unesco Equation of State for sea water (Millero, 1980) is used to calculate fluid densities D in g/cm³ or in units of sigma-t =(D-1)*1000 from salinity S (PSS), temperature T (°C) and pressure P (bars) from the following set of polynomials:

A= 8.50935e-5+T(-6.12293e-6+T*5.2787e-8)

B= 3.239908+T(1.43713e-3+T(1.16092e-4-T*5.77905e-7))

C=19652.21+T(148.4206+T(-2.327105+T(1.360477e-2-T*5.155288e-5)))

E= A+S(-9.9348e-7+T(2.0816e-8+T*9.1697e-10))

F= B+S(2.2838e-3+T(-1.0981e-5-T*1.6078e-6))+S³ᐟ²*1.91075e-4

G= C+S(54.6746+T(-0.603459+T(0.0109987-T*6.167e-5)))

H= G+S³ᐟ²(0.07944+T(0.016483-T*5.3009e-4))+P(F+P*E)

J=999.842594+T(0.06793952+T(-9.09*29e-3+T*1.001685e-4))

K= J+T*(-1.120083e-6+T*6.536332e-9)

L=0.824493+T(-4.0899e-3+T(7.6438e-5+T(-8.2467e-7+T*5.3875e-9)))

M=-5.72466e-3+T(1.0227e-4-T*1.6546e-6)

N= J+S*K+S³ᐟ²*M+S²*4.8314e-4

D= N/1000/(1-P/H) = density in gr/cm³

Similar to the polynomials of the Practical Salinity Scale, these are valid for salinities ranging from 0 to 42 PSS. They also simplify since P=0 for laboratory (atmospheric pressure).

The relation between salinity and density, plotted from the above polynomials, is nearly linear over the extended range of salinities for the temperatures used in laboratory experiments (see figure A-2). Densities so determined were used to compute estimates of the membrane salt flux during the experiments.

Figure A-1. CONDUCTIVITY RATIO vs SALINITY
for laboratory temperatures
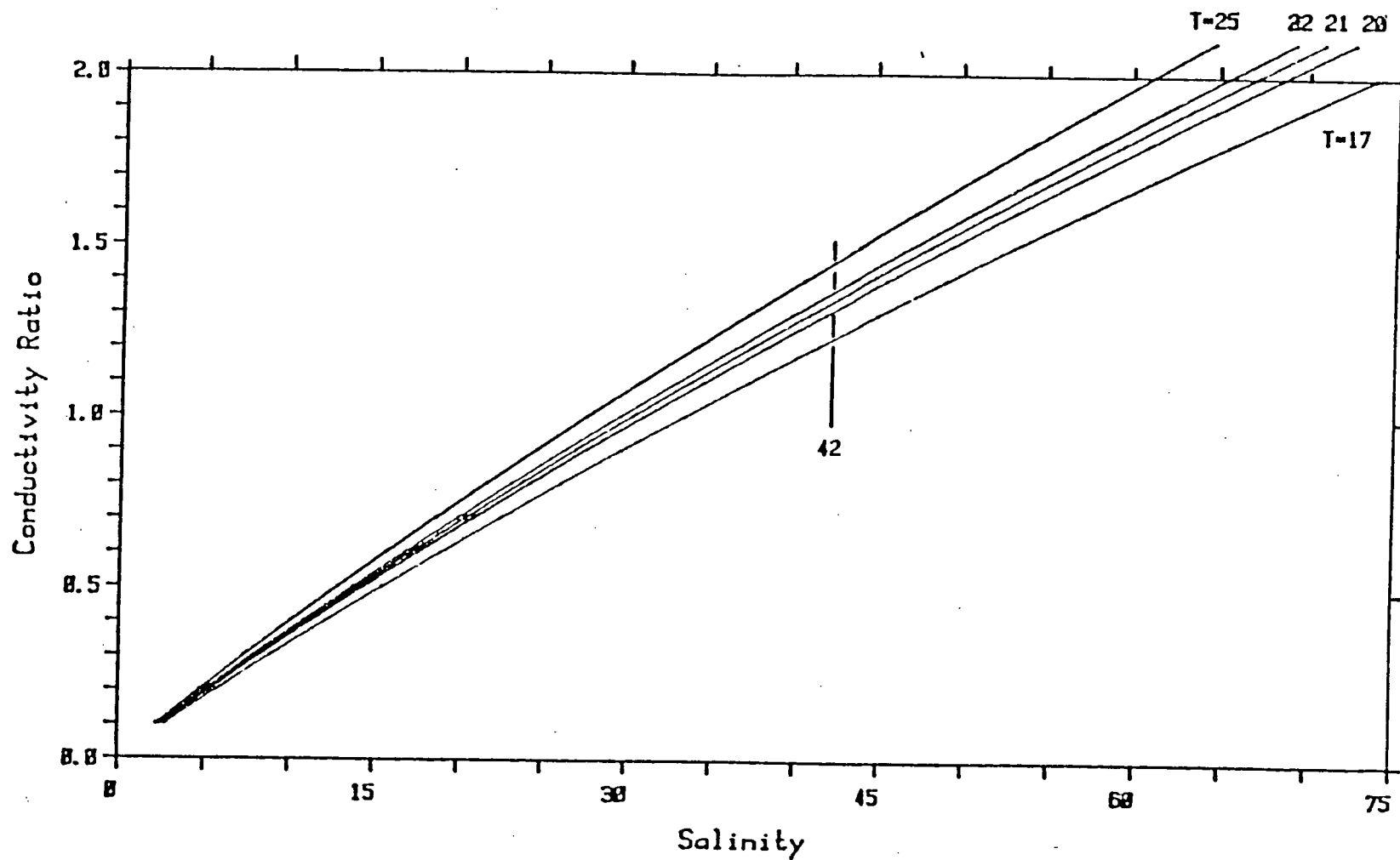
Figure A-2.  DENSITY vs SALINITY
for lab temperatures
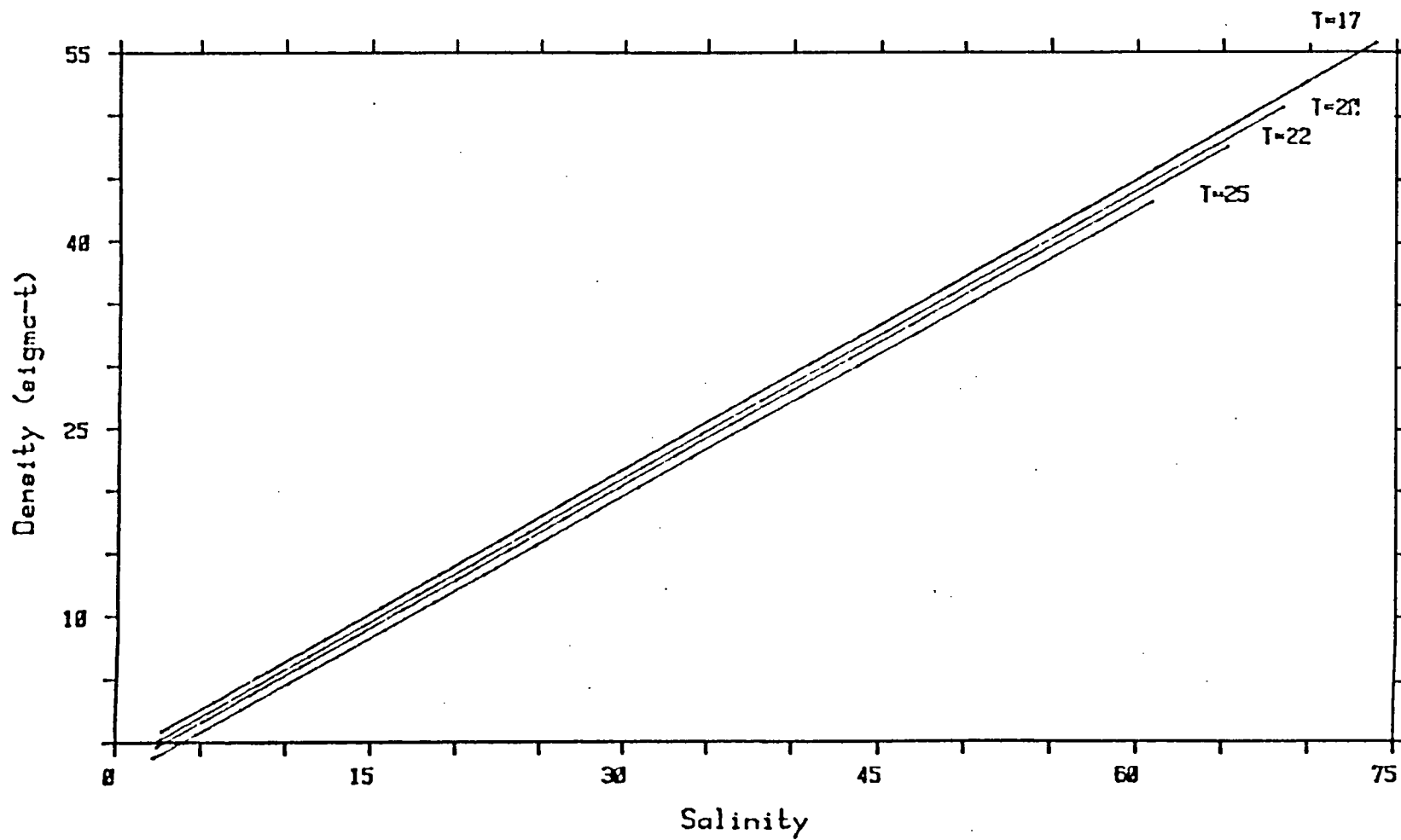
CONDUCTIVITY MICRO-CELLS

A set of small volume four-electrode conductivity cells was developed to determine the salinity of fluid in an experimental tank. As fluid is syphoned through one of these micro-cells, at a flow rate of about 2 drops/sec (0.15 ml/s), the electrical conductance inside the cell changes with the salinity of the fluid. A small electronic circuit converts this conductance into an output voltage, which was calibrated to yield the conductivity ratio of the fluid.

Thermistors were added at the inlet and outlet of the micro-cell, and the salinity of fluid in the micro-cell is calculated from the conductivity ratio and the average temperature of the thermistors, using the polynomials of the Practical Salinity Scale (see appendix A.1). The fluid density at the intake point in the tank is computed from this salinity and the temperature from another thermistor located in the tank, using the Unesco Equation of State for Sea Water (appendix A.2).

## B.1 Cell construction

The micro-cells, constructed by technical support staff at the Institute of Ocean Sciences, consist of four ring-shaped electrodes made of 0.002" thick platinum foil and separated by segments of 1.8 mm I.D. glass tubing of 0.6 mm wall thickness. Figure B-1 shows a diagram of the cell with the principal dimensions.

```
25
mm

10mm

18
mm

10mm

25
mm
```

GLASS TUBING SECTIONS
1.8mm I.D. - 3mm O.D.

COLOR CODED LEADS
FROM ELECTRODES

ORANGE

·RED

0.002" PLATINUM
FOIL ELECTRODES,
EACH 5mm WIDE

·BROWN

BLACK

PVC TUBING COVER
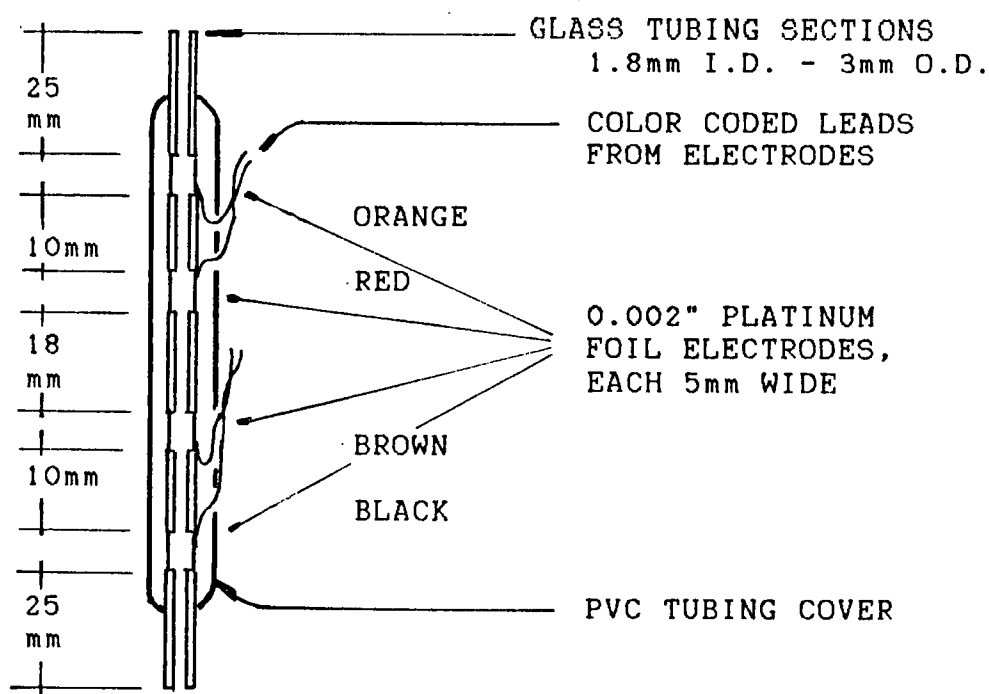
Figure B-1. Diagram of micro-cell assembly

The electrodes and glass spacers were held in place by sections of heat shrink tubing, and color coded electrical leads were soldered to the electrodes. The completed assembly was sealed with epoxy in a protective PVC sleeve. Three such micro-cells were made, using the same materials and physical dimensions.

## B.2 Micro-cell electronics

The four electrodes of the micro-cell were connected to an electronic circuit which converts the conductance (1/R) of the microcell into a linear function of the output voltage (VC).

Fluid samples of a known salinity, determined with a Guild-line Autosal bench salinometer, were used to obtain values for micro-cells calibration constants K, expressed in ohms of cell resistance at a salinity of 35 ppt and a temperature of 15 °C.

The conductivity ratio (RR) obtained from the micro-cell is the product of conductance and cell constant:

$$1/R = A + B.VC$$

1/R = cell conductance

VC = output voltage

or: $$RR = K.(A + B.VC)$$

RR = conductivity ratio

K = cell constant

and coefficients:

A = -2.6008e-8

B = -4.5954e-4

The coefficients A and B were determined with a high precision decade resistor box, and checked after about 6 months of use. There was no drift or temperature dependence found in the output voltage of the circuit. A least squares linear fit to the data was used to calculate A and B. The standard deviation was 2.2065e-4 with a correlation factor better than 0.9999 .


## B.3 AM/CT Datalogger conductivity electronics

The AM/CT Datalogger had a slightly different conductivity circuit. It was originally designed for cells with a constant of about 100 ohms but was modified for use with the micro-cells which have a much higher cell constant of about 1800 ohms. The relation between N-number and conductivity ratio is given by:

$$RR = K'.(A + B.NC)$$     with  NC = AM/CT datalogger output

K'= cell constant

and coefficients:  A = 5.53084e-5

B = 1.3290e-7

A number of trial runs were done to determine the stability and variability of measurements at several constant salinities. In several of the tests, the variability of the raw temperature data was less than $\pm$ 2 in the last digit ($\pm0.007$ °C), and for raw conductivity about $\pm$ 3 units (corresponding to $\pm0.025$ PSS).

As a larger range of conductivities was used with the three micro-cells, the variability in the output of the datalogger conductivity circuit increased. Several series of observations were taken over longer periods of time, using three micro-cells simultaneously. Deviations in the observations could be caused by sudden variations in the flow rate caused by small particles obstructing the flow. Filtering all fluids did not eliminate the problem. Small bubbles adhering to a micro-cell electrode could change the conductance in the cell.

The tests did show that any abrupt change in the flow causes an immediate change in the computed salinity which in about 5 to 20 seconds returns to the previous level. The computed value of salinity and the variability did not depend on the magnitude of the flow through the micro-cells. The use of a peristaltic pump to draw the fluid through the cells more than doubles the variability, possibly due to shocks which cause small particles or bubbles to disrupt the potential or the current pattern inside the cell.

## B.4 Determination of calibration constants

The micro-cells were calibrated by using fluid samples of known salinity. Cell constants were then chosen which yield a calculated salinity equal to that determined with a Guildline

Autosal bench salinometer. The fluid was syphoned through each micro-cell at several different steady flow rates counted to be between 1 and 4 drops per second (about 0.05 to 0.20 ml/s). An integer value was chosen for K to make the calculated S agree with the value determined using the Autosal.

These calibrations were repeated at several temperatures and salinities. The values of K were plotted against temperature at which they were calculated to check for temperature dependence (figure B-2). Shifts in conductivity were found to occur when the cell outlet tubing made electrical contact with the fluid which was pumped back to the tank instead of dripping to break the flow. An external current loop formed via the pump or one of the other cells and caused a change in apparent conductivity and thus in the cell constant. For cell #2, the data without an external loop had an average value for K of 1765 with a standard deviation of 1.89 , which changes the calculated salinity by 0.024 at a salinity of 20 PSS and a temperature of 20 °C.

Initially, the current electrodes were those closest to the centre of the cell, but exchanging the leads of potential and current electrodes reduced the variability in the calculated salinity from the Datalogger to nearly half the initial value. This exchange of electrodes changed the effective potential path inside the cell and caused a small change in the values of cell constants.

# MICRO-CELL CALIBRATION , CELL#2

## T = TEMP (°C)
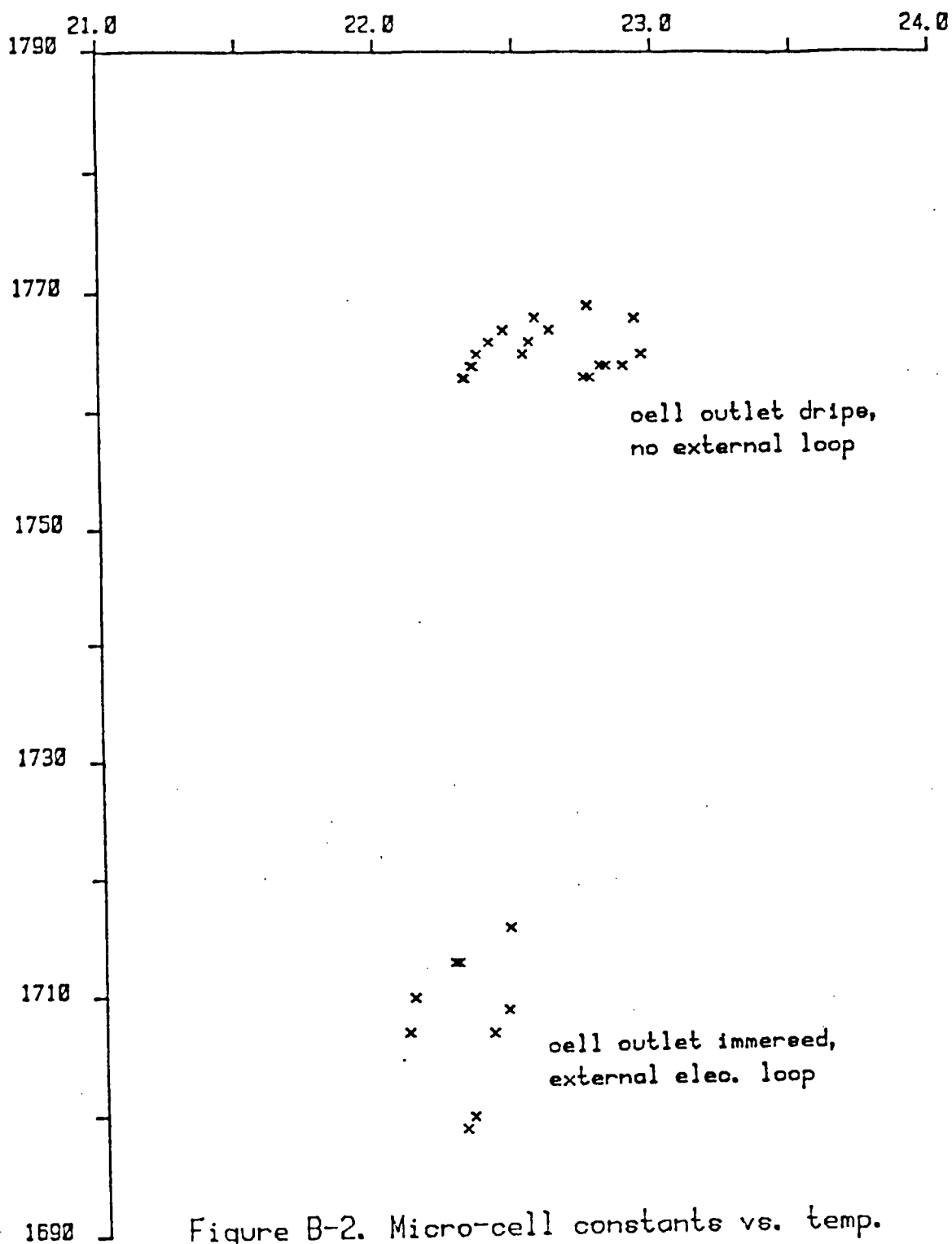


Figure B-2. Micro-cell constants vs. temp.

cell outlet drips,
no external loop

cell outlet immersed,
external elec. loop

Cells have been reported to 'age' in successive cycles of wetting and drying. This may alter the surface characteristics of the electrodes of the new cells, and cause some shift in K. No significant change was found in the constant of the first cell in more than a year. The conductance in the cell is strongly affected by minute particles or bubbles due to the small size of the cell. In some instances, using a well mixed fluid of constant salinity, the time-series plot of calculated values of S from the Datalogger output did show a drift down in salinity, followed by a jump back to the former constant value. This apparent drop in salinity could be caused by a decreasing contact surface at an electrode due to trapped and coalescing bubbles. Occasional light tapping on the cell may dislodge any particle or bubble trapped in the cell and restore the correct calibration value.

The AM/CT datalogger conductivity circuit used different current and voltage values for the cell electrodes, resulting in values for the cell constants K which differ significantly from those obtained with the small electronic circuits as was explained previously.

Calibration checks were frequently done for both systems to track the long term behaviour of the micro-cells. Print-outs of each date are included in this appendix and the averaged value of calibration constants for each cell are shown in table B.1 below. Each calibration constant listed below is an average of 4 to 8 observations.

### Table B.1 Micro-cell calibration constants

| Day # | Date | Sal. (PSS) | Temp. (°C) | datalogger K1 | K2 | K3 | small electr. K1 | K2 | K3 |
|---|---|---|---|---|---|---|---|---|---|
| 11 | 85-12-11 | 31.15 | 22.0 | 1879 | 1787 | 1815 | 1799 | 1749 | 1783 |
| 11 | 12-11 | | | 1878 | 1789 | 1815 | | | |
| 12 | 12-12 | 31.34 | 21.7 | 1882 | 1791 | 1816 | 1801 | 1753 | 1786 |
| 13 | 12-13 | 31.50 | 21.8 | 1885 | 1792 | 1818 | 1802 | 1753 | 1787 |
| 13 | 12-13 | 31.34 | 21.8 | 1876 | 1784 | 1811 | 1796 | 1746 | 1779 |
| 20 | 12-20 | 7.83 | 21.1 | 1886 | 1790 | 1823 | | | |
| 28 | 12-28 | 7.52 | 20.7 | 1891 | 1802 | 1831 | | | |
| 34 | 86-1-3 | 2.74 | 19.1 | 1897 | 1796 | 1826 | | | |
| 34 | 1-3 | 4.83 | 19.2 | 1897 | 1793 | (1837) | | | |
| 34 | 1-3 | 30.3 | 20.5 | 1888 | 1796 | 1826 | | | |
| 37 | 1-6 | 4.97 | 20.5 | 1885 | (1818) | 1832 | | | |
| 51 | 1-20 | 5.95 | 21.0 | 1878 | 1794 | 1832 | | | |
| 53 | 1-22 | 31.5 | 21.0 | | | | 1808 | 1754 | (1738) |
| 53 | 1-22 | 6.10 | 20.5 | | | | (1771) | (1717) | (1755) |
| 54 | 1-23 | 6.11 | 21.1 | | | | (1709) | 1748 | (1763) |
| 55 | 1-24 | 33.66 | 20.0 | | | | (1816 | 1758 | 1793 |
| 55 | 1-24 | 6.59 | 20.0 | | | | (1767) | (1711) | (1753) |
| 62 | 1-31 | 20.56 | 21.6 | 1884 | 1795 | 1822 | 1799 | 1750 | 1785 |
| 66 | 2-4 | 22.60 | 20.9 | | | | 1801 | 1748 | 1787 |
| 81 | 2-19 | 25.85 | 21.1 | 1884 | 1792 | 1816 | 1803 | 1752 | 1786 |
| 81 | 2-19 | 25.94 | 21.3 | | | | 1798 | 1752 | 1782 |
| 86 | 2-24 | 27.40 | 21.3 | | | | 1802 | 1751 | 1786 |
| 89 | 2-27 | 35.56 | 21.6 | | | | (1811) | 1758 | 1790 |
| 99 | 3-9 | 28.02 | 21.9 | 1877 | 1792 | 1814 | 1800 | 1751 | 1782 |
| 106 | 3-16 | 28.36 | 21.4 | (1845) | (1774) | -- | -- | -- | 1785 |
| 143 | 4-22 | 31.60 | 21.3 | 1888 | 1798 | 1825 | | | |
| 159 | 5-8 | 16.40 | 20.4 | 1892 | 1795 | 1817 | | | |
| 165 | 5-14 | 28.49 | 19.6 | 1884 | 1793 | 1818 | | | |
| 196 | 6-27 | 26.83 | 21.3 | 1885 | 1795 | 1821 | 1803 | 1746 | 1782 |

|  |  | Average cell constants: | 1885 | 1793 | 1821 | 1801 | 1752 | 1785 |
|  |  | with standard deviation: | 6.34 | 4.20 | 6.70 | 5.64 | 3.50 | 6.63 |

The constants in brackets differed substantially from the expected value and were not included in determining the average values and standard deviations. Some of these differences could be caused by contamination of the electrodes inside a cell by particles or bubbles. A time-series plot of the cell constant values (figure B-3) shows that any drift is much less than the

variability in the observations. The conductivity may affect the field distribution and current path in the cell and thus alter the cell constant. Some dependence is seen in a plot of cell constant versus salinity during calibration (figure B-4).
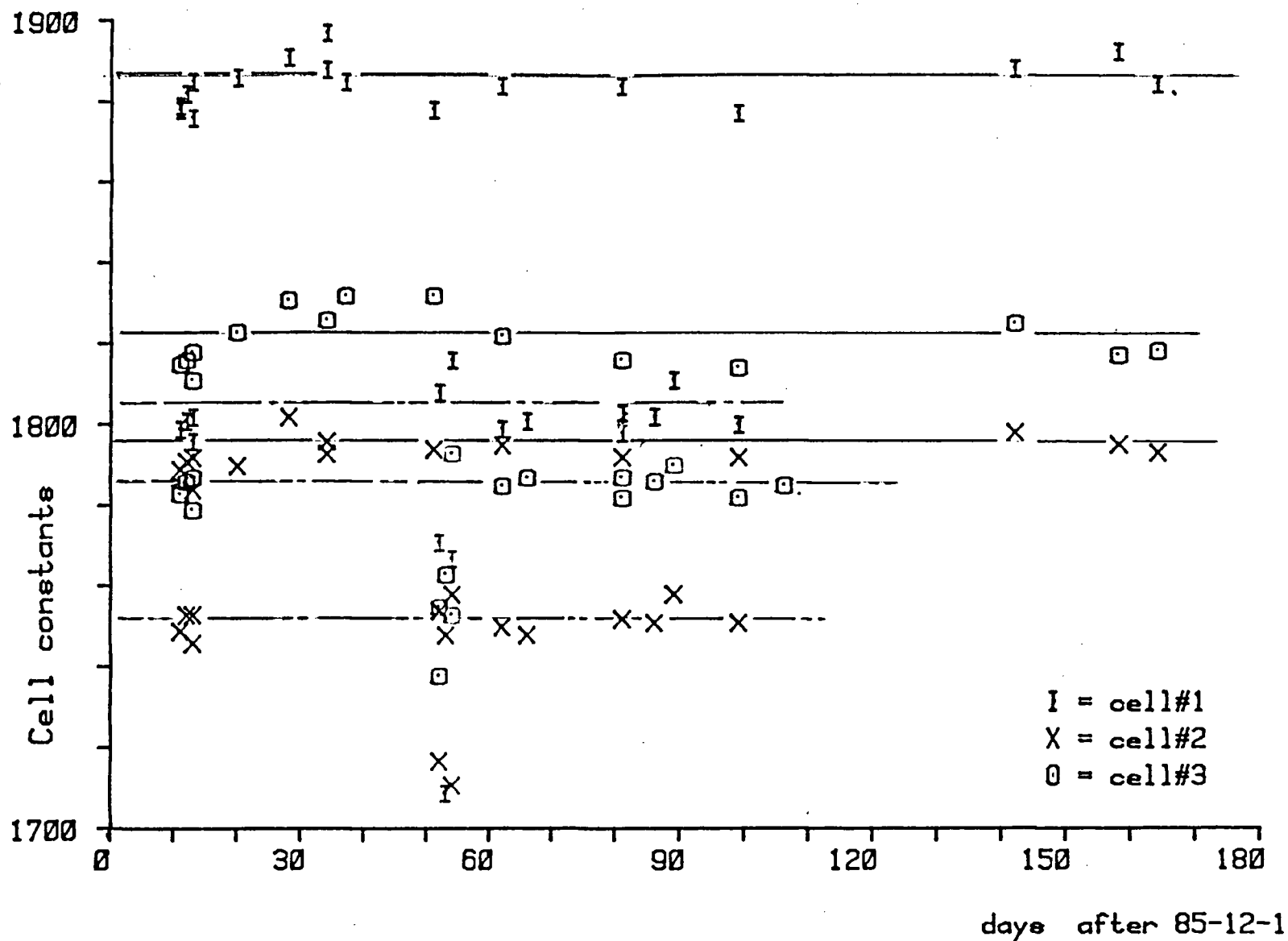
Figure B-3    Time-series of micro-cell calibration constants
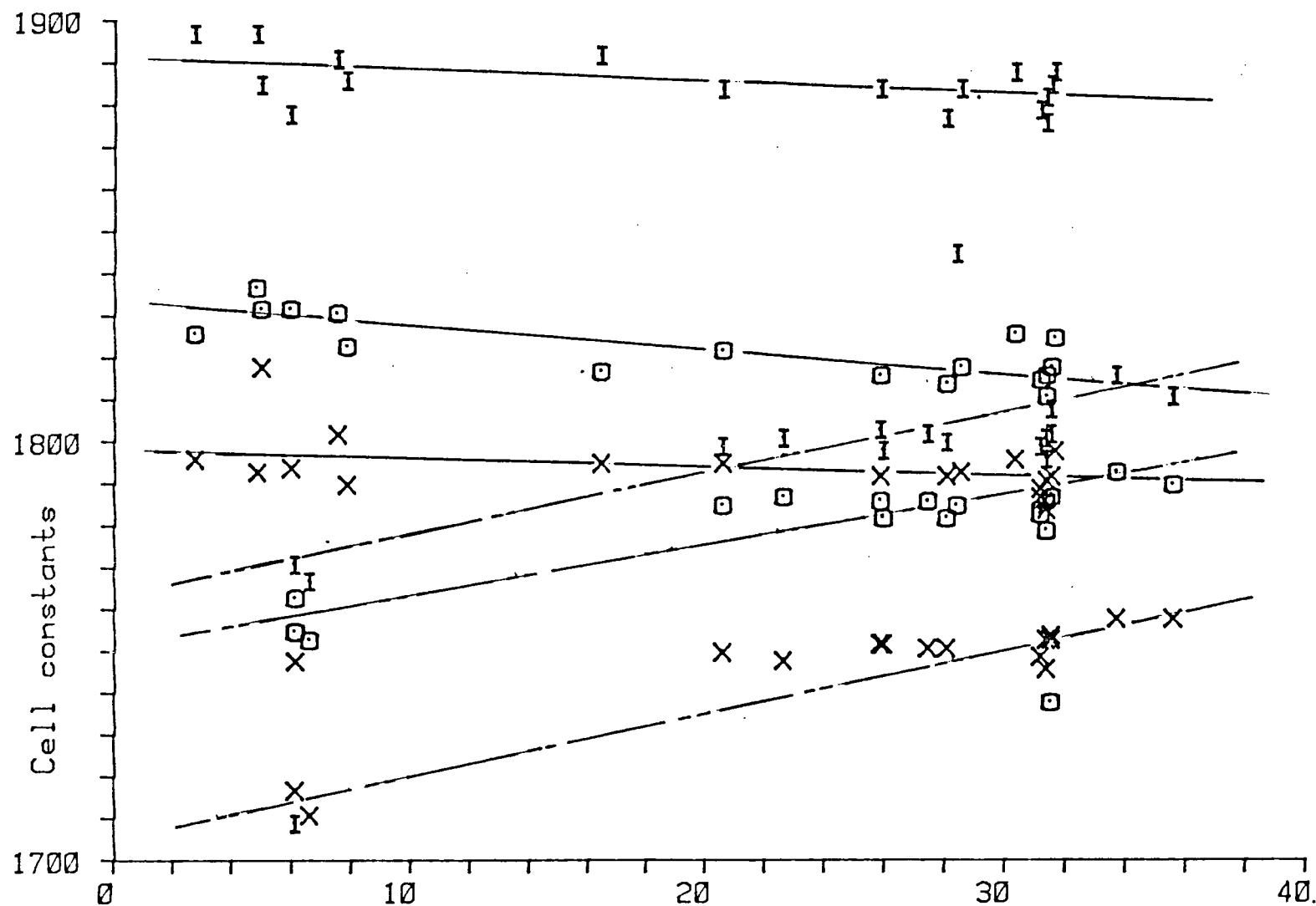
Figure B-4. Cell calibration constants vs. Salinity

90

## B.5 Micro-cell time response

The response of the cell to an abrupt change in salinity has been investigated to determine the volume required (or the time required at a selected flow rate) before the calculated salinity reaches the new value. After a step-change in the salinity at the intake point, the length of time for the cell to respond depends on the flushing characteristics of the cell. In initial attempts to determine the time response of the micro-cell with the AM/CT datalogger, the minimum sampling was about 4 seconds and the output showed excessive variability caused by problems with the A/D converter of the conductivity circuit. To get more accurate data and faster sampling, an HP-3497A Data Acquisition System was used. The arrangement is shown in figure B-5.
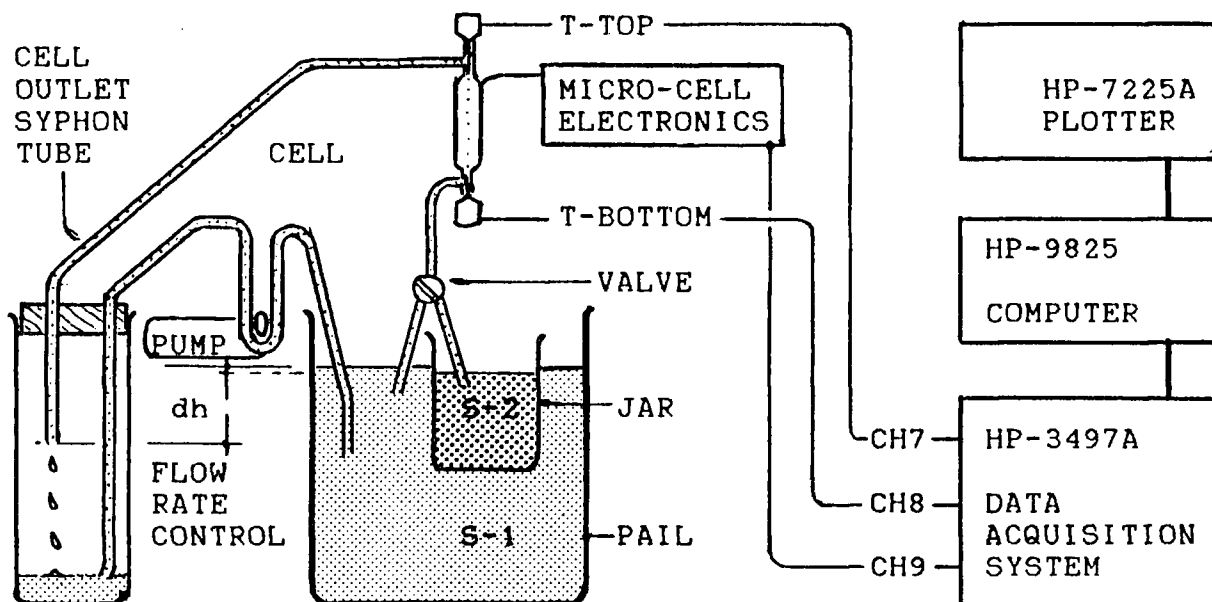
Figure B-5. Time Response - Experimental Arrangement

The intake of the micro-cell was connected to a valve which could switch the flow from a jar of one salinity

to a pail of another. The jar was floated in the larger pail to minimize temperature differences and to get a nearly constant drop in height between the fluid levels and the cell outlet. The gravity-driven flow through the cell did remain nearly constant when switching between salinities. Actual flow rates during each run were measured by counting the number of drops over time at the outlet for different settings. These ranged from about 0.5 to 4 drops per second. Counting showed about 825 drops in 50 ml.

Each cell was connected to a micro-cell conductivity circuit and continuously powered during a run, which avoids transients caused by switching. The output of this circuit and of the micro-cell thermistors were then connected to the HP-Datalogger System, which was controlled by an HP-9825 computer. A program for this system was modified to use the average temperature from both thermistors for calculating the salinity and to store the calculated values on tape. The computed salinities were plotted during each run and the observed flow rates were marked on the plots in number of drops counted per stopwatch seconds. At low flows, the difference in fluid levels of pail and jar resulted in a change in flow when switching between salinities. Flow rates were counted and marked for both heights. The time to adjust to this change is unknown but believed to have a negligible effect on the response time.

From the first time-series at constant salinity it was found that the overall variability of this system was about 0.01 S.

The next series of runs was done to look at the characteristics of the response for a range of salinity values and at flowrates used in experiments. The output of these runs consists of plots of calculated salinity for each of the three cells at different but steady flow rates from 0.5 to 4 drops per second, and for steps of 0.5 to 4.0 S in the salinity. These time-series plots are included in this appendix.

The typical shape of the response curves consist of:
- a nearly horizontal part after switching the intake,
- a steep linear section of rapid change in salinity
- an exponential tail approaching the final salinity

The time required after a switch in salinity at the intake, for the calculated salinity to reach 90% or 95% of the final value, was graphically determined from this first set of plots: On these plots, the time at which the intake was switched was marked as $t0$ and the start of rapid change as $tc$; $t90$ and $t95$ were the times at which the calculated value had changed by 90% or 95% of the step in salinity. The rapid change starting at $t=tc$ appears linear over part of the change, except at flows of less than about 1 drop per 2 seconds (.03 ml/sec). This is followed by a curve as the calculated value approaches the final salinity. Distances measured along the time axis were converted to volume by multiplying with the flow rate.

For obtaining density profiles in the tank a reasonable flow rate is needed to take successive readings at different depths within the time in which larger patterns in the convection tank

change. A steady slow flow through the micro-cell minimizes the disturbance at the intake point. The length of time before the rapid change (t0-tc) depends on the length and diameter of the tube through which the fluid moves before reaching the cell and on the flow rate. The volume of fluid entering the cell in time (t0-tc) should be constant for steady flow, but the flow is briefly interrupted while switching salinity at the intake. The starting point and flow rate are approximate which explains the range in initial volume from 0.28 to 0.66 ml. The plotted data show that for a change to 95% of the final value takes 30 to 90 seconds and between 2 and 7 ml of fluid.

The shape of the response curve changes with the flow rate. In a next set of runs the calculated temperatures, conductivity ratios and salinities were recorded. The time-series plots show a series of calculated salinity curves at different flow rates. These have been normalized for salinity change and each section has been replotted in terms of volume required from the time of a switch in salinity. A plot of normalized salinity change vs. volume (text fig. 2-5) shows that the response curves collapse into a single curve at higher flow rates. The flow rate and the start and end time for each segment are also marked on the plots. Several time-series of computed salinities, temperatures and conductivity ratios were plotted at the same time-scale to check their relative effect.

At the higher flow rates (40/15 dr/s or 0.16 ml/s) it takes 2 to 3 ml of fluid for a change of 90% to 95% of the new value over respectively 12 to 19 seconds. To get a density profile of

fluid in the experimental tank, the flow rate is set by adjusting the drop in height between the fluid level in the tank and the cell outlet. If the Datalogger multiplexer cycle is started 20 seconds after the intake is moved to the next height, then the calculated salinity (Sc) will be close to 95% of the change in salinity or, assuming S1 < S2:

$$Sc=S1 + 0.95(S2-S1)$$

which yields: $\quad S2 = (Sc - .05S1)/.95$

For continuous monitoring of the salinity in the tray or in the mixed layer below it at a fixed point, a much slower flow rate can be used since the average changes over time are much smaller and slower than those observed in the test profiles.
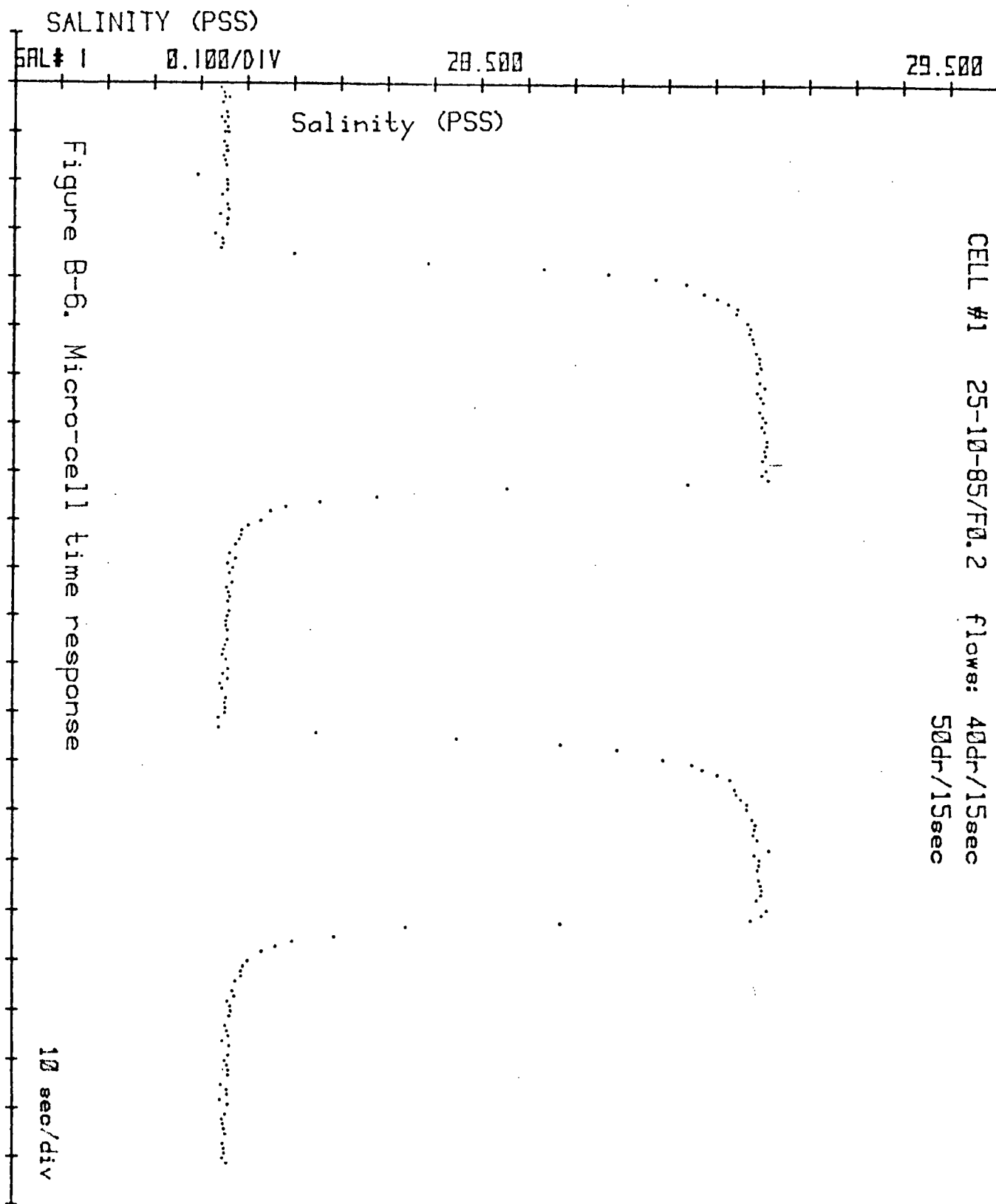
SALINITY (PSS)

SAL# 1    0.100/DIV        20.500              29.500

Salinity (PSS)

CELL #1   25-10-85/F0.2   flows: 40dr/15sec
50dr/15sec

Figure B-6.  Micro-cell time response

10 sec/div
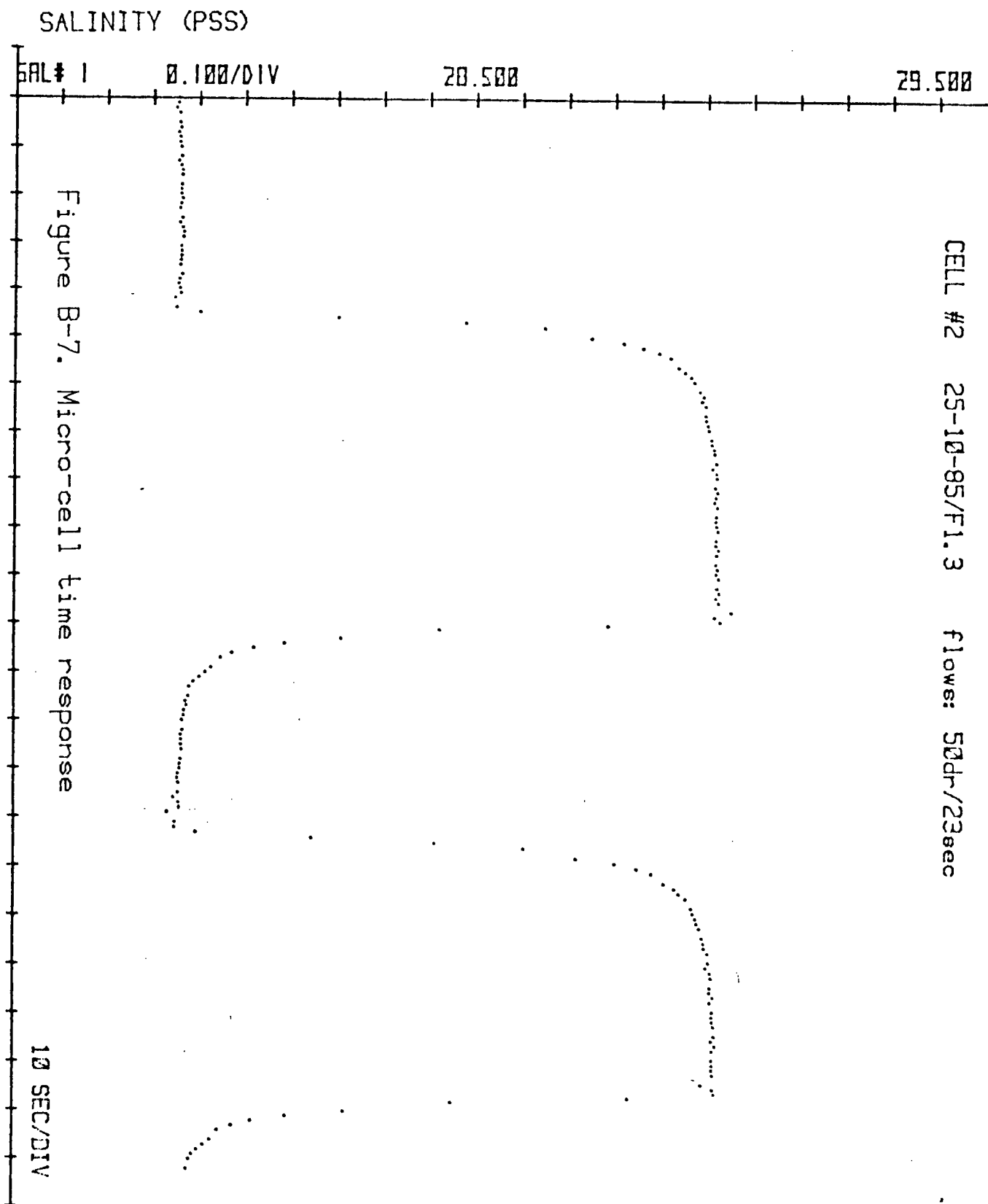
Figure B-7. Micro-cell time response
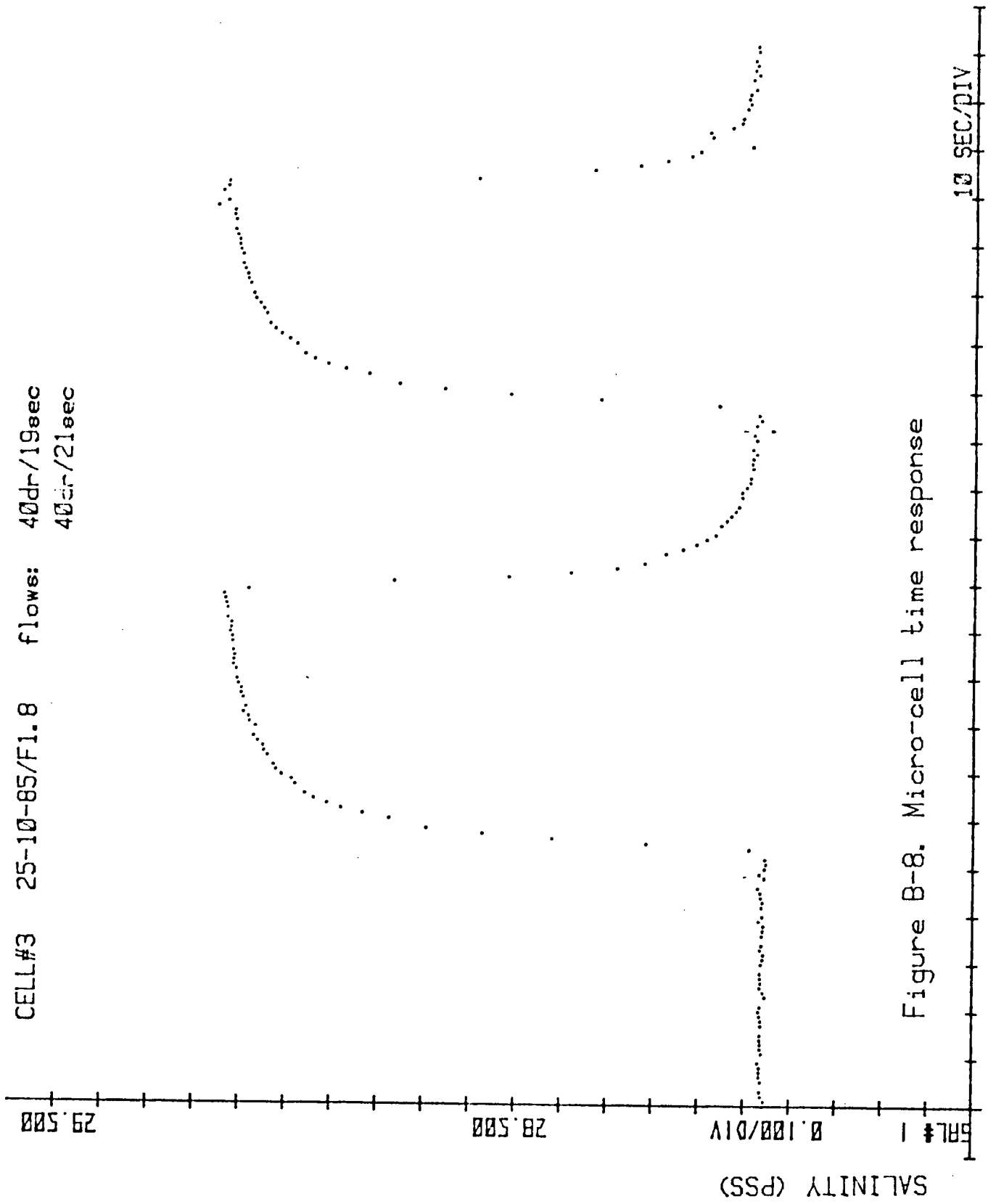
Figure B-8. Micro-cell time response

Figure B-9.  MICRO-CELL TIME RESPONSE
CELL#1 25-10/0.4

S1-S2 = 27.95-29.10
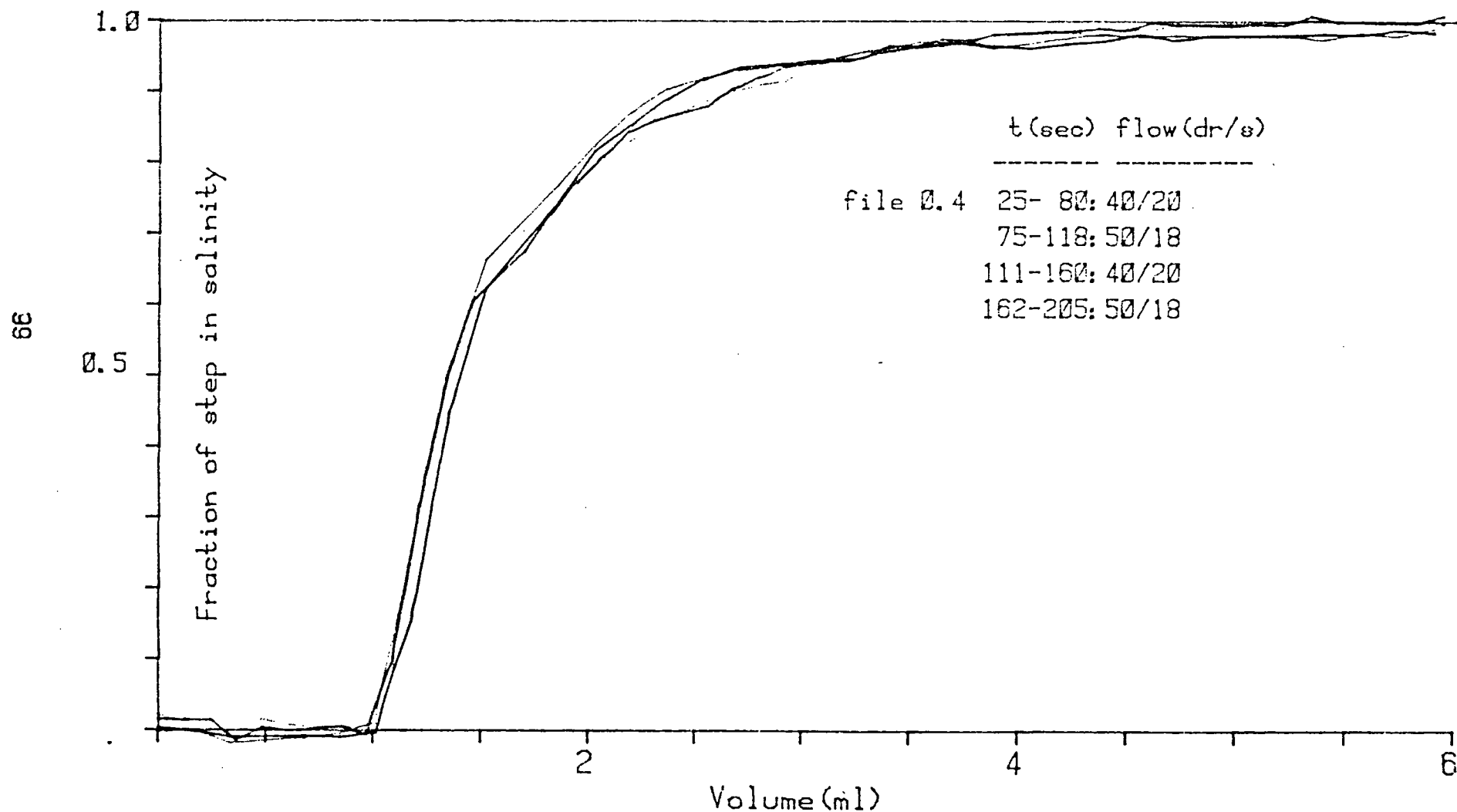
Figure B-10.     MICRO-CELL TIME RESPONSE
CELL#2 25-10-85/1.1 -1.2

S1-S2 = 27.85-29.02

**Fraction of step in salinity** (y-axis, values 1.0 and 0.5 marked)

F1.1 flow=50/15 dr/sec
        18-68
        68-140
        141-180
        180-215

F1.2 flow=50/16 dr/sec
        22-61
        61-95
        95-128
        128-169
        169-208

Volume (ml) (x-axis, values 1 2 3 4 5 6)
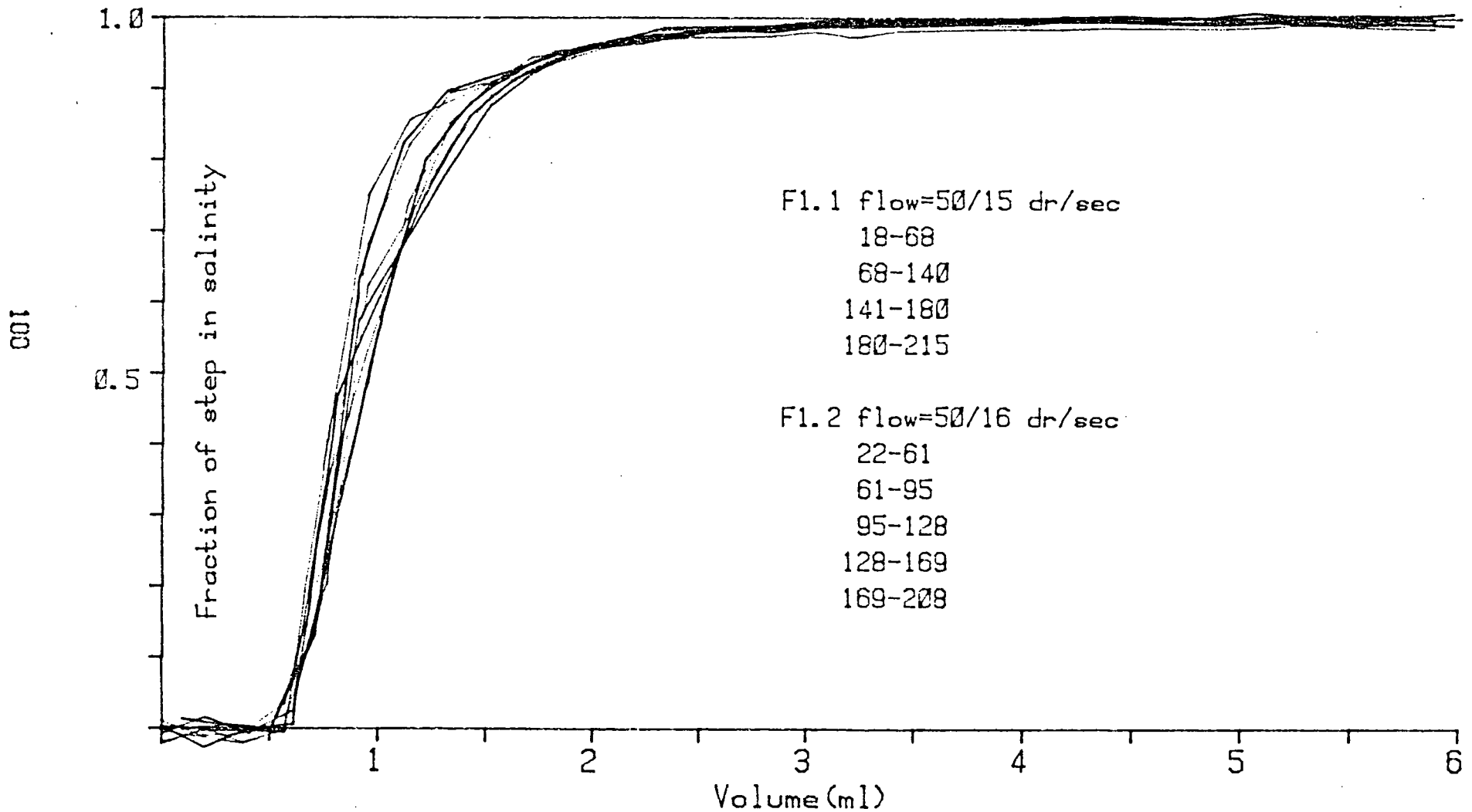
Figure B-11.  MICRO-CELL TIME RESPONSE
CELL#3 25-10/  FILES F1.7-F1.10

S1-S2 = 27.97-29.13
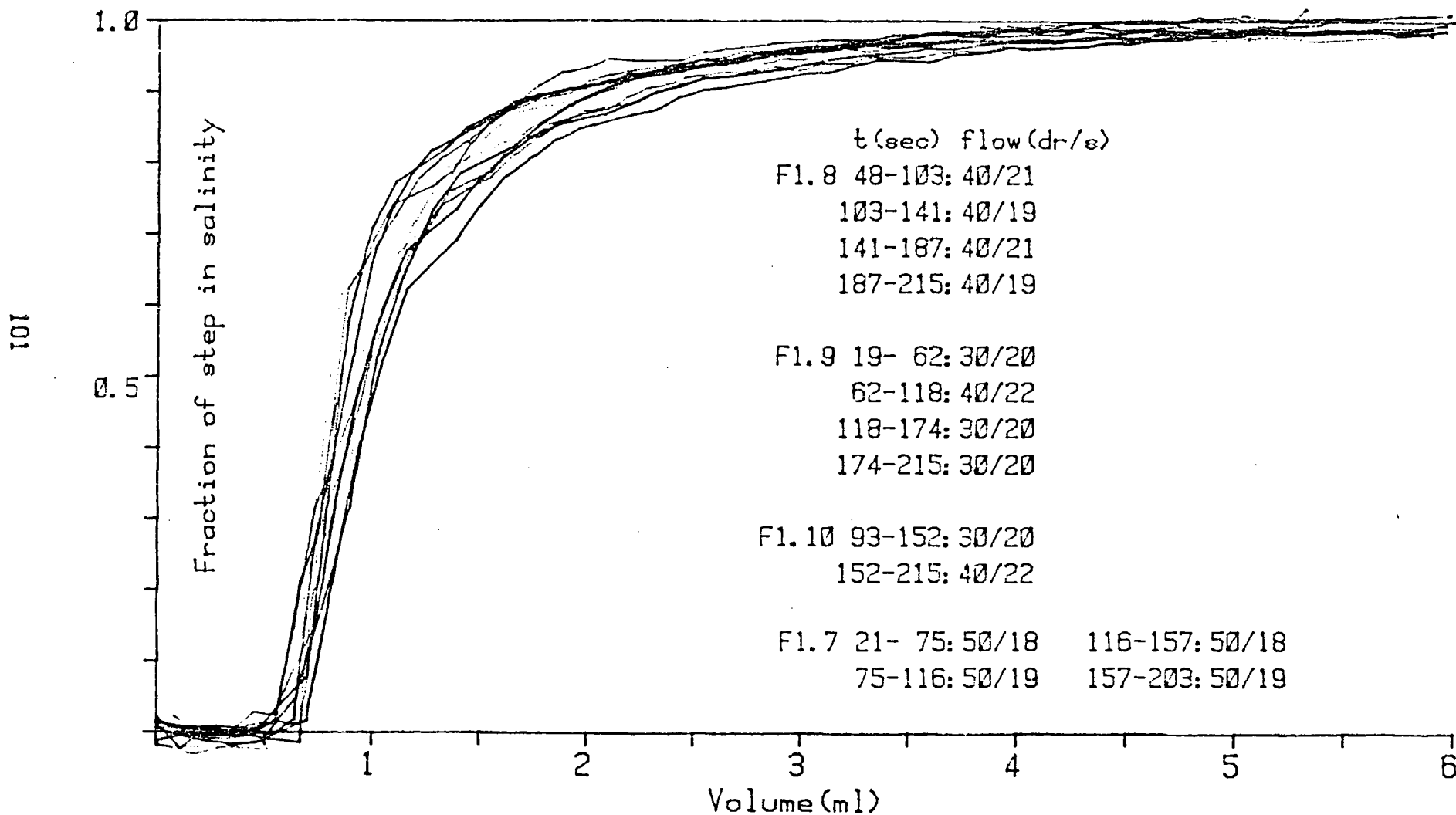
## B.6 Spatial resolution of the micro-cells

A two-layer system was used to check how well an apparently sharp step in salinity at the interface is represented in a salinity profile from micro-cells data taken at closely spaced points.

The lighter fluid of lower salinity was first placed in the container and the heavier fluid was then slowly added at the bottom. The density interface was visible in the shadowgraph image as a narrow bright line of light which slowly broadened due to diffusion and turbulence from filling. It was sharpened by withdrawing fluid from a point below the line.

Fluid was then syphoned through the micro-cell at about 2 to 3 drops per second in several runs with different steps in salinity. Measurements were while syphoning fluid through the micro-cell at a fixed rate, lowering the cell intake to a depth and taking a reading after allowing enough time to flush the cell (30 sec), then moving the intake to the next depth.

Salinity profiles were obtained by plotting the calculated salinities against depth (figures B-6,7 ). Several plots show a spread in depth between the layers of constant salinity. This can indicate either a lack of resolution or the actual shape of the interface which showed long period oscillations in one case. In the profile dated 15-4-86 a sharp interface is seen of 0.5 PSS over 3 mm thickness, in which the salinity increases in 8 steps of 0.4 mm each.

# SALINITY PROFILE
## 11-4-86 CELL SPATIAL RESOLUTION



flow through cell:
25 dr/ 23 eeo
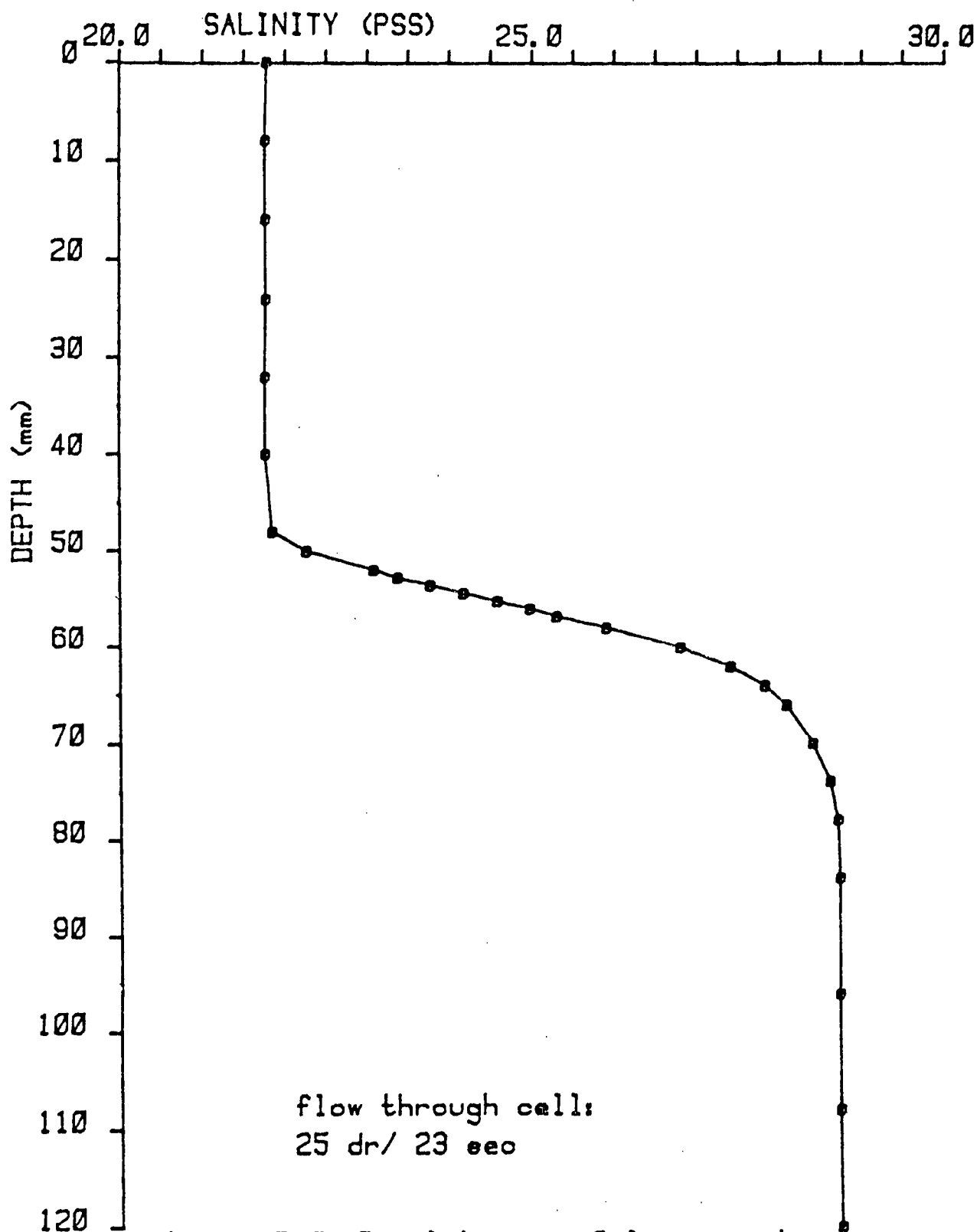
Figure B-12. Resolution in 2-layer system.

# SALINITY PROFILE
## 15-4-86 MICRO-CELL SPATIAL RESOLUTION
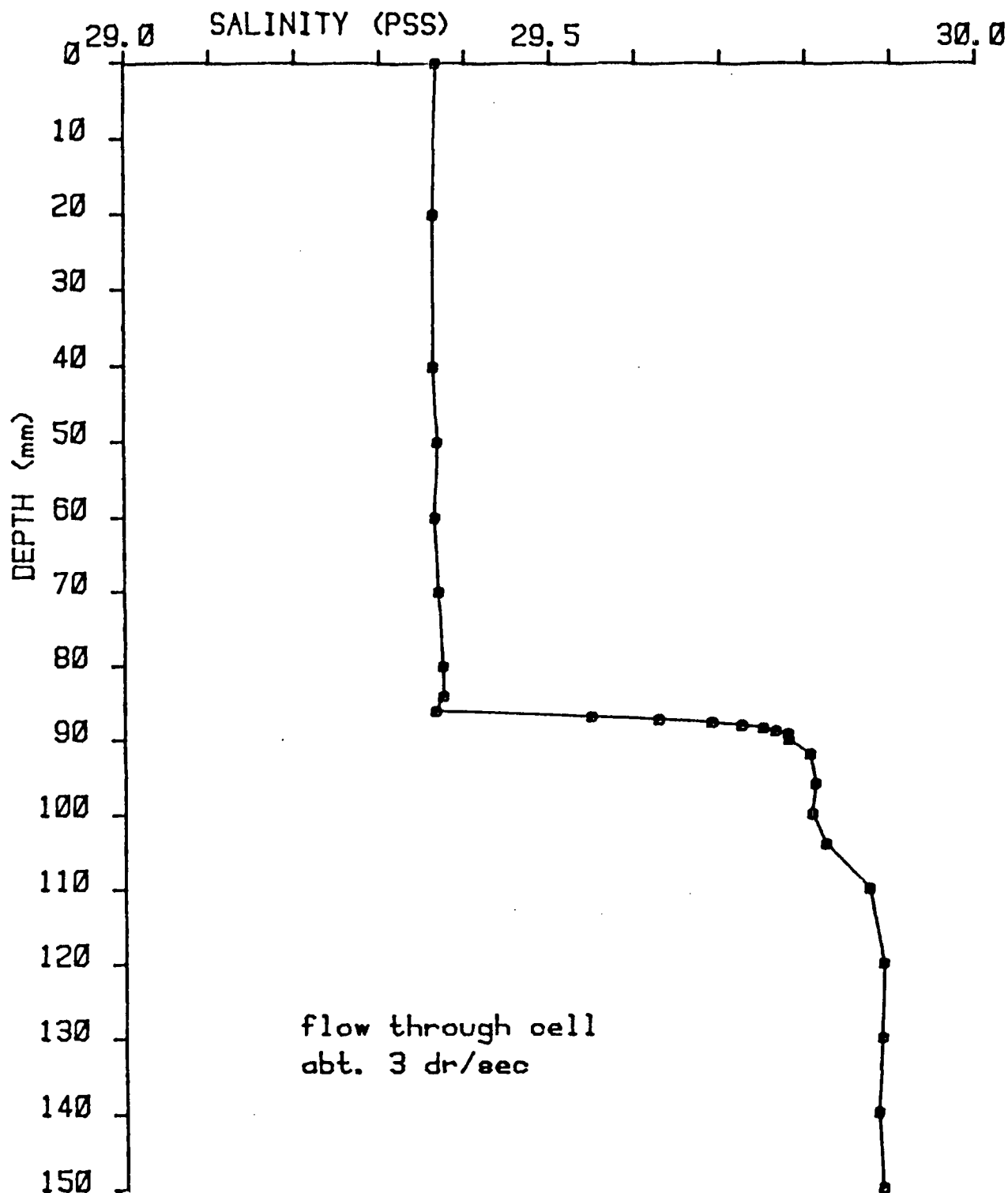


Figure B-13. Resolution in 2-layer system.

Thermistors

## C.1 Thermistor use

Thermistors were used to determine the temperature of fluid inside each micro-cell and in the experimental tank, to enable accurate calculation of the salinity and density of the fluid. The type of thermistor used in these experiments consisted of a small bead mounted in the tip of a hollow needle, and placed in in the tank and at the inlet and outlet of each cell.

Initially, a single thermistor was inserted in the flow at the outlet of the micro-cells through a small glass tee. The difference between the temperature of fluid in the experimental tank and ambient room temperature caused the value determined from this thermistor to differ from that at the centre of the cell by some amount which depends on the rate of flow through the cell and on the magnitude of the temperature difference. To reduce this error and to check on the output of these older thermistors (some of which were found to develop electrical leaks over time) a second thermistor was installed at the inlet of each cell. The average of the temperatures at the inlet and outlet of the cell was used in the calculation of salinity (see appendix A.1). This was then combined with the temperature in the experimental tank to determine the density of fluid at the intake point (see appendix A.2).

Figure C-1 below shows the micro-cell with the two thermistors.
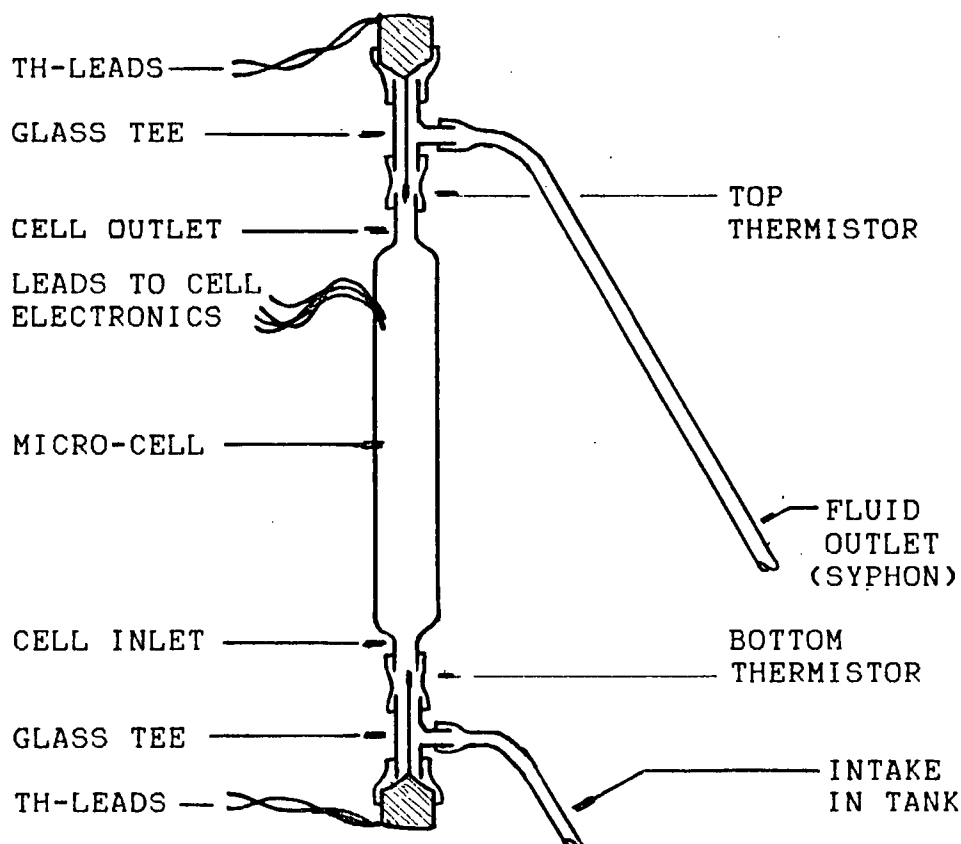
Figure C-1. Thermistors at micro-cell inlet and outlet.

Temperatures are calculated from the measured resistance of calibrated thermistors. The temperature T (in °C) for a given resistance RT (in ohms) and calibration constants A, B and C is then computed from:

$$T = 1/[A + B*\ln(RT) + C*(\ln(RT))^3] - 273.15$$

## 1.1 Leaks

In initial tests with the thermistors at top and bottom of each cell, significant differences were found in several cases between the calculated temperatures above and below the cell. Electrical leaks were found in some thermistors. These leaks form an external current path parallel to the internal path,

107

with a resistance which may vary with the conductivity of the fluid or with variations in temperature, which can change the contact-surface resistance in minute cracks. Any current leak lowers the true resistance value as a parallel resistance, which corresponds to a higher apparent temperature:

$$1/Rapparent = 1/Rtrue + 1/Rleak$$

For a leak of 1 megohm and a true resistance of 2000 ohm, the apparent resistance becomes 1996 ohm. For thermistor #31 the calculated temperature would change from 20.281 to 20.338 °C and the salinity at 20-30 PSS would change by 0.3-0.4 PSS. The discrepancies in temperatures were reduced by replacing the thermistors which were found to have leaks.


## C.2 Re-calibration for extended range

The thermistors were originally calibrated at temperatures close to 0 °C. For laboratory use, the resistance of the needle mounted thermistors was determined at temperatures up to 25 °C in a controlled temperature bath against recently calibrated thermistors. The HP utility-program FITTER was used to generate a new set of calibration constants for these thermistors, which are listed in table C.1 below. Some typical examples of the output from the curve fitting program for the re-calibrated thermistors is included at the end of this appendix. This lists date, data used for the fit, generated calibration constants, and the maximum error and standard error of the estimate.

## Table C.1 Thermistor Calibration Constants

| Therm# | A = | B = | C = |
|---|---|---|---|
| 17 | 0.928120e-3 | 3.216646e-4 | 3.286378e-7 |
| 20 | 1.072391e-3 | 2.936491e-4 | 1.741109e-7 |
| 22 | 1.060989e-3 | 2.973808e-4 | 1.586510e-7 |
| 23 | 1.076479e-3 | 2.937859e-4 | 1.670782e-7 |
| 34 | 1.053861e-3 | 2.975737e-4 | 1.544686e-7 |
| 37 | 1.015587e-3 | 3.013717e-4 | 1.391556e-7 |
| 40 | 1.143266e-3 | 2.841332e-4 | 2.267124e-7 |
| 44 | 1.027313e-3 | 2.924027e-4 | 1.616634e-7 |
| 526 | 1.3262863e-3 | 2.5896285e-4 | 1.3697736e-7 |

$$T (°C) = 1/[A + B*\ln(RT) + C*(\ln(RT))^3] - 273.15$$

## C.3  Datalogger calibration correction

Recalibration did correct the error in observations when a digital voltmeter was used but temperatures determined from the datalogger input still did not agree for different thermistors. The conversion from datalogger N-number to resistance value was done with a linear fit for the resistance values for a range of laboratory operating temperatures returned by thermistor #41, (used initially at the exit of the first cell but replaced due to an electrical leak). This linear fit was given by:

$$RT = 2526 - NT*0.25373$$

where RT = resistance value (ohm)

NT = datalogger N-number

Many of the thermistors cover a slightly lower range of values. A second order fit to the datalogger output NT-numbers yields a better fit over the range of resistance values from 1600 to 2500 ohms, with a standard error of 0.854221 :

$$RT = 2527.62 + NT*(-0.261192 + NT*4.771296E-6)$$

A thermistor resistance of 1800 ohms corresponds to an N-number of 2861 when using the coefficients of the linear fit, but with the second order fit this N-number (2861) yields a resistance of 1818.4 ohms. Using the calibration constants for thermistor #40, 1800 ohms corresponds to a temperature of 23.72 °C while 1818 ohms would be 23.44 °C.

After implementing the above corrections, the values of the observed temperatures were found to be in good agreement with expected values for fluid in the tank and for ambient air temperatures.

Title: THERM# 31
X-Variable:        R       Y-Variable:          T
Created 07-04-85

Observation 1:    X = 3961.72      Y = 1.953
Observation 2:    X = 3854.75      Y = 2.648
Observation 3:    X = 3580.44      Y = 4.539
Observation 4:    X = 3101.18      Y = 8.282
Observation 5:    X = 2692.32      Y = 12.053
Observation 6:    X = 2329.38      Y = 16.009
Observation 7:    X = 2155.63      Y = 18.167
Observation 8:    X = 1943.39      Y = 21.097
Observation 9:    X = 1691.93      Y = 25.1


### FINAL RESULT OF CURVE FIT

Dataset title: THERM# 31
Model used:
Thermistor Equation: $F(X)=1/(A1+A2*\ln(X)+A3*\ln(X)^3)-273.15$


The estimated parameter values after 7 iterations:

A[1]= 1.035417e-03
A[2]= 3.033537e-04
A[3]= 1.520697e-07

Maximum error is 1.220309e-03
The overall standard error of estimate is 8.155511e-04

Title: THERMISTOR# 37
X Variable:      R      Y-Variable:      T
Created 08-13-85

Observation 1:      X = 3534.3      Y = 8.241
Observation 2:      X = 3309.97     Y = 9.96
Observation 3:      X = 3006.92     Y = 12.512
Observation 4:      X = 2646.11     Y = 15.971
Observation 5:      X = 2415.55     Y = 18.483
Observation 6:      X = 2322.26     Y = 19.582
Observation 7:      X = 2111.23     Y = 22.27
Observation 8:      X = 1985.75     Y = 24.022
Observation 9:      X = 1913.41     Y = 25.091
Observation 10:     X = 1854.23     Y = 26.002

FINAL RESULT OF CURVE FIT

Dataset title: THERMISTOR# 37
Model used:
Thermistor Equation: $F(X) = 1/(A1 + A2 \cdot \ln(X) + A3 \cdot \ln(X)^3) - 273.15$

The estimated parameter values after 8 iterations:

A[1]= 1.015587e-03
A[2]= 3.013717e-04
A[3]= 1.391556e-07

Maximum error is 1.324976e-03
The overall standard error of estimate is 8.015290e-04

Figure C-2. Calibration curve — Thermistor# 37
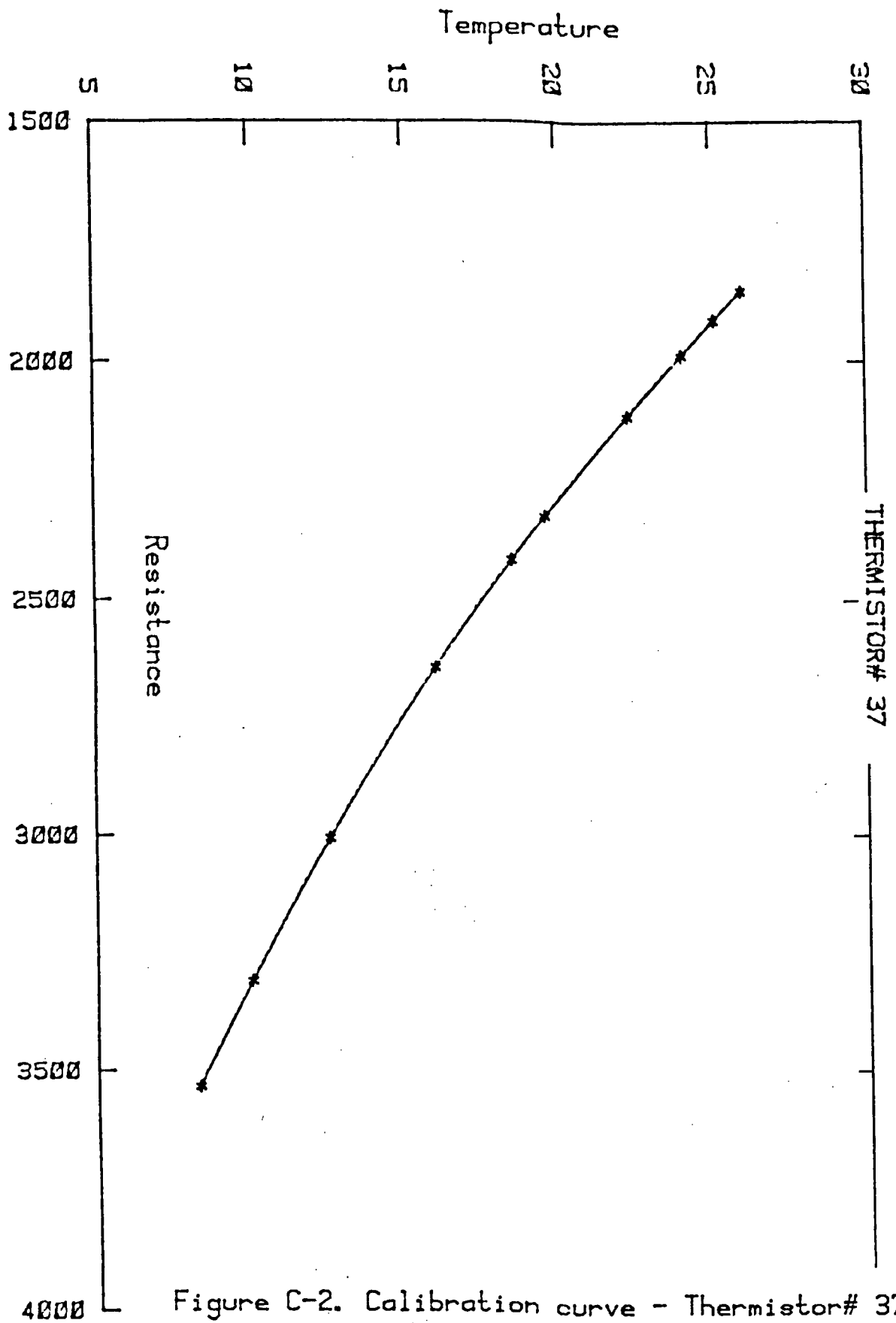
Dataloggers

APPENDIX D

114

In this series of experiments, two types of datalogger were used at different times. The first was an Applied Microsystems C/T datalogger, modified to bring the digitized output in range for input from the thermistors and micro-cells. When available, an HP-3497A Data Acquisition System was used with individual conductivity circuits for the micro-cells. The output in both cases was directed to an HP-9825 computer.

## D.1 Applied Microsystems C/T Datalogger

An Applied Microsystems Datalogger (S/N 170) was adapted for use with the micro-cells: an input panel allows a number of cells and thermistors to be connected to designated channels. The temperature and conductivity electronics in this AM/CT Datalogger were modified for the range of conditions expected to be used in laboratory experiments.

Triggered manually or at some pre-set clock rate, the multi-plexer cycles through the pre-set pattern of input channels. Analog input signals are converted into a digital output line which contains serial number, time, and numbers for temperature and conductivity. This line is translated by an A.M. serial converter and entered into the HP-9825 via an RS-232 interface.

The sampling cycle frequency or clock rate is set by connecting pin #32 of the edge-connector on the Sequencer board to the appropriate pin on the Clock board edge connector. Table D.1 lists the function for each pin of the Clock board. After switching on the datalogger, the sampling cycles are initiated

automatically at the rate set on the clock or can be triggered manually by pressing the button marked "start".

The pattern of C and T channels which the sequencer cycles through was programmed on a ROM-chip in the Datalogger. Up to four different micro-cells can be selected, each with two thermistors, and up to four additional thermistor inputs can be added to determine the temperature at points in the tank. These patterns are listed in table D.2 . Dip-switches S1-S5 of SW1 on the multiplexer (MUX) board are pre-set to the desired pattern number:

$$MUX\# = 1 +S1 +S2 +S3 +S4 +S5$$

Here and in the following dip-switch patterns, Si=0 if open and Si=$2^{(i-1)}$ if closed. Dip-switches S6-S8 of MUX-SW1 should be closed for 12-bit data. The number of channels output by the Datalogger to the Serial Converter is set with switches S1-S5 of SW1 on on the Storage Formatter (FMT) board:

$$\#CHNLS = 1 +S1 +S2 +S3 +S4 +S5$$

The first two channels are instrument serial number and time in seconds (approximately),and each temperature and conductance requires an additional channel. The HP-9825 programs prompt for number of cells and extra thermistors and display settings for MUX-SW and FMT-SW1. Dip-switches S6-S8 of FMT-SW1 set the number of times that the data words are output (once if all are open). Dipswitches S1-S6 of FMT-SW2 set the data output rate in milliseconds:

$$Time/bit = 5.15*(1 +S1 +S2 +S3 +S4 +S5)$$

For 12-bit word output S7 of FMT-SW2 is closed (10-bit if open).

116

# Table D.1. Clock Board Edge Connector Pin Functions

| Pin# | Function | Pin# | Function |
|---|---|---|---|
| 1 | o/p 256 hours | 18 | o/p 30 minutes |
| 2 | o/p 128 hours | 19 | o/p 56.25 seconds |
| 3 | parallel transfer pulse | 20 | o/p 28.125 seconds |
| 4 | serial data output | 21 | serial data input |
| 5 | o/p 32 hours | 22 | o/p 112.5 seconds |
| 6 | o/p 16 hours | 23 | o/p 1.75 seconds |
| 7 | o/p 8 hours | 24 | o/p 3.51 seconds |
| 8 | o/p 64 hours | 25 | o/p 7.03 |
| 9 | o/p 27.466 microseconds | 26 | o/p 14.0625 |
| 10 | o/p 1 hour | 27 | o/p 429.153522 microsec |
| 11 | shift clock | 28 | o/p 6.86 msec |
| 12 | o/p 2 hours | 29 | o/p 3.43 msec |
| 13 | o/p 4 hours | 30 | clock reset pulse out |
| 14 | o/p 15 minutes | 31 | clock reset |
| 15 | o/p 225 seconds | 32 | parallel transfer |
| 16 | o/p 7.5 minutes | 33 | Vss |
| 17 | time code increment o/p | 34 | Vdd |
|  |  | 35 | Vss |

# Table D.2. Multiplexer Input Channel Cycling Pattern

| MUX# = | 1 | 2 | 3 | 4 | 5 | 6 | 7 | 8 | 9 | 10 | 11 | 12 | 13 | 14 | 15 | 16 | 17 | 18 | 19 | 20 |
|---|---|---|---|---|---|---|---|---|---|---|---|---|---|---|---|---|---|---|---|---|
| **CHANNELS:** |  |  |  |  |  |  |  |  |  |  |  |  |  |  |  |  |  |  |  |  |
| T1-C1-T6 | x | x | x | x | x | x | x | x | x | x | x | x | x | x | x | x | x | x | x | x |
| T2-C2-T7 |  | x | x | x |  | x | x | x |  | x | x | x |  | x | x | x |  | x | x | x |
| T3-C3-T8 |  |  | x | x |  |  | x | x |  |  | x | x |  |  | x | x |  |  | x | x |
| T4-C4-T9 |  |  |  | x |  |  |  | x |  |  |  | x |  |  |  | x |  |  |  | x |
| T11 |  |  |  |  | x | x | x | x | x | x | x | x | x | x | x | x | x | x | x | x |
| T12 |  |  |  |  |  |  |  |  | x | x | x | x | x | x | x | x | x | x | x | x |
| T13 |  |  |  |  |  |  |  |  |  |  |  |  | x | x | x | x | x | x | x | x |
| T14 |  |  |  |  |  |  |  |  |  |  |  |  |  |  |  |  | x | x | x | x |

The datalogger greatly simplified the nearly simultaneous collection of data from all thermistors and conductivity cells during the slope flow experiments. However, while the data from the temperature circuit gave very stable output, there were some spurious jumps in the output from the conductivity circuit. The N-numbers did jump at times by up to 10 or more units, which corresponds to a variability of almost 0.1 PSS. Several efforts were made to improve the reliability by replacing components in the datalogger and by increasing the delay between switching a cell on and reading the output, but the conductivity readings still became noisy occasionally without known cause.

## D.2 HP-3497A Data Acquisition System

The HP-3497A System was only available on occasion. It was used in determining the time response characteristics of the micro-cells and to obtain data for simultaneous profiles in the last two slope flow experiments. When using this system, each micro-cell was continuously powered by a separate conductivity circuit. This reduced any transients caused by switching the cells on but caused some cross-talk between the cells which was eliminated by shifting the individual operating frequencies. Small shifts found after collecting experimental data were seen to occur when the syphon outlets of the micro-cells were moved relative to each other.

The HP-datalogger allowed much higher sampling frequencies as well as averaging of rapid multiple readings of each sensor, which further reduced the noise in the data.

Membrane Salt Flux Calibration

**E.1 Salt and volume flux and driving pressure**

The surface salt flux due to the freezing of sea water was simulated in these experiments by a percolation of sea water through a porous membrane in a tray. This membrane was mounted between two layers of circuit board, with perforations of about 1 mm diameter spaced uniformly at 4 per cm along and across the tray. The tray was suspended level with the surface of fluid in the experimental tank, which was partly filled with a mixture of sea water and filtered tap water.

The method used for estimating the magnitude of the volume and salt flux through the membrane is detailed in section 2.6 in the text. In a series of flux calibration runs, in which the bottom of the tank was kept horizontal, the salinity of fluid at the center of the tank was taken as average for the whole tank since the mixed layer extends to the bottom. The net salt flux is the high salinity inflow reduced by the low salinity return flow to the tray, per unit time and unit area. It was expressed as:

$$Bn = Vw.\frac{(S2.D2-S1.D1)}{1000} = \frac{d[S1.D1]}{dt}.\frac{V1}{1000}\frac{}{A} \qquad (E-1)$$

Bn= net salt flux $(g/cm^2/s)$

Vw= volume flux $(cm^3/cm^2/s)$

Si= salinity in tray(2) and tank(1) (g/kg or PSS)

Di= density in tray(2) and tank(1) $(g/cm^3)$

V1= volume of fluid in the tank $(cm^3)$

A = area of the tray bottom $(cm^2)$

The flux is driven by the pressure caused by the difference in density between the fluid in the tank and that in the tray or rather, the weight of a column of fluid in the tray and that of a column of the same height in the edge between tank and tray:

$$P = (D2-D1).g.h \qquad (E-2)$$

P = pressure (g/cm/s²)

Dl= density (g/cm³)

g = gravity = 981 (cm/s²)

h = effective height of fluid (cm)


The fluid in the edge space between tank and tray became stably stratified as the return flow which rises from the mixed layer in the tank slowly increases in salinity. The less saline fluid formed a surface layer of about 2 mm in the tray, which can not be mixed well without disturbing the surface (and thus the pressure and associated flux). Fluid in the tray and in the edge space were approximated as 2-layer systems with the same salinity in the upper 2 mm layer, and the effective height used to compute pressures was the tray fluid height reduced by 2 mm.


## E.2 Flux calibration experiments

To estimate the magnitude of the salt flux, time-series data of conductivity and temperature were collected from tank and tray in a series of calibration experiments without a bottom slope. The salt flux was varied by using different starting salinities and depths of fluid in the tray. The meniscus in the

edge space made it difficult to determine the exact height of the fluid. Shadowgraph patterns during these runs show a nearly uniform distribution of convective motions in the tank except near the tank end-walls where these motions appear reduced in a triangular section widening with depth. This is caused by the small downflow under the end-walls of the tray and the very slow upward motion in the edge space. Any similar effect at the side walls cannot be distinguished since the shadowgraph image integrates over the width of the tank, but injected dye did not show any mean circulation in a cross-section of the tank.

Salinity profiles were plotted from data taken during several salt flux calibration runs, along the centerline and in the edge space between the tank and tray.(figures E-1 to E-3). Vertical salinity gradients were found just below the membrane and in some cases close to the bottom, possibly due to incomplete mixing after a local spill. The profiles indicate that salinity of fluid sampled at a point near the centre of the tank may be taken as a reasonable estimate of the average for the tank.

The initial series of calibration runs did show a general similarity in the shape of the time-series plots of calculated salinities. Estimated values for volume fluxes were obtained with the expressions formulated above, using a finite differences method: the rate of change in salinity and in density was approximated by the difference between successive observations divided by the time interval. Interpolated time, salinity and density are taken as the average of each pair. The volume

fluxes and pressures found by substituting these values into the above expressions were plotted for successive runs to obtain a single flux calibration graph for the system. There is a doubling of variability by using this method since a point too high in one step will be too low in the next. The plotted results from a first series of experiments did not form a single characteristic curve of volume flux versus pressure. The tray bottom was disassembled to inspect the membrane, which appeared to be clogged and discolored in spite of filtering through water-purifying cartridges. This could be caused by organic activity or mineral precipitation, and by dust from the laboratory ventilation system.

A new membrane with 5 micron pore size was installed in the tray, and all fluids were pumped through a 0.45 micron filter. After adjusting the salinities, and adding a small amount of bleach to control biological activity, the fluids were pumped through a 0.8 or 5 micron filter into the tank and reservoirs before each calibration run. The salt flux plots from these experiments were combined in a single graph (figure E-3). This shows that, with some scatter, repeatable results for salt flux estimates were obtained for a range of fluxes. Membrane volume flux calibrations were done before and after the first slope flow experiment and a curve through the combined plots (figure E-2, also in text) was used to compute salt flux estimates.

The following pages contain a typical print-out of the data and calculated values, the time-series plot of salinities and the calibration plots of membrane volume flux versus pressure.

Figure E-1. MICRO-CELL TIME SERIES PLOT
Membrane flux calibration: 26-2-86

124
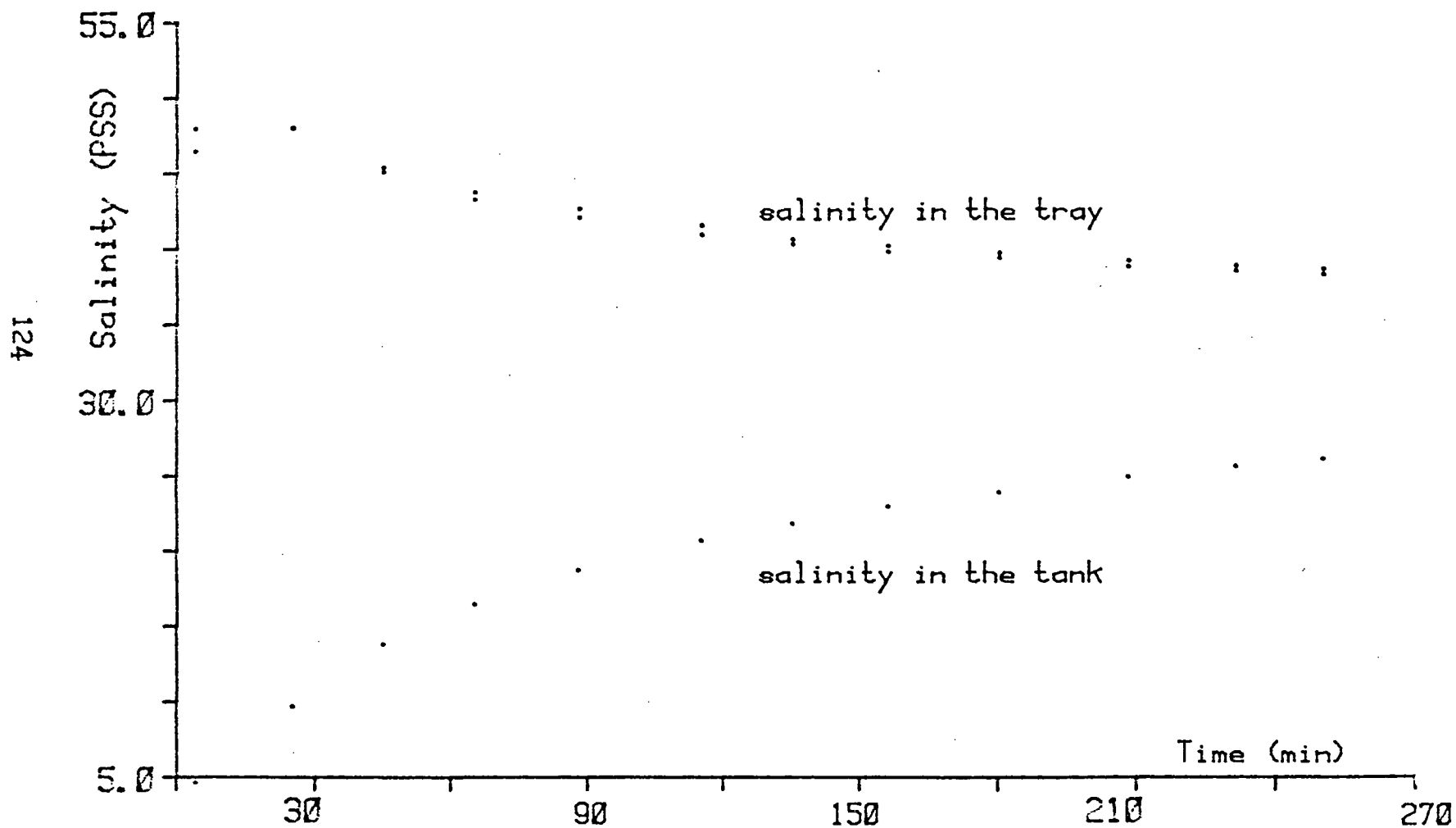
Figure E-2. Membrane volume flux calibration before and after first slope flow experiment.
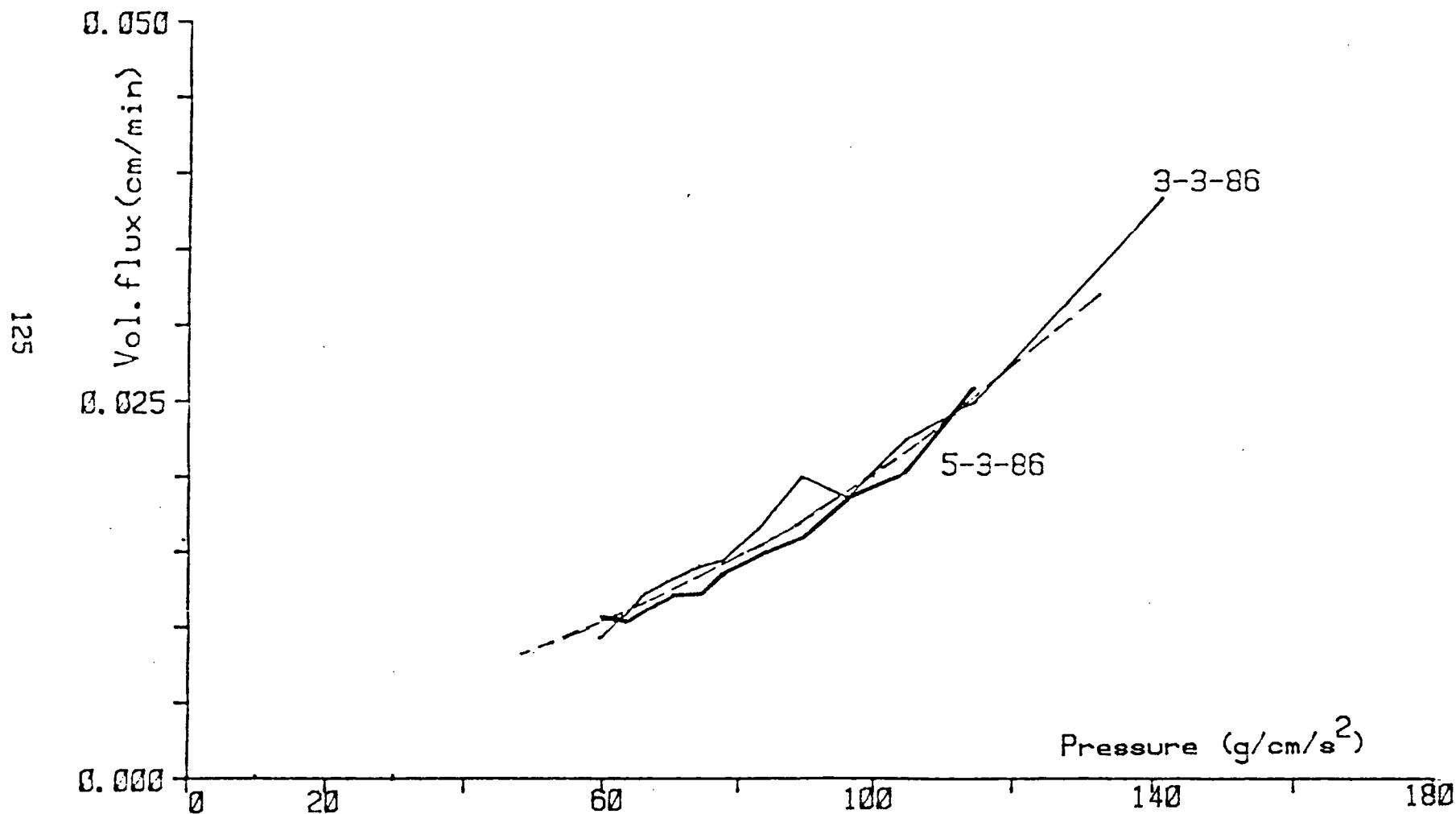
Figure E-3. Membrane volume flux calibration

126
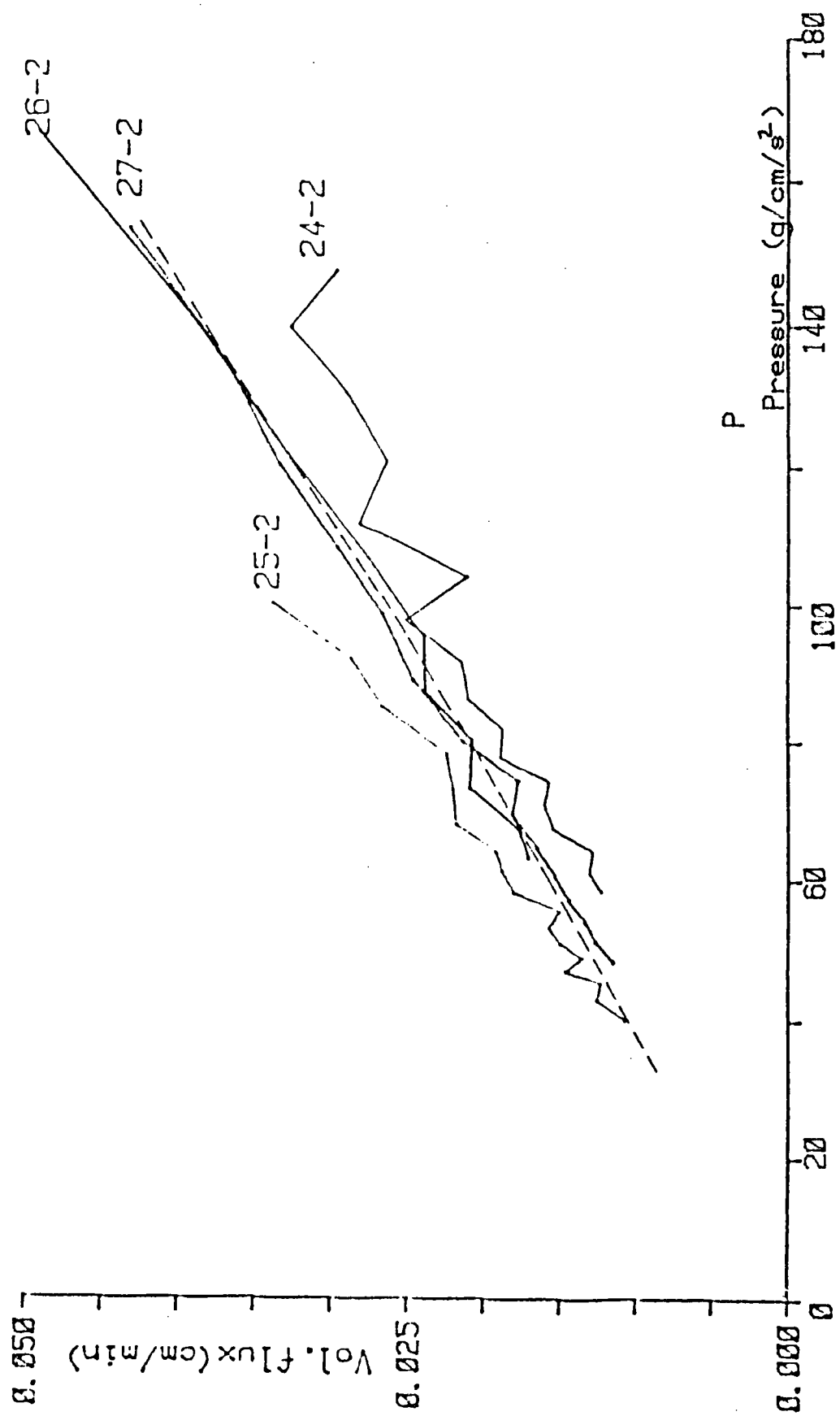
DESCRIPTION OF EXPERIMENTS

This appendix contains a brief description of the individual slope flow experiments. Included are the slope angle, starting salinities of fluid in tank and tray, special features observed during the individual experiment, the tabulated values of tray salinities from the manually collected data, velocity maxima measured from dye features in the slope flow, the estimates of the membrane salt flux at the times that flow velocities were determined, time-series plots of salinities during the experiments and the lineprinter output of the raw data and computed values from the datalogger.

In the first slope flow experiment, the bottom slope angle was 3.3 degrees and the depth in the tank under the tray was 7 mm at the raised end and 63 mm at the deep end. The tray was filled with fluid of 59 ppt to a height of about 34 mm, while 800 ml of fluid of 15 ppt was added to the edge between tank and tray to keep the levels equal. A bottom slope flow became visible on the shadowgraph before filling and levelling was completed. Velocity maxima in the slope flow were determined from color slide sequences of dye streaks.

Salinity profiles were plotted from micro-cell data taken at port#6 over t=11-38 min (fig. F-2).'Quasi-instantaneous' profiles were obtained fitting a second order curve through the profile points in the mixed layer (figure F-3) and subtracting the fit from the profile points:

$$S(instant)= S(profile)- S(fit)+ S(t1)$$

The adjusted profiles (figure F-4) show a slope flow depth of 14 to 17 mm, with a rise in salinity of 0.6-0.7 PSS.

Micro-cell data were also taken to check the distribution of salinity in the tank along the bottom slope and along the top under the tray (figure F-5), but a time-series plot of these points (figure F-6) gives insufficient detail about the lateral distribution.

Table F1 lists the computed values of salinities, densities and driving pressures at those times that slope flow velocities were measured, and the volume and salt fluxes derived from them as described in the text (section 2.6).

Table F1. Saltfluxes and flow velocities - sloperun#1

| | | | |
|---|---|---|---|
| From dye seen in slide# | | 12-13 | 17-19,20-21 |
| taken at time (min) | t = | 25 | 30 (lineprinter time) |
| max. velocity (cm/s) | v = | 0.510 | 0.401-0.519 |
| salinity-tray (g/kg) | S2 = | 57.926 | 57.676 from C#3 data fit |
| salinity-mixed layer | S1 = | 20.541 | 21.395 from printer C#2 |
| temperature (°C) T-tank = | | 21.67 | 21.64 thermistor #526 |
| tray density(sigma-t) | D2 = | 41.867 | 41.683 Unesco Eq.of State |
| mixed layer density | D1 = | 13.357 | 14.010 " " |
| driving pressure | P = | 89.50 | 86.87 g*h*(D2-D1)/1000 |
| volume flux (cm/sec) | Vw = | 2.95e-4 | 2.82e-4 from fig.2-15 |
| salt flux (g/cm²/s) | B = | 1.780e-5 | 1.694e-5 |

Figure F-1. MICRO-CELL TIME SERIES PLOT
SLOPE FLOW EXPERIMENT #1

131
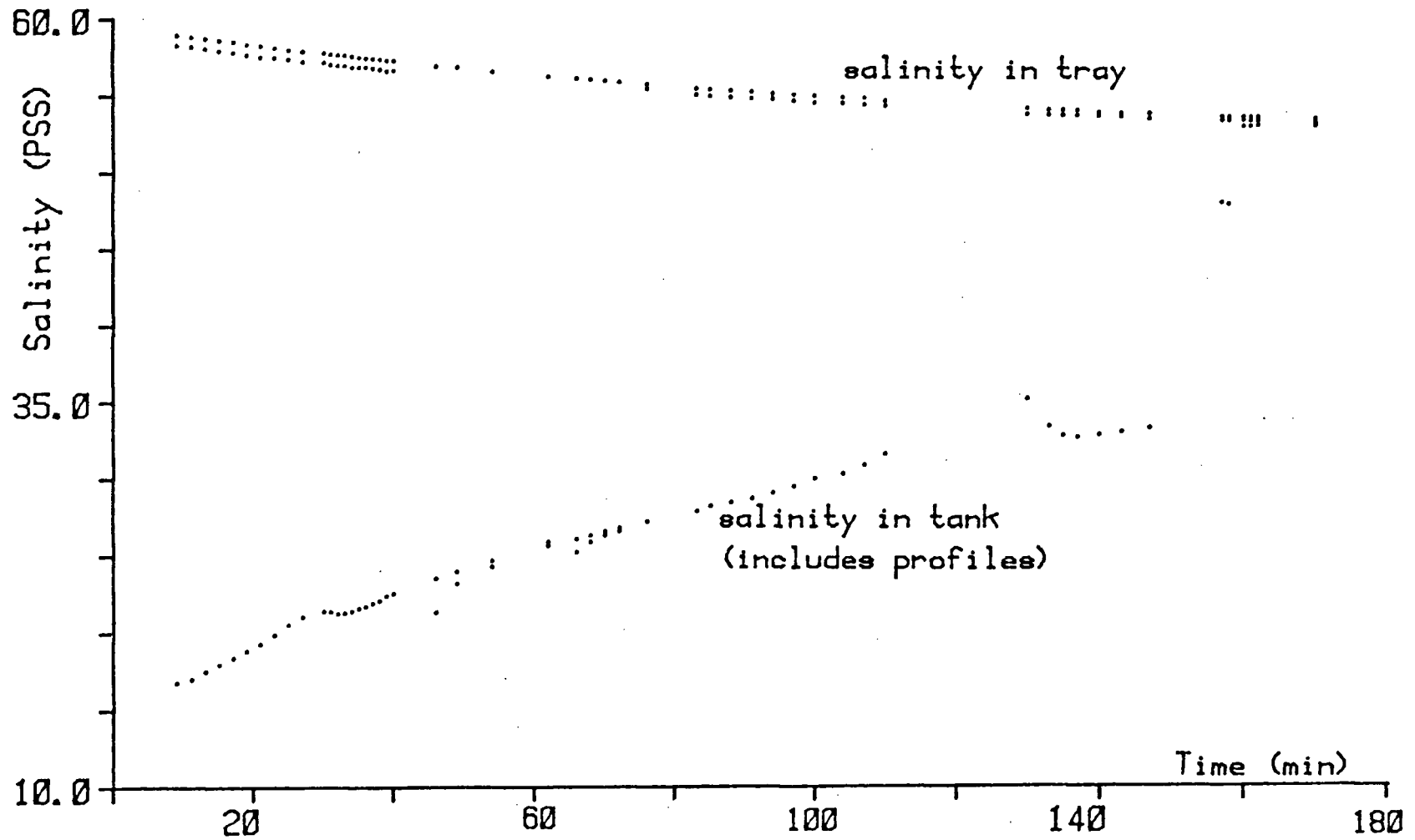
Figure F-2. SALINITY PROFILE
SLOPE FLOW EXP#1

PROFILES IN PORT #6
t=11-27 min going down- 2 min intervals
t=30-38 going up- 1 min intervals

bottom

SLOPE FLOW EXP#1

profile points
(see fig. F-4)

$S(fit)=14.118+ t(0.2874- t*2.1194E-3)$

time-series during profiling

point-wise connected observations
and second order fit to mixed
layer data:

Salinity

time (min)
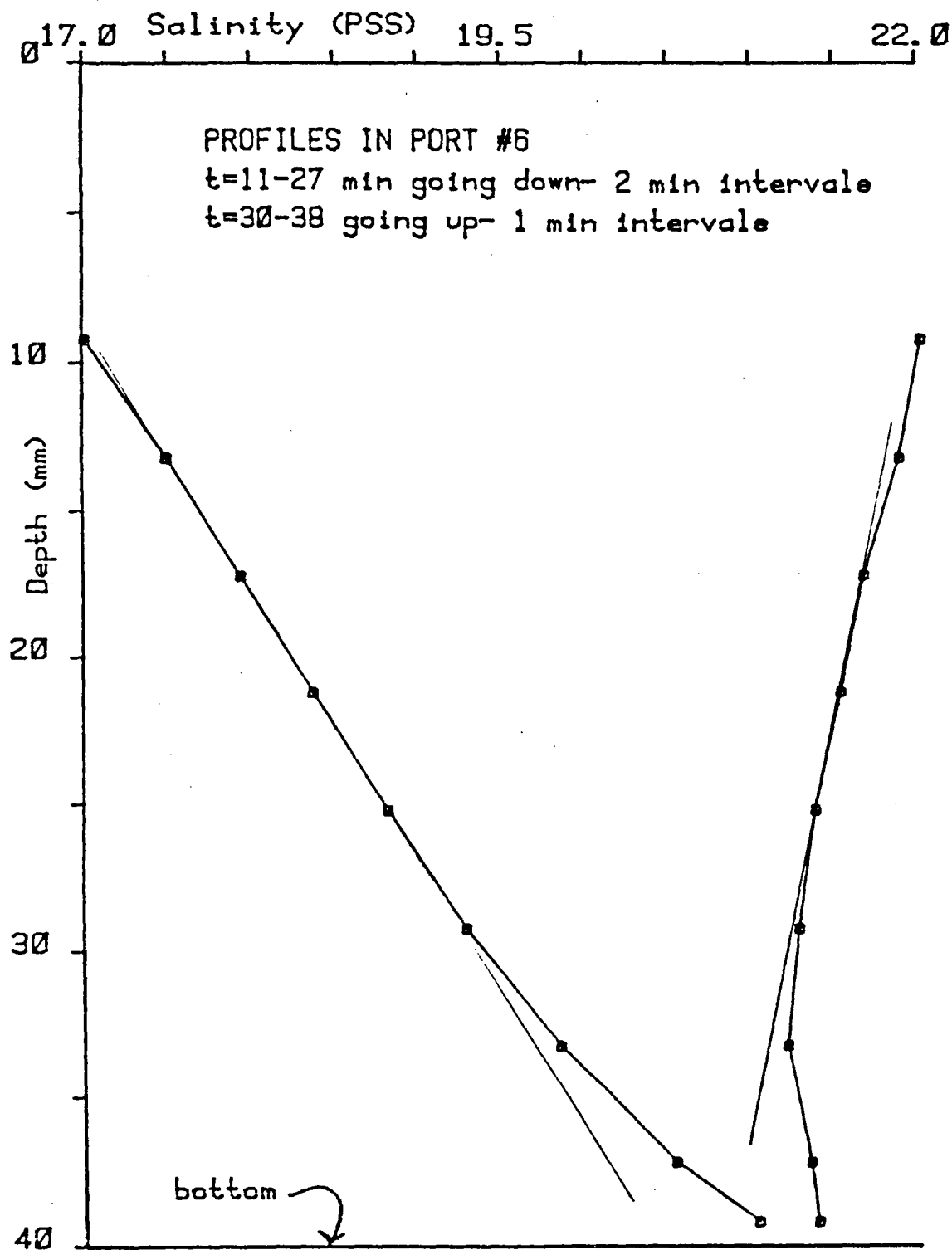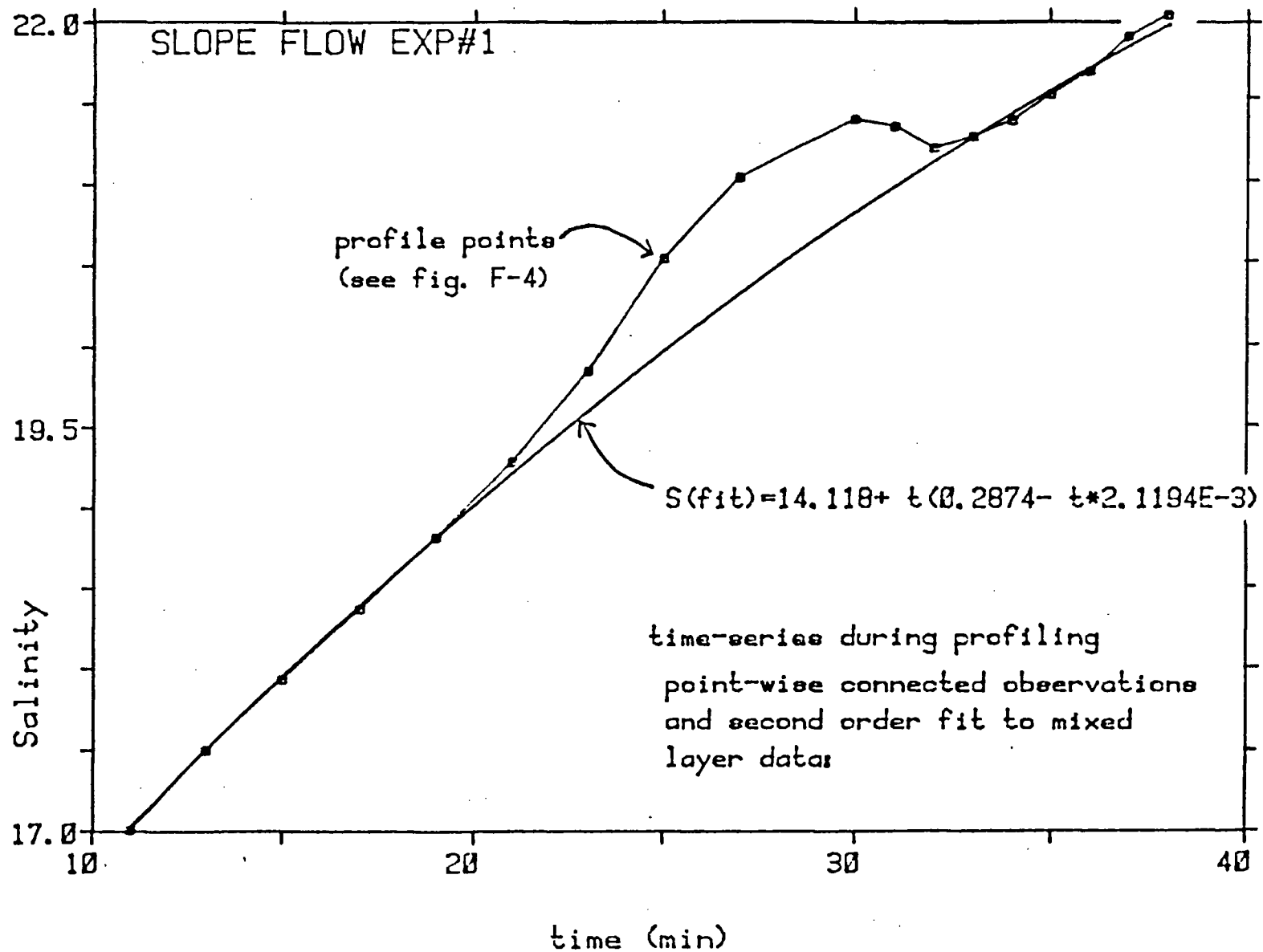
Figure F-3. Time-series plot of profile points.

133

# Figure F-4.    SALINITY PROFILE
## SLOPE FLOW EXP#1



Salinity (PSS)

16.90         17.30              17.70

·Profiles in port #6
t=11-27 going down (o)
t=30-38 going up   (x)

S(profile)=S(actual) − S(t) + S(t0)
S(t)= 14.1185 +t(.28736 −t*.0021194)
(2nd order fit to mixed layer data)
(S(t0)= S(t=11)

bottom

Figure F-5. Distribution.

SLOPE FLOW EXP#1

time-series plot of data from successive port#'s:
x = 5mm below the tray bottom,
o = 2mm above the bottom slope

$S(t)=34.2406+t(-0.23219+t*1.87359e-3)$
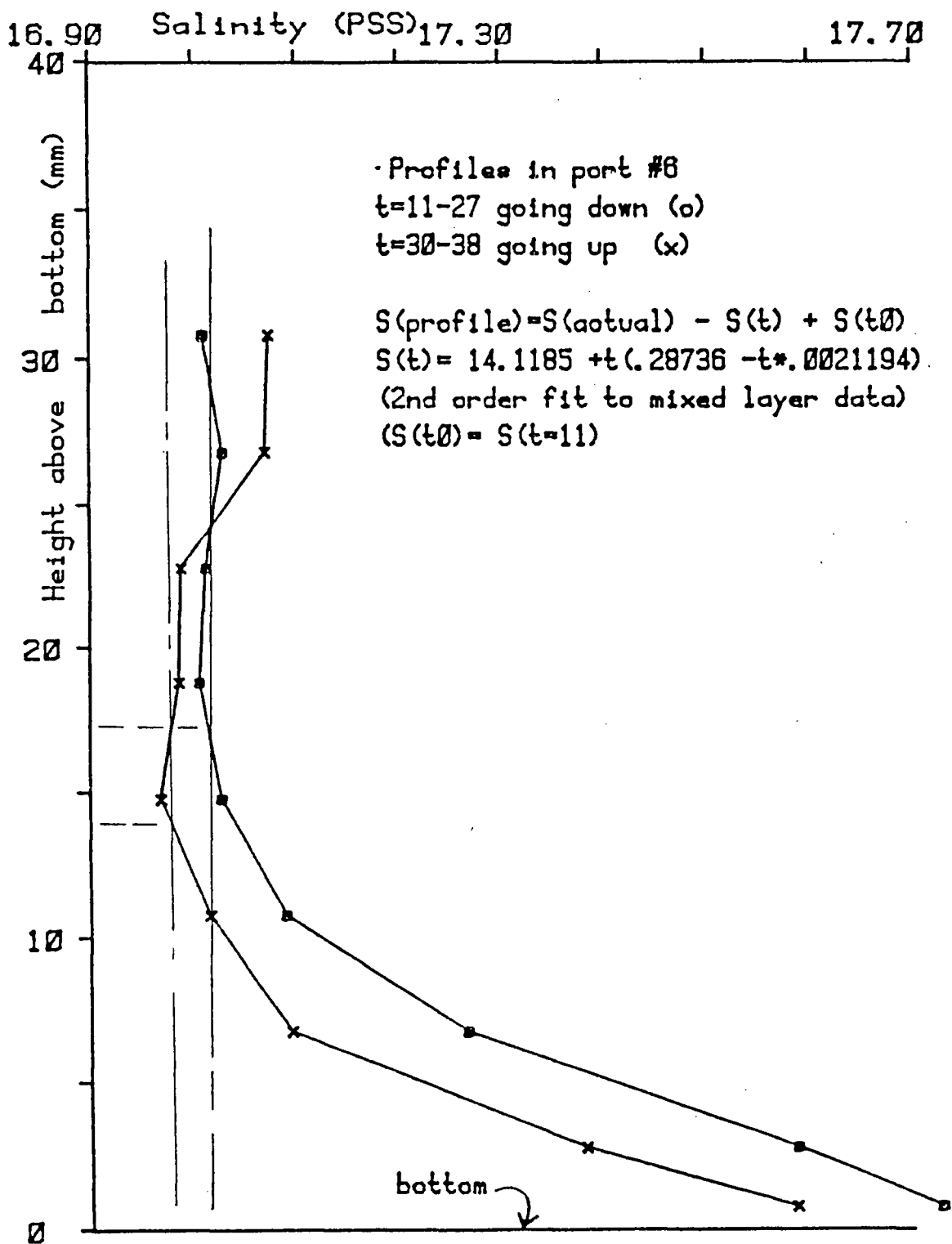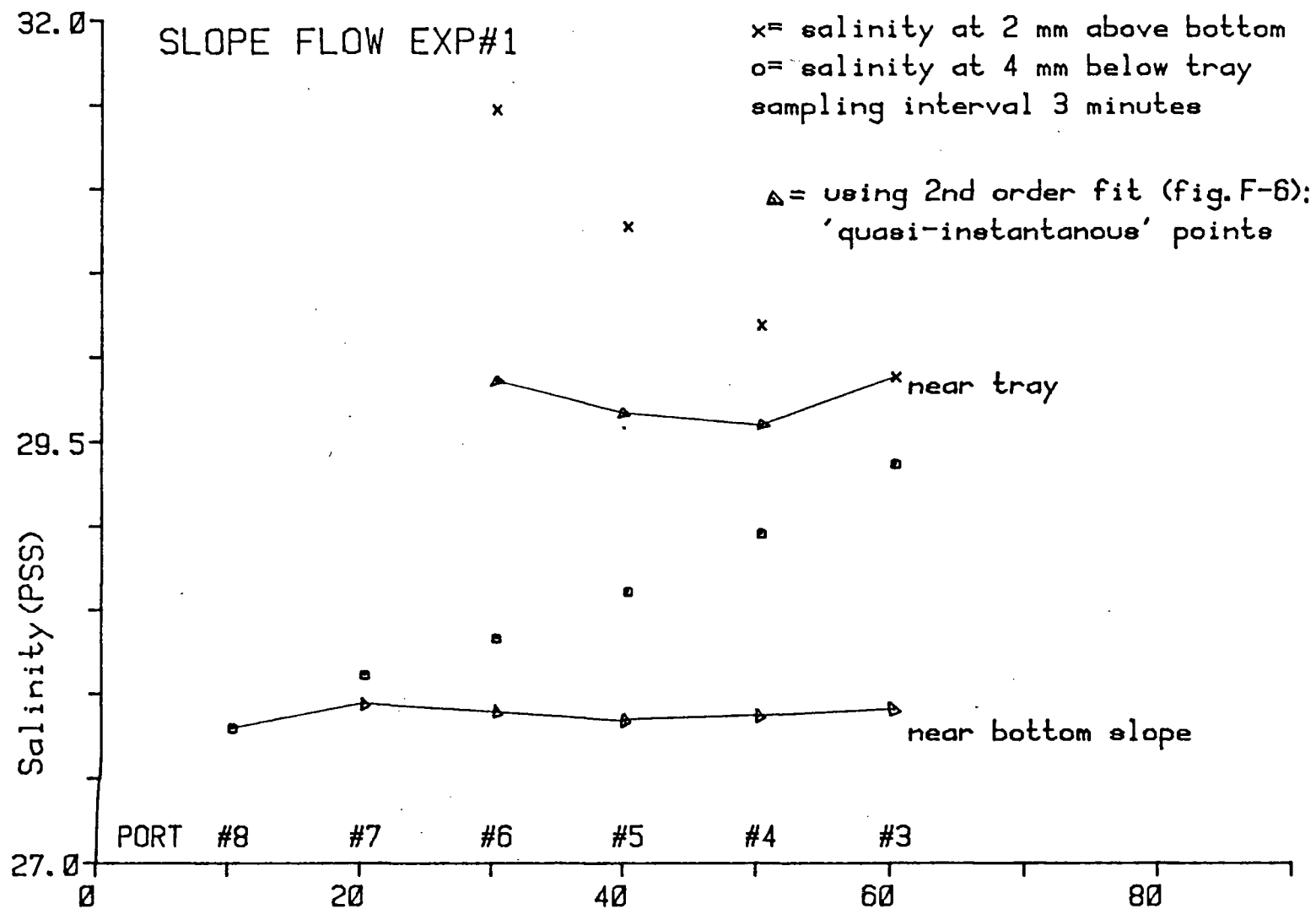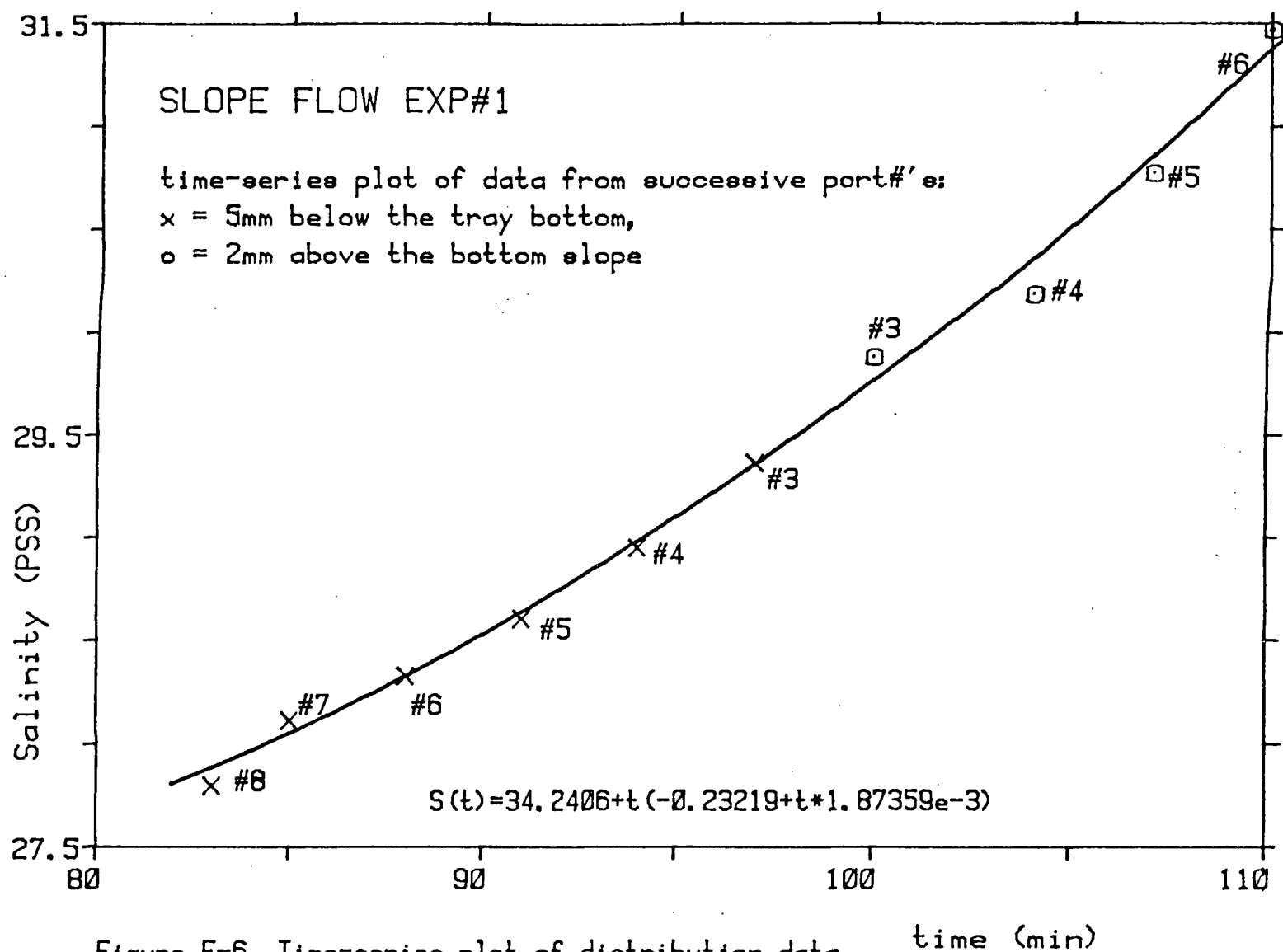
Figure F-6. Time-series plot of distribution data

In slope flow experiment #2, the slope angle was 3.8 degrees and the fluid depth below the tray was 7 mm at the shallow end and 65 mm at the deep end. The AM/CT datalogger was used with micro-cells #1 and #2 to obtain data for fluid in the tank. Profile data were taken in port #6 at t=39-56 min (figure F-9) and at t=112-130 min (figure F-11) after the start. A least squares linear fit to data taken simultaneously with the second micro-cell at fixed depth in the mixed layer (figure F-8, F-10) was used to obtain the quasi-instantaneous profiles. Salinity maxima in the slope flow were 0.4 to 0.5 ppt above those in the mixed layer.

Table F2.   **Flow velocities from photos - sloperun #2**

| Photos #                      :   | 7-10         | 14-17         |
|-----------------------------------|--------------|---------------|
| min after start (clock time):     | 55 (15:25)   | 125 (16:35)   |
| scale  : ports(cm)/photo(mm):     | 20/74        | 30/81.8       |
| dye moved on photo(mm/10sec):     | 16           | 8.5           |
| flow velocity max. (cm/sec) :     | 0.43         | 0.312         |

Tray fluid data were only taken at the start and end of the run. Salinities at other times were estimated from conservation of volume and salt:

$$V1*S1(t)*D1(t)+V2*S2(t)*D2(t)= G(t)$$

in which V1 and V2 were the tank and tray volumes, S1 and S2 the salinity in the mixed layer and in the tray and D1 and D2 corresponding densities. The arbitrary function G(t) represents

137

the salt loss to the bottom flow, and was linearly proportioned over the profiling time. Table F3 shows the salinities computed from data of micro-cell #3, with V1=7.08 and V2=26.5 liters. Table F4 lists the computed salinities, densities and pressures and the derived salt fluxes at the times that flow velocities were determined.

Table F3.  Salinity of tray fluid - sloperun #2

|  | -VC#3 | RT#22 | RT#40 | T(deg.C) | S(ppt) |
|---|---|---|---|---|---|
| start: | 2.217 | 1950 | 1883 | 22.45 | 57.64 |
| t=55 : | (estim.) |  |  |  | 55.21 |
| t=125: | (estim.) |  |  |  | 52.42 |
| end: | 2.026 | 1956 | 1889 | 22.37 | 52.04 |

Table F4.  Saltfluxes and slope flow velocities - sloperun#2

| At time (min) | t[prt]= | 55 | 125 | from: |
|---|---|---|---|---|
| Sal.-mixed layer | S1 = | 15.694 | 25.006 | C#2 print-out |
| Salinity-tray | S2 = | 55.21 | 52.04 | estim.(table F3) |
| temp(deg.C) | T-tnk = | 21.286 | 21.585 | thermistor #526 |
| tray dens(sigma-t) | D2 = | 39.890 | 37.652 | Unesco polynom. |
| dens mix.layer | D1 = | 9.794 | 16.754 | " " |
| driving pressure | P = | 94.48 | 65.60 | (D2-D1)/1000*g*h |
| volume flux (cm/s) | Vw= | 3.17e-4 | 2.00e-4 | from figure 2-15 |
| membrane salt flux | B = | 1.820e-5 | 1.712e-5 | $B=F*S2*(\frac{D2}{1000}+\frac{1}{1000})$ |
| max.flow velocity | v = | 0.43 | 0.312 | (cm/sec) |

Figure F-7. MICRO-CELL TIME SERIES PLOT
SLOPE FLOW EXPERIMENT #2

solid line connects mixed layer points
indiv. pts include profile data

139
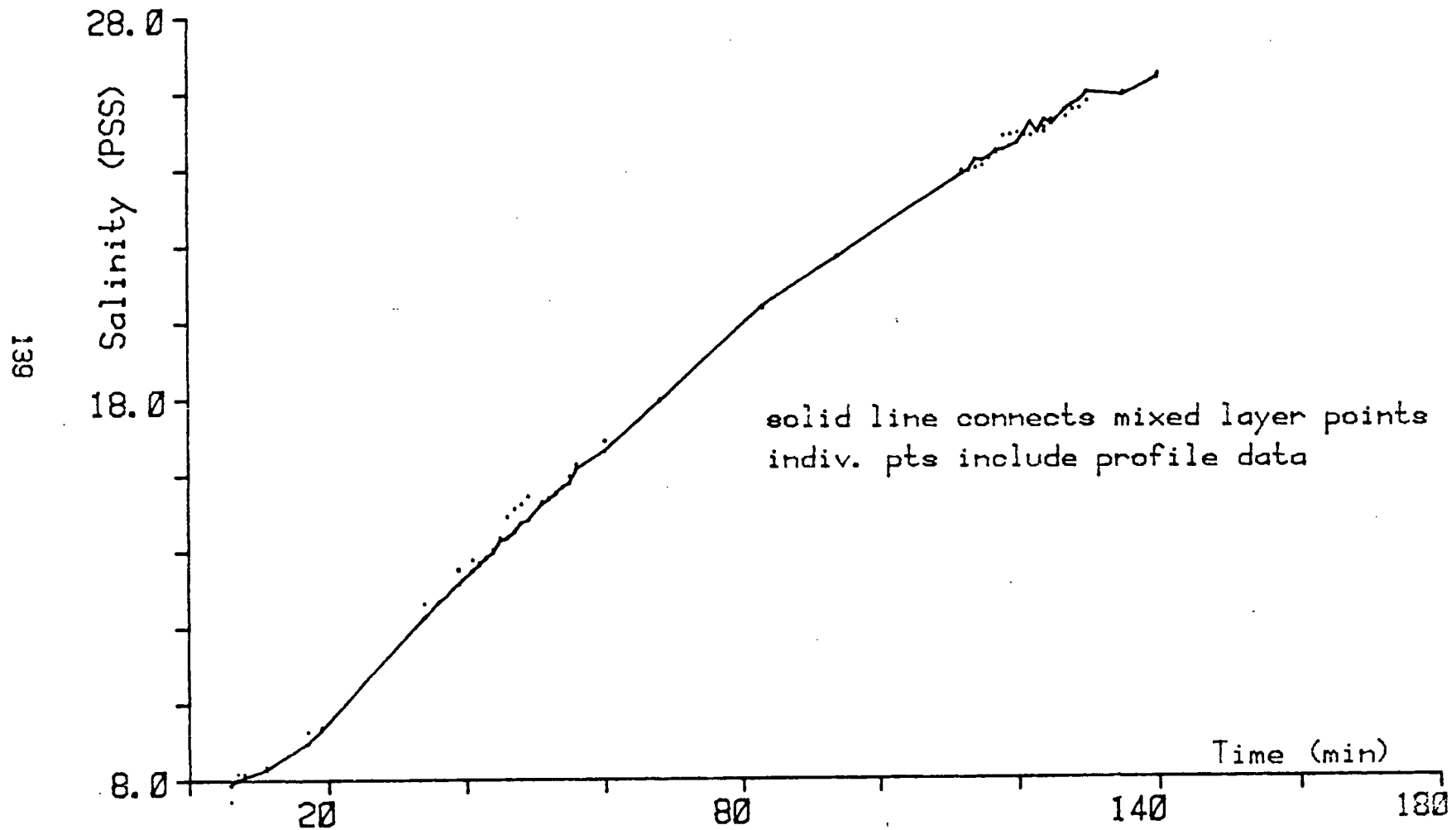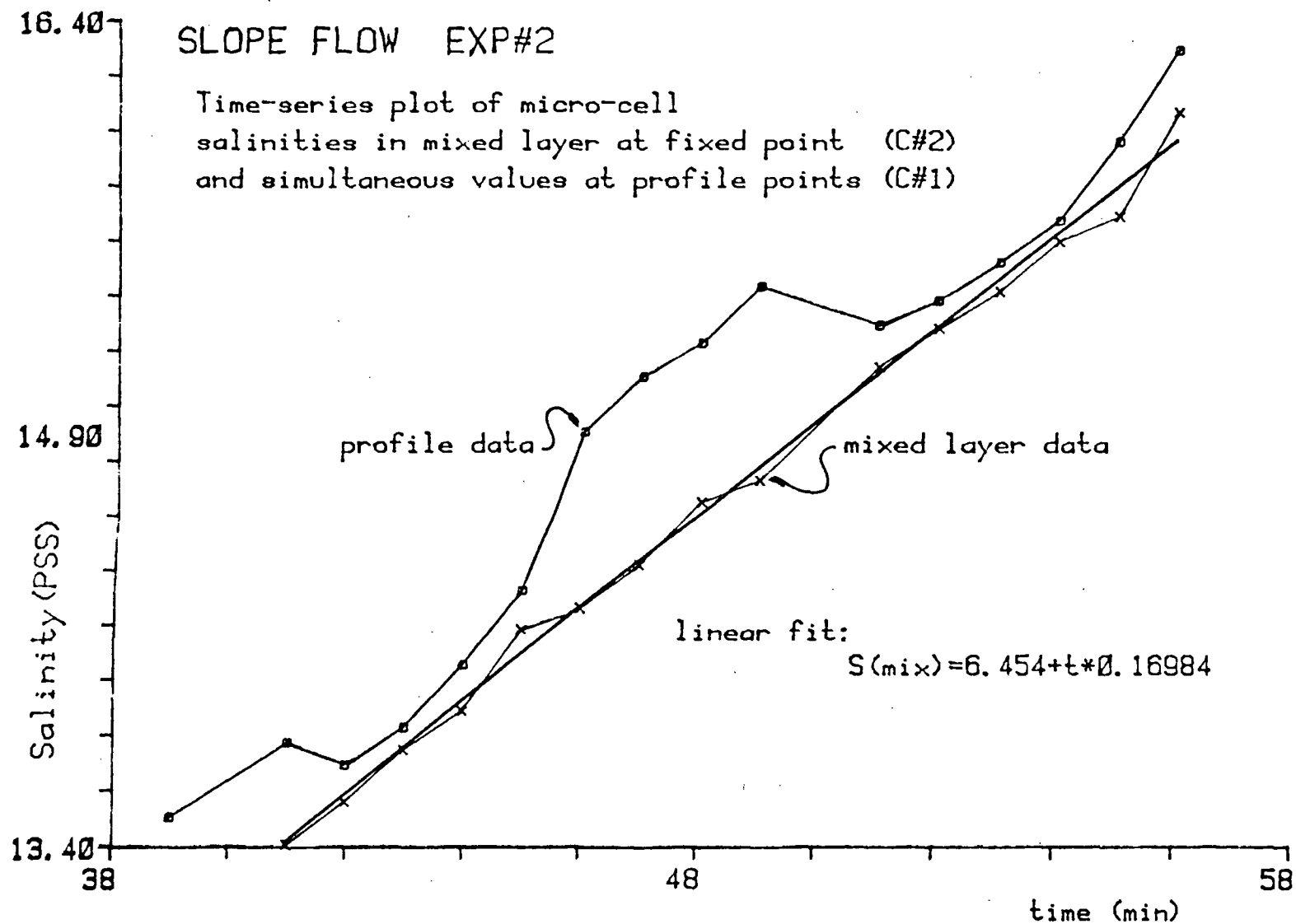
Figure F-8. Time-series and linear fit

Figure F-9. SALINITY PROFILE
6-3-86 SLOPERUN #2

SALINITY (PSS)

13.00    14.60    16.20

DEPTH (mm)

PORT #6
time=39-56
x =actual profile
o =fixed depth backgnd
+ =adjusted profile
   (linear fit)

bottom

Figure F-10. Time-series and linear fit

Text within the figure:

SLOPE FLOW EXP#2

Salinity from data at fixed depth in
mixed layer used to adjust profile

x = calculated salinity C#2
straightline = least squares
linear fit:
S = 11.1487 +.11222*t

SALINITY (PSS)

time (min)

142

Figure F-11.  SALINITY PROFILE
6-3-86 SLOPERUN #2

t = 112-130

PORT #6
x = actual
    profile
o = mixed
    layer
+ = adjusted
   (linear fit)
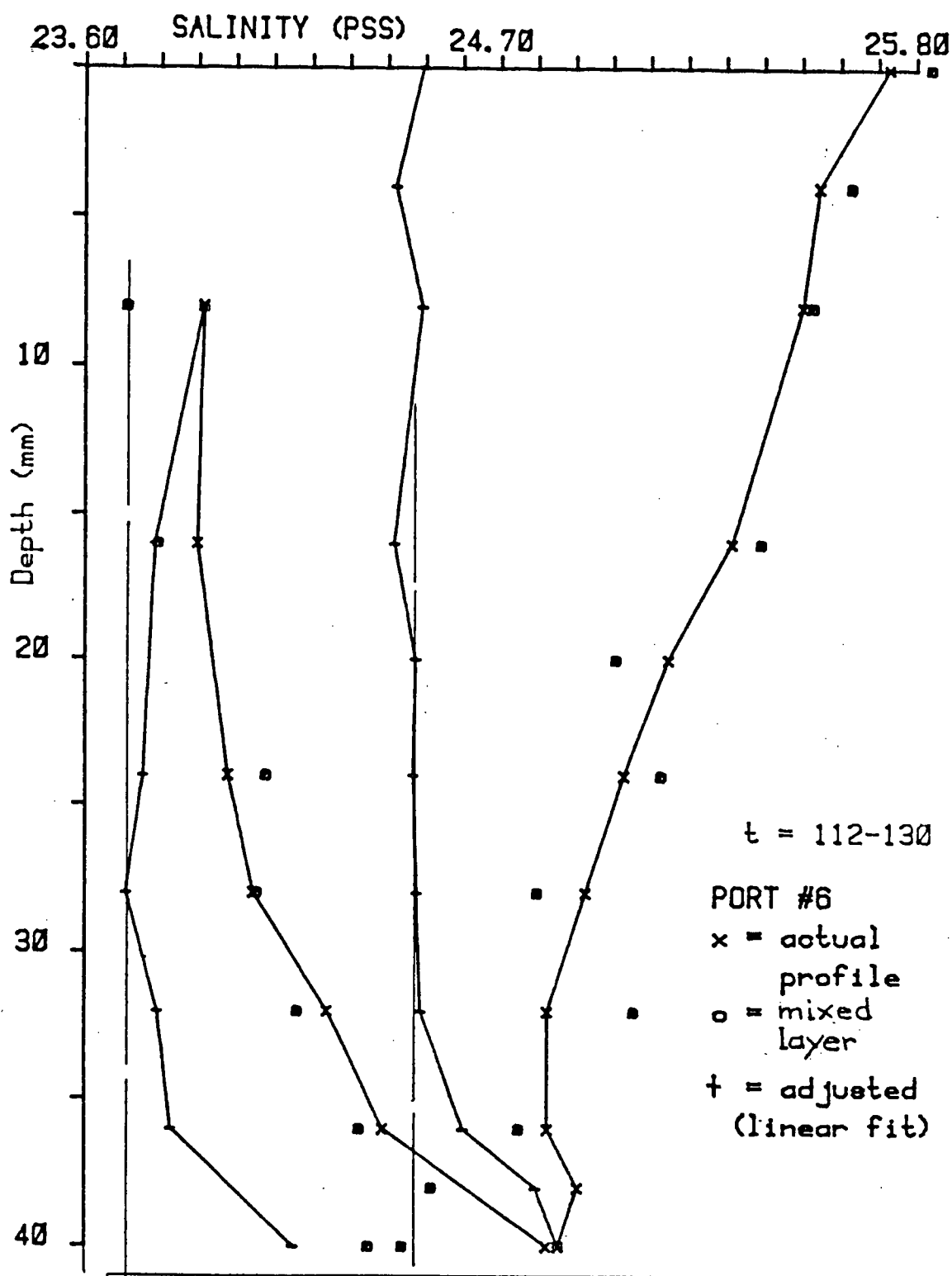
In slope flow experiment #3 the slope angle was 2.2 degrees. The depth below the tray was 20 mm at the shallow end and 51 mm at the deep end. The AM/CT Datalogger was used with micro-cell #1 for profiles,with micro-cell #2 fixed at 15mm below the tray for salinities in the mixed layer and with thermistor #526 for temperatures in the tank. Salinities in the tray were computed from volt-meter readings of micro-cell #3.

After filling the tray to start the experiment, the tank was briefly stirred to remove circulation patterns which might have been formed by uneven flux during the filling. The slope flow re-established itself within one minute, starting at about 30cm from the shallow end. A counter-rotating flow cell, also found in the previous experiment, was seen in the shadowgraph upslope from this point. This uphill flow disappeared when the starting point of the down-slope flow moved slowly towards the shallow end. Sketches of the typical flow patterns and the double flow cells are included in the text.

Salinity profile data were taken in port #8 at t=105-129 min after the start. A linear fit to salinities computed from data taken at a fixed depth in the mixed layer during the profiling (figure F-13) was used to obtain 'quasi-instantaneous' profiles (figure F-14). These show the convectively mixed layer and a sharp rise in salinity of 0.8 PSS starting at 12-18 mm above the bottom. Maxima in the slopeflow velocity were measured from the distance dye moved in photo sequences.

Table F5.  Flow velocities from photos - sloperun #3

min after start  (clock time):      60 (10:30)       135 (11:45)

dist. dye moved on photo (mm):      11-11.5          10.5-11.0

time between photos        :        11.5             12.5

slopeflow velocity (cm/sec) :       0.259-0.270      0.227-0.238


Table F6.  Saltflux and slopeflow velocity - sloperun #3

lineprinter time    = 60        135          min. after start

mixed layer    S1 = 21.561      29.106       (PSS)time-series fit

tray salinity  S2 = 54.583      52.695       (PSS)time-series fit

temperature T-tnk = 21.420      21.877       (°C) thermistor #526

tray density   D2 = 39.366      37.775       (sigma-t)Unesco eqn.

tank density   D1 = 14.192      19.781           "              "

pressure        P = 81.50       58.25        (gr/cm/s²)

volume flux    Vw = 2.50e-4     1.67e-4      (cm/s) flux cal.plot

membr.salt flux B = 1.418e-5    0.946e-5     gr/cm2/s

slopeflow   max. v =0.259-0.270  0.227-0.238  cm/s    from photos

Figure F-12. MICRO-CELL TIME SERIES PLOT
SLOPE FLOW EXPERIMENT #3

line connects points from
C#2 (mixed layer, fixed)

146
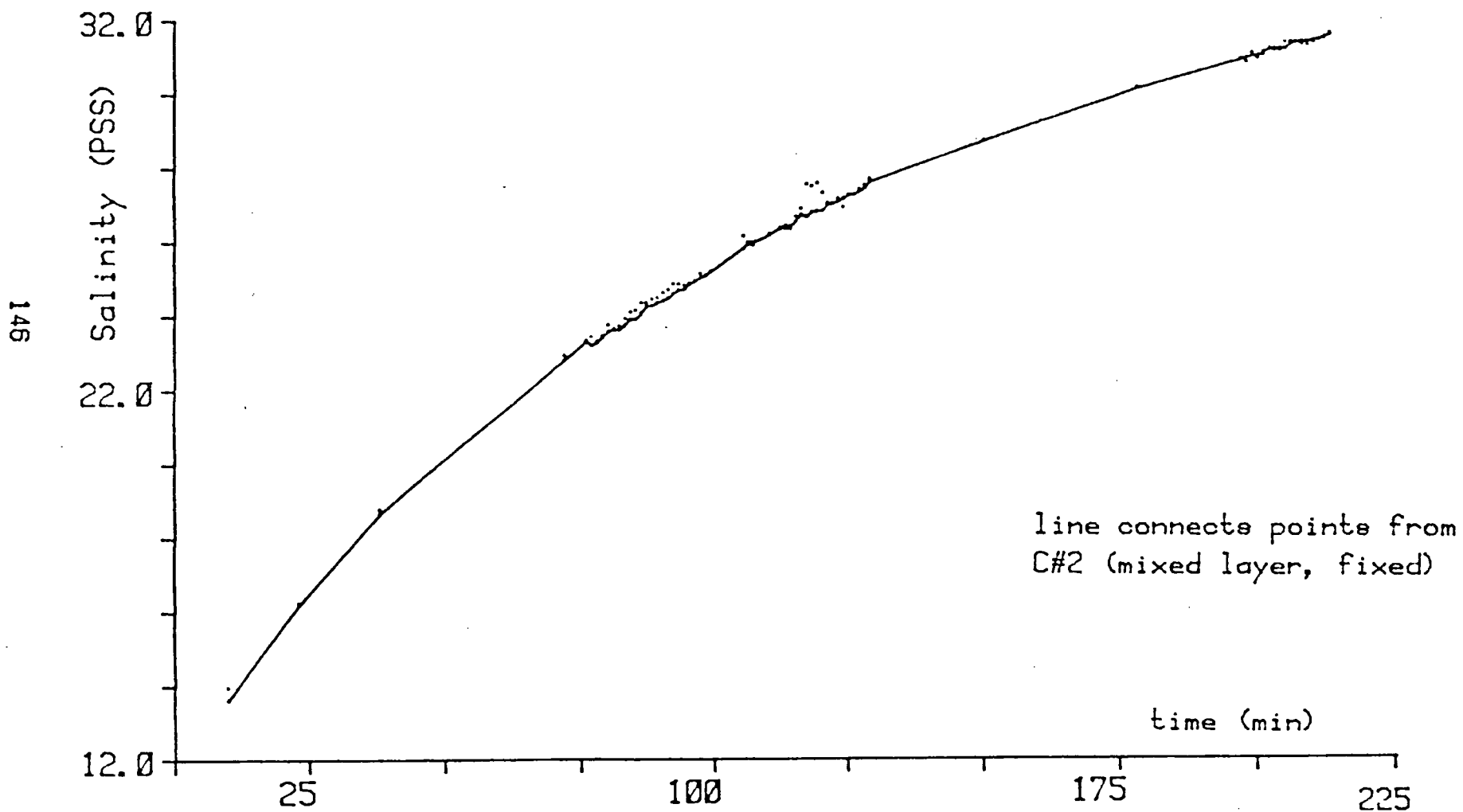
11-3-86 SLOPE RUN #3 background salinity
during profiling

Figure F-13.

linear fit: S(t)=25.5008+.0695(t-100)

time ( min )

105                                                              130

147
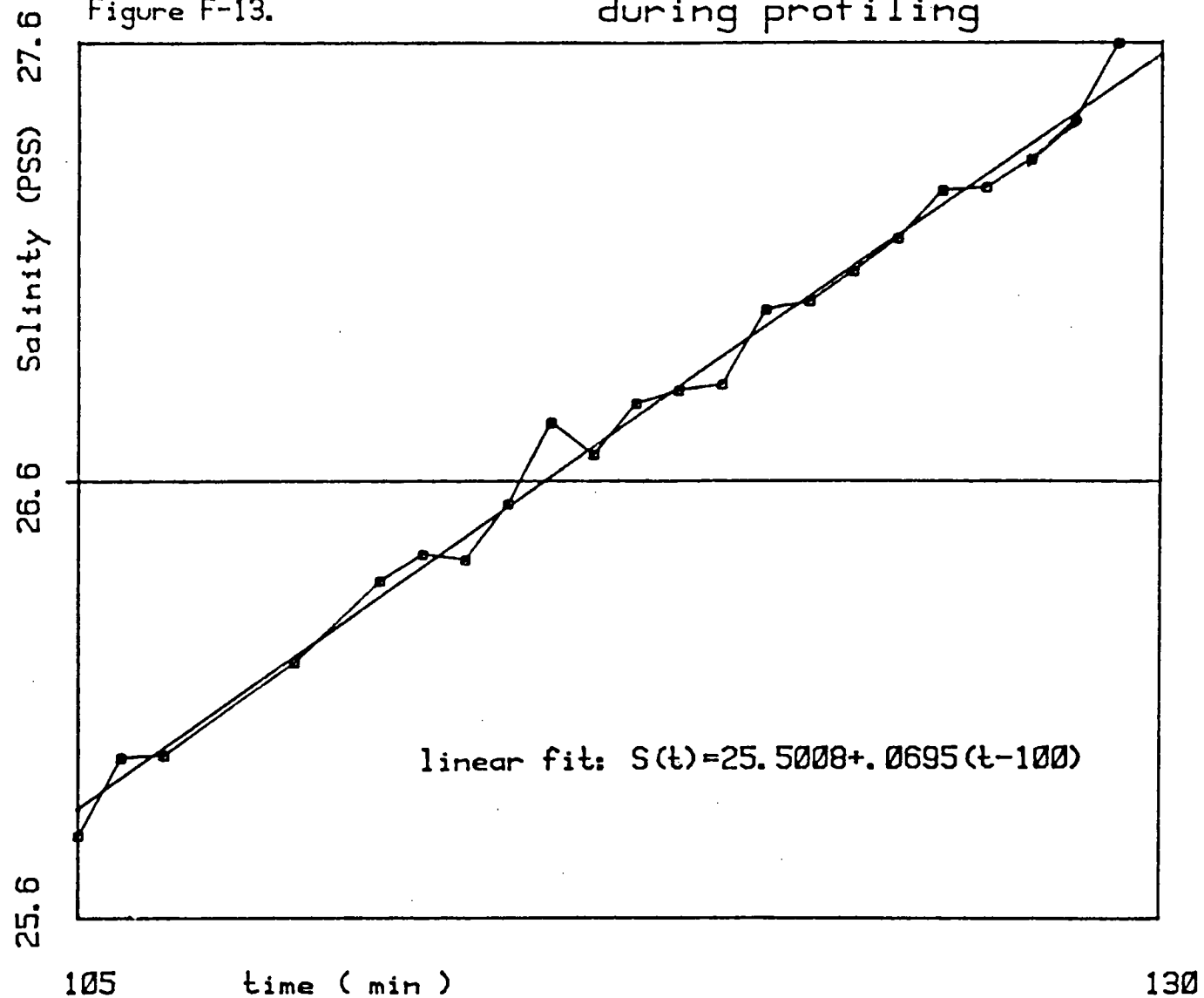
Figure F-14. SALINITY PROFILE
11-3-86 SLOPERUN #3

PORT #8

SALINITY (PSS)

actual profiles
adjusted profiles by
linear fit to data
from fixed depth

DEPTH (mm)
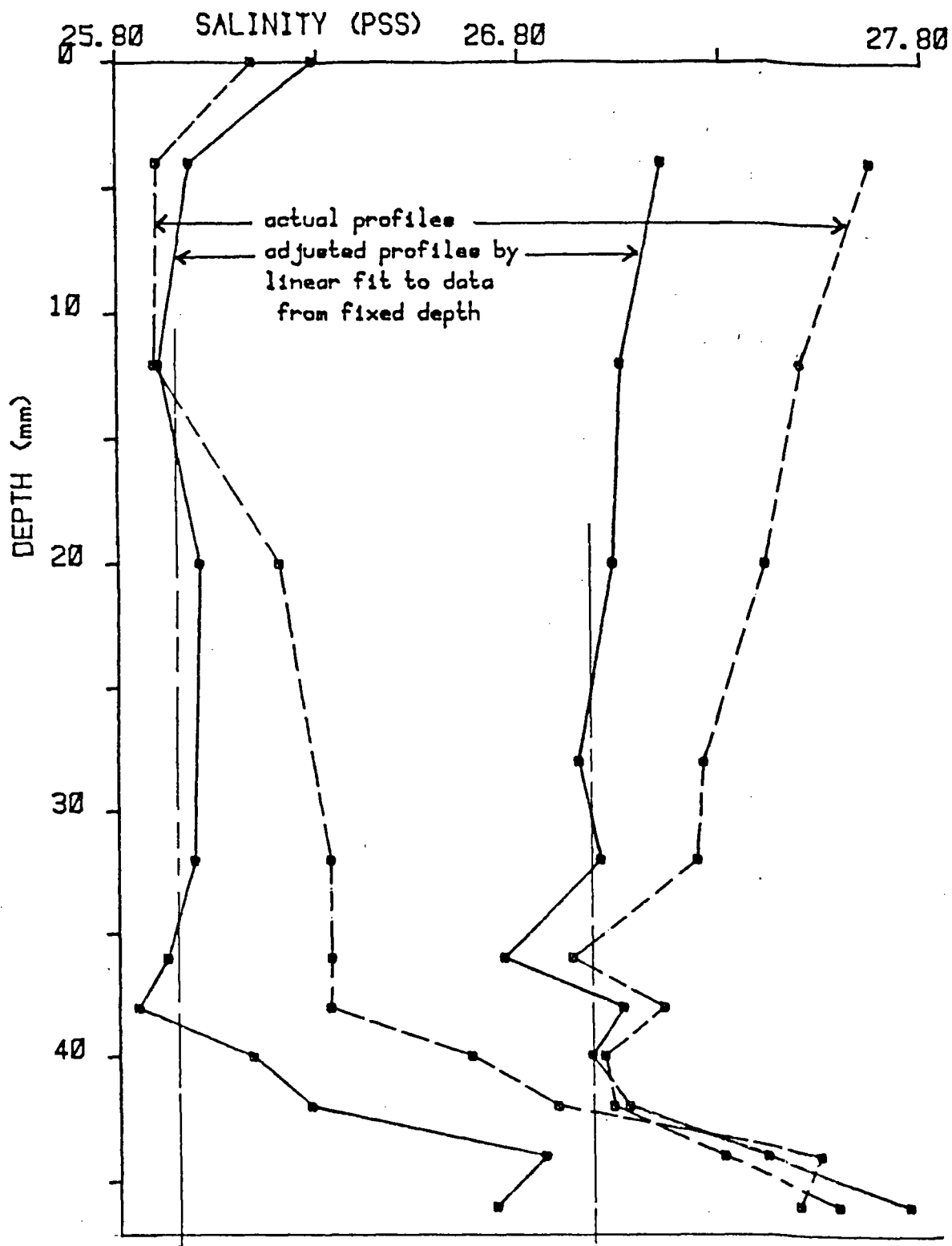
In slope flow experiment #4, the slope angle was 5.2 degrees. The depth below the tray was 2 cm at the shallow end and 10 cm at the deep end. The AM/CT Datalogger was again used with micro-cells #1 and #2 and with the tank thermistor, and digital voltmeters were used with micro-cell #3 to monitor the salinity of fluid in the tray.

Table F7.  Salinities in the tray - sloperun #4

| time | min | -VC#3 | RT#22 --> | T(°C) | S(ppt) |
|------|-----|-------|-----------|-------|--------|
| 15:00 | 30 | 2.012 | 2000 | 21.746 | 52.381 |
| 15:23 | 53 | 1.982 | 2006 | 21.662 | 51.585 |
| 15:37 | 68 | 1.967 | 2008 | 21.634 | 51.171 |
| 15:55 | 85 | 1.947 | 2011 | 21.592 | 50.623 |
| 16:17 | 107 | 1.927 | 2012 | 21.578 | 50.043 |
| 16:40 | 130 | 1.907 | 2014 | 21.550 | 49.480 |
| 16:55 | 205 | 1.899 | 2013 | 21.564 | 49.226 |
| 17:25 | 235 | 1.880 | 2007 | 21.648 | 48.566 |

Salinity profiles were plotted from data taken in port #5 over t=97-131 min after the start, corrected for the salinity change in the mixed layer (figure F-16). Data were also taken along the bottom of the tank at port #8 through #2 and back to port #7. Three data points were taken in rapid succession in each port at about 2 mm above the bottom, and the pointwise time-corrected averages were plotted (figure F-17).

The slopeflow velocities were measured from video footage of dye carried along by the bottom flow, using the 10 cm spacing of sampling ports in the tray for scale where visible or taking the average of vertical lines at the back (spaced 5 cm) and the units on a scale along the front of the tank.

Table F8.  Flow velocities and saltfluxes - sloperun #4

| At clock time = | 14:50 | 15:21 | 16:12 | 16:48 | hr:min |
|---|---|---|---|---|---|
| lineprinter t = | 20 | 50 | 102 | 138 | min |
| tray fluid S2= | 52.708 | 51.585 | 50.175 | 49.3445 | ppt |
| mixed layer S1= | 7.011 | 9.557 | 12.720 | 14.847 | ppt |
| tank temp. T = | 21.053 | 21.392 | 21.639 | 21.715 | °C |
| tray dens. D2 = | 38.033 | 37.068 | 35.911 | 35.252 | sigma-t |
| tank dens. D1 = | 3.295 | 5.138 | 7.464 | 9.049 | sigma-t |
| pressure P = | 112.5 | 103.4 | 92.09 | 84.83 | gr/cm/s$^2$ |
| volume flux Vw= | 4.00e-4 | 3.50e-4 | 3.00e-4 | 2.67e-4 | cm/s |
| salt flux B = | 2.19e-5 | 1.87e-5 | 1.56e-5 | 1.36e-5 | gr/cm$^2$/s |
| max.flowspeed = | 0.45-0.49 | 0.45-0.49 | 0.39-0.41 | 0.33-0.36 | cm/s |

Figure F-15. SALINITY PROFILE
SLOPE RUN #4
Port #5 t= 97-111 min
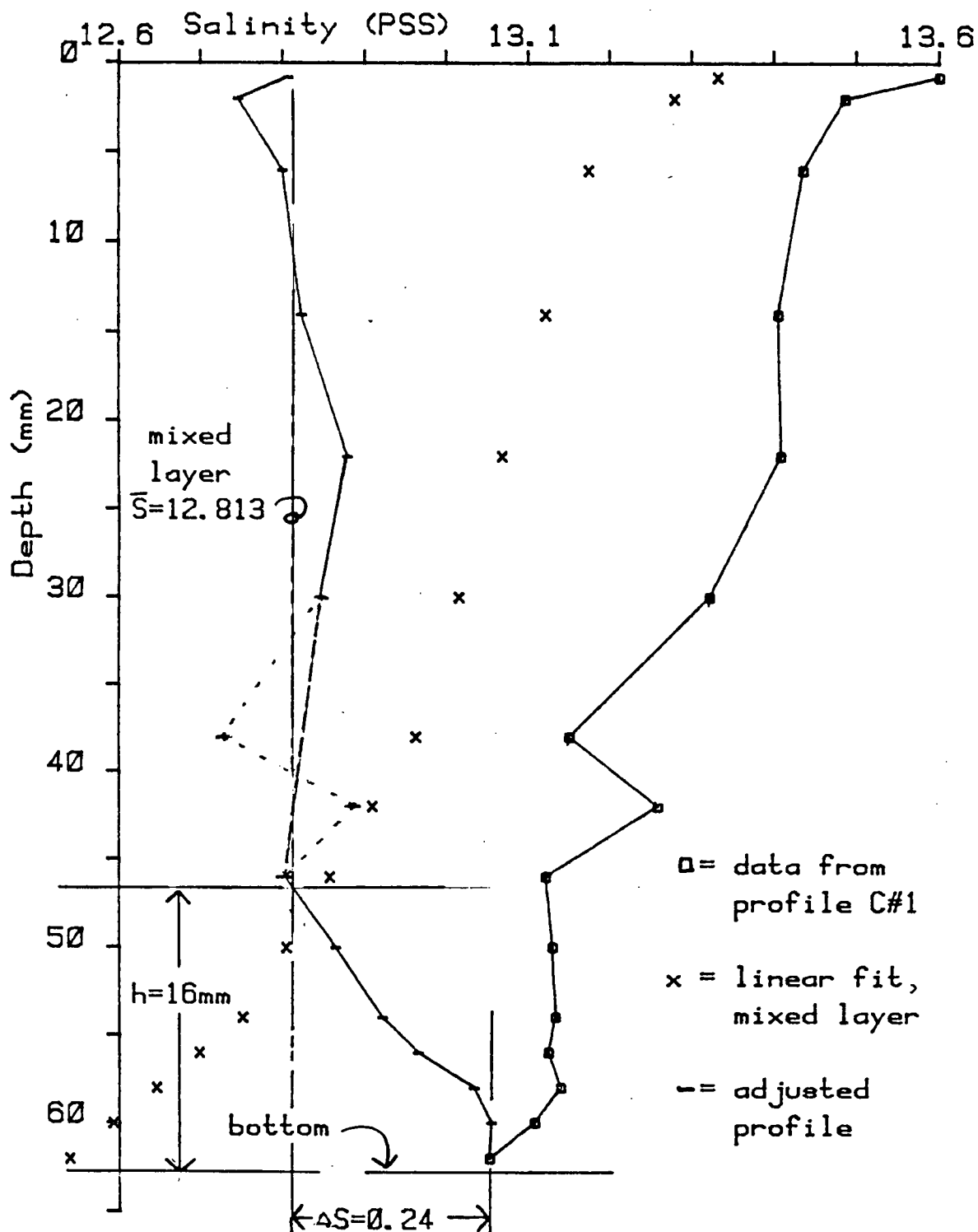
Figure F-16. SALINITY PROFILE
SLOPE RUN #4
Port #5   t=111-126 min
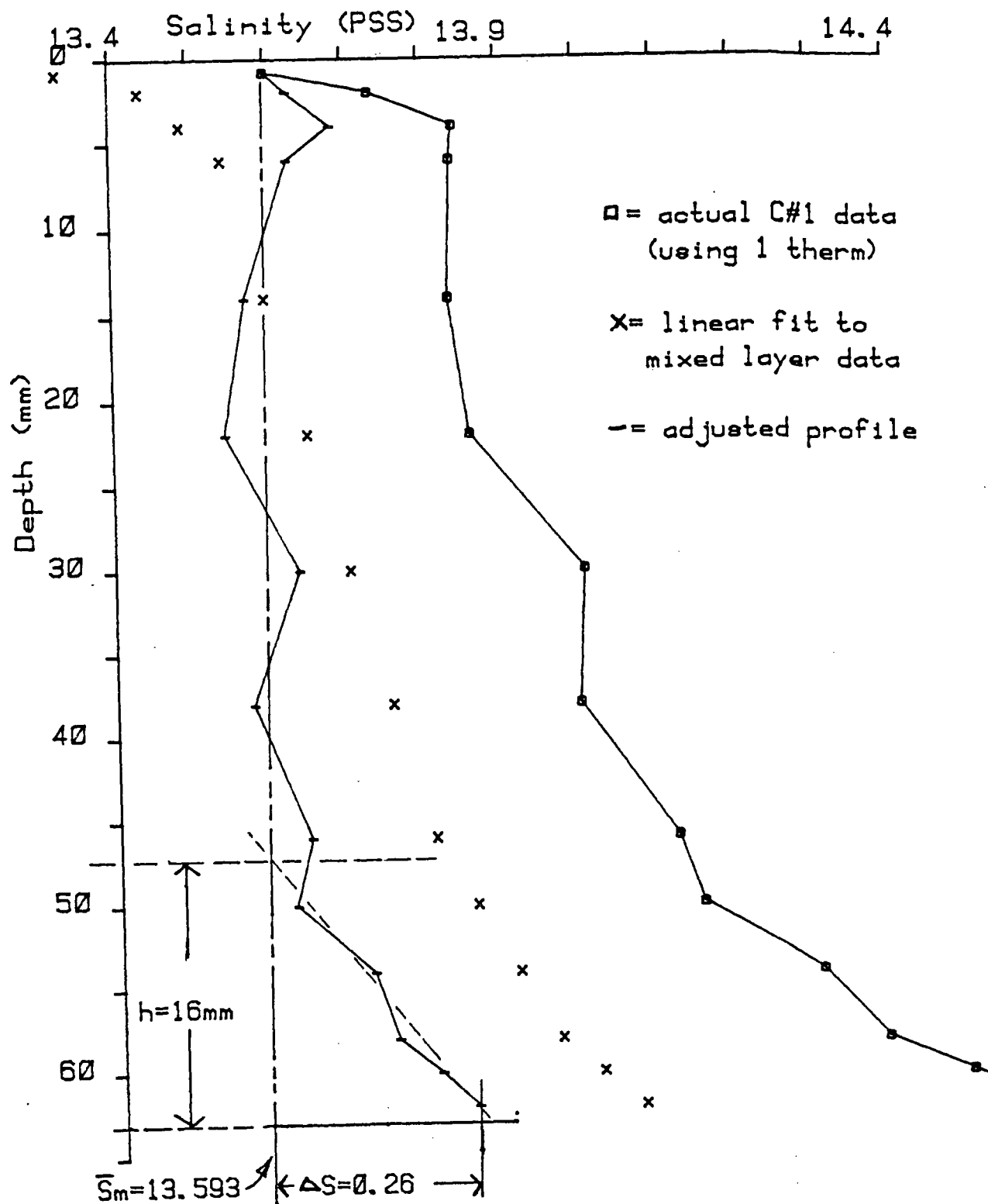
$\bar{S}_m = 13.593$   $\leftarrow \Delta S = 0.26 \rightarrow$

h=16mm

□ = actual C#1 data
(using 1 therm)

X = linear fit to
mixed layer data

— = adjusted profile
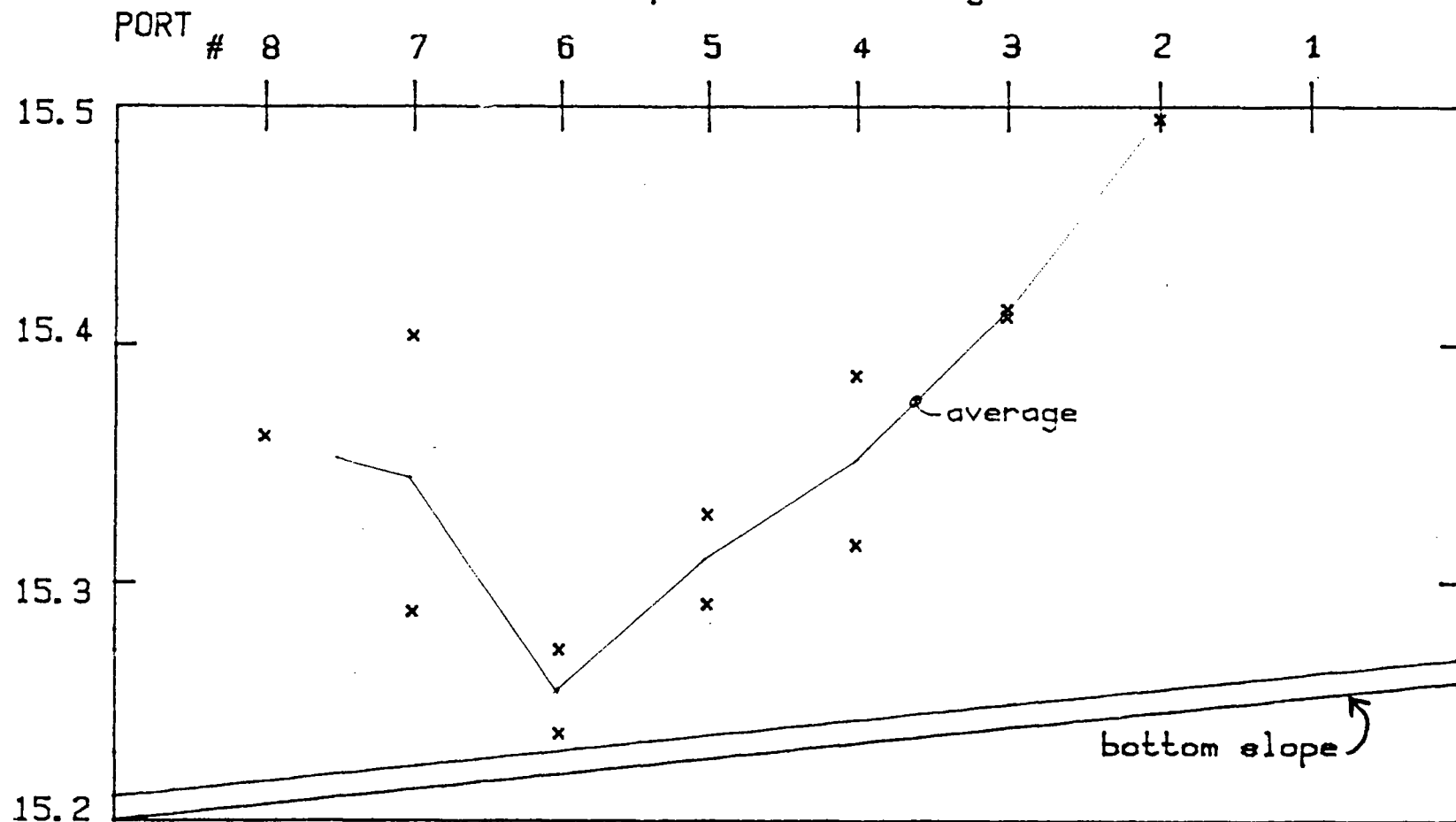
Figure F-17. Salinity distribution along bottom slope.

153

In this experiment the slope angle was again 5.2 degrees and
the depth 2 cm at the shallow end and 10 cm at the deep end.  A
new  membrane was installed in the tray.  Micro-cells #1 and #2
were  connected  to the AM/CT datalogger and cell #3  was  used
with the DVM's for tray. Starting salinities were 52 ppt in the
tray and 13 ppt in the tank.

Table F9.      Salinities in the tray during sloperun #5

| time | min | -VC3 | RT#44 | RT#23 | T-avg | S(K=1782) |
|---|---|---|---|---|---|---|
| 12:30 | 30 | 1.9961 | 2497 | 2059 | 21.644 | 52.030 |
| 12:40 | 40 | 1.9659 | 2496 | 2058 | 21.656 | 51.110 |
| 12:50 | 50 | 1.9336 | 2496 | 2058 | 21.656 | 50.147 |
| 13:01 | 61 | 1.9100 | 2494 | 2056 | 21.679 | 49.416 |
| 13:10 | 70 | 1.8942 | 2494 | 2056 | 21.679 | 48.948 |
| 13:30 | 90 | 1.8610 | 2494 | 2056 | 21.679 | 47.967 |
| 13:40 | 100 | 1.8449 | 2494 | 2056 | 21.679 | 47.492 |
| 14:03 | 123 | 1.8160 | 2496 | 2057 | 21.663 | 46.663 |
| 14:20 | 140 | 1.7971 | 2496 | 2058 | 21.656 | 46.116 |
| 14:50 | 170 | 1.7711 | 2496 | 2058 | 21.656 | 45.356 |
| 15:32 | 212 | 1.7418 | 2498 | 2060 | 21.631 | 44.528 |
| 16:20 | 260 | 1.7222 | 2502 | 2063 | 21.589 | 44.002 |
| 16:30 | 270 | 1.7203 | 2501 | 2062 | 21.601 | 43.934 |
| 17:00 | 300 | 1.7111 | 2500 | 2063 | 21.600 | 43.668 |

Salinity profiles from data taken in port #5 at t=80-97  min
(figure  F-19) and in port #3 at t=125-141 min after the  start

(figure F-20) were made instantaneous by subtracting the change in simultaneously taken mixed layer salinities. They show a well mixed convective layer and a slope flow region of 9 to 15 mm thickness where the salinity increases by about 0.3 PSS. Another profile was plotted from data taken in the edge space between tank and tray (figure 2-12 in text).

Shadowgraph images and motions of injected dye were recorded on videotape during part of this run. This includes footage of the counter-cell which formed upslope from the place where the bottom flow first established itself.

Velocity maxima in the flow were measured from videotape footage, and the temperature and salinity of fluid in the mixed layer and in the tray at those times were obtained by linear interpolation of the time-series data of calculated values.

Table F10.  Flow velocities and saltfluxes - sloperun #5

| clock time  t = | 13:11 | 200(15:20) | 16:21 | 16:42 | hr:min |
|---|---|---|---|---|---|
| printer  t(p) = | 71 | 200 | 261 | 282 | min |
| trayfluid  S2 = | 48.948 | 44.765 | 43.995 | 43.828 | PSS |
| mix.layer  S1 = | 15.835 | 24.773 | 26.406 | 26.915 | PSS |
| temp    T-tnk = | 21.568 | 21.843 | 21.863 | 21.872 | deg.C |
| tray dens  D2 = | 34.991 | 31.707 | 31.112 | 30.982 | sigma-t |
| tank dens  D1 = | 9.831 | 16.510 | 17.740 | 18.123 | sigma-t |
| pressure    P = | 81.45 | 49.20 | 43.29 | 41.63 | g/cm/s² |
| vol.flux  Vw = | 2.50e-4 | 1.35e-4 | 1.25e-4 | 1.22e-4 | cm/min |
| membr.flux  B = | 1.267e-5 | 0.623e-5 | 0.567e-5 | 0.551e-5 | gr/cm²/s |
| slopeflow    v = | 0.474-0.665 | 0.269-0.279 | 0.248-0.312 | 0.259-0.273 | cm/s |

Figure F-18.  MICRO-CELL TIMESERIES
18-3-86 SLOPERUN #5 d=2-10 K1,2=1878,1793 new membr
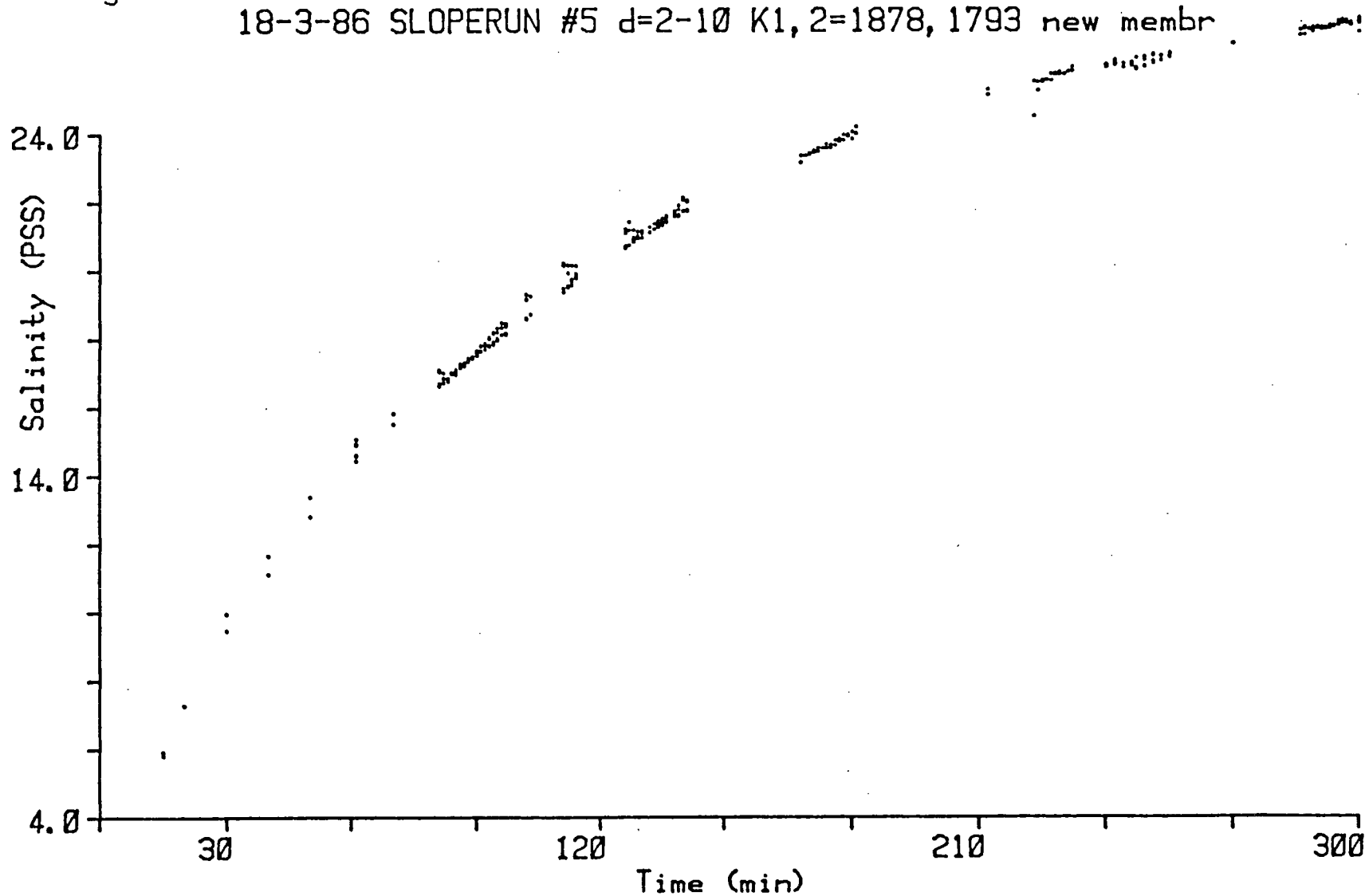
# SALINITY PROFILE
## 18-3-86 SLOPERUN #5

Figure F-19:

SALINITY (PSS)

PORT #5

t≈82-87 (13:20-13:37)
x - actual profile data
o - fixed depth backgnd
♠ - corrected profile
(pointwise diff.)
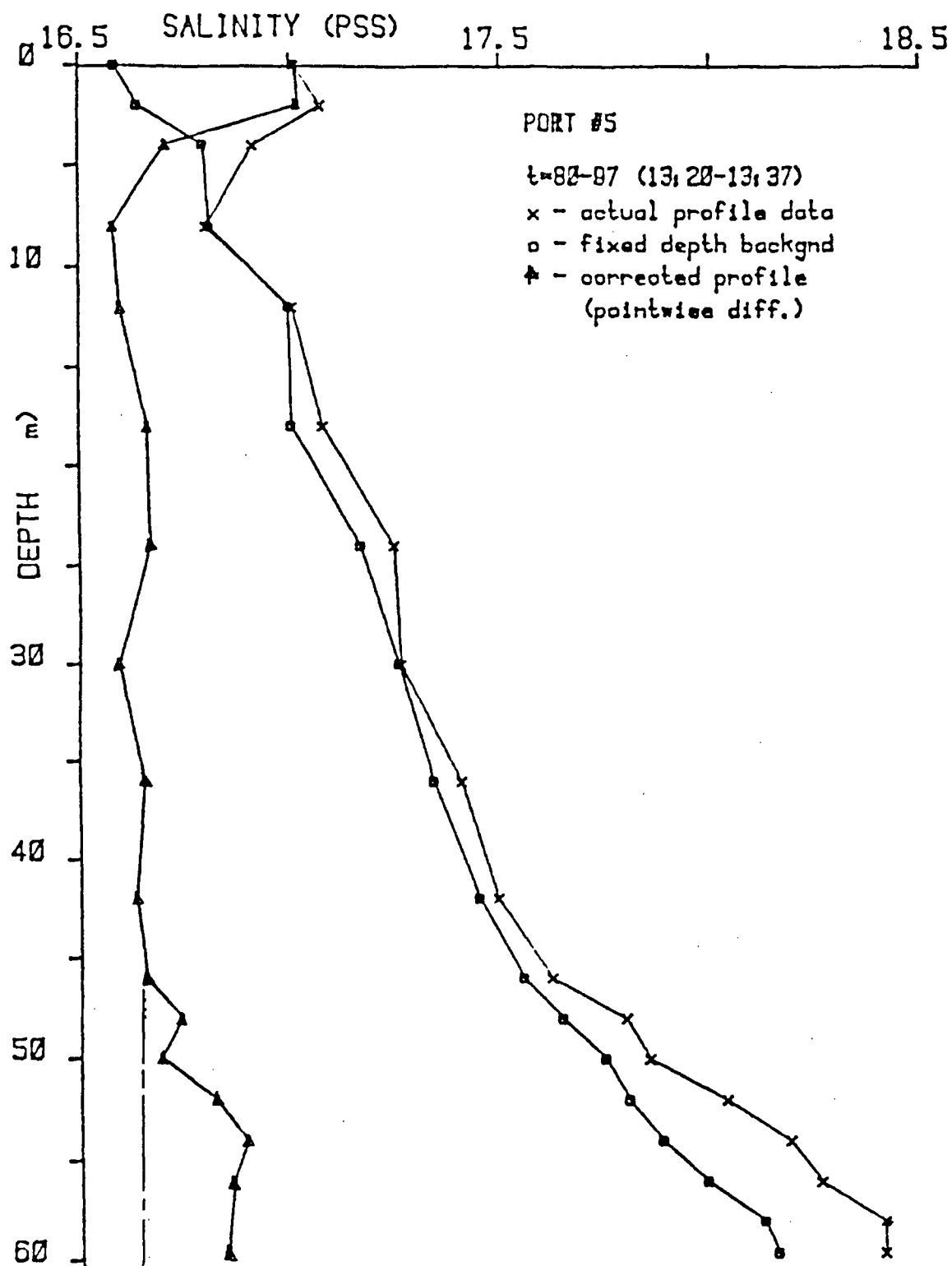
Figure F-20 : SALINITY PROFILE
18-3-86 SLOPERUN #5

SALINITY (PSS)

PORT#3

t = 125-141
X = actual profile
o = fixed depth
- = pointwise corrected
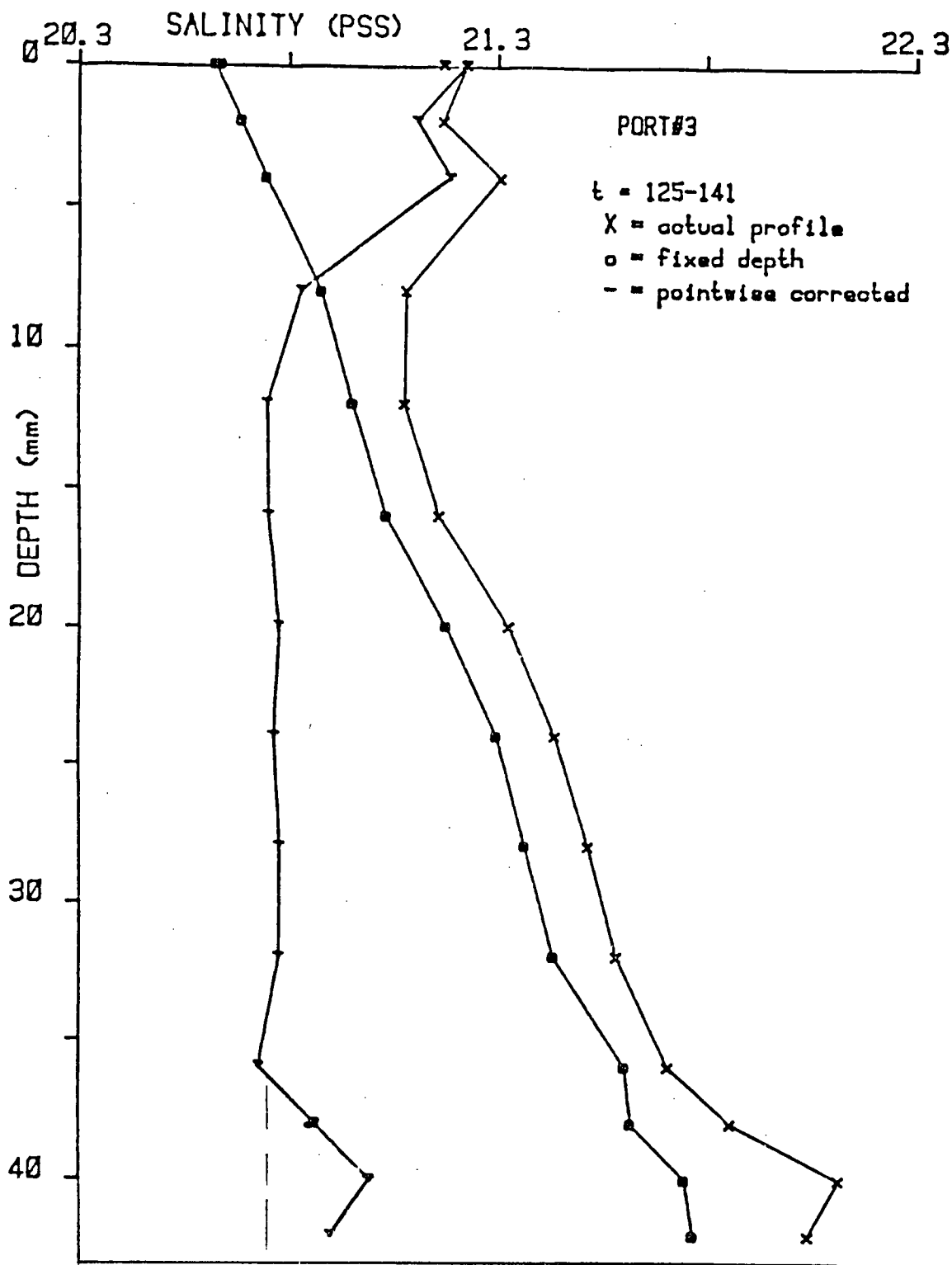
In slope flow experiment #6, the slope angle was 2.3 degrees
and  the depth below the tray was 20 mm at the shallow end  and
57 mm at the deep end.  A convergence near the top of the mixed
layer was seen to occur in several of the previous experiments.
This  convergence was centered near the point where  the  down-
slope flow was separated from the uphill flow cell which formed
during start-up. The object of this experiment was to check for
variations in  the mixed layer salinity along the length of the
tank.   Any  sag in the bottom or a slight bow in the sides  of
the  tray would increase the local height of the heavier  fluid
column and thus the saltflux.

The AM/CT datalogger was used with all three micro-cells  to
sample  fluid  in the upper part of the mixed layer  along  the
centerline,  about 1 cm below the tray:  micro-cell #1 was used
at port #5 near the center, #2 at port #2 near the shallow end,
and  #3 was used at port #7 near the deep end but  occasionally
moved to the tray to determine the salinity there.

The tray was filled between 11:10 to 11:20 to a height of 34
mm  while  fluid of 10 PSS was added to the edge space  between
tank and tray.  The video timer was started at 11:23:30 but the
time-series  data are printed in minutes after 11:00 and  thus:
t(printer)= t(video)+ 23.5 min.

During the first 40 minutes in the time-series, the salinity
was higher by 0.2 to 0.5 PSS near the center, and a convergence
just below the tray was visible in the shadowgraph.  At  t=29 or

t(video)=5 min, the tank was stirred to remove patterns formed during filling. The downslope/uphill flow patterns re-formed in a short time and dye injected at points along the centerline confirmed this. In later measurements, the mixed layer salinity was higher towards the shallow end, explained by mixing of salt into a smaller depth. The counter-cell which was visible in the shadowgraph image decreased to the shallowest 10 cm of the tank but persisted throughout the run. It might have been sustained by the difference in saltflux near the end wall due to the area without salt flux below the end of the tray.

The shadowgraph images and streaks from injected dye were recorded on video tape during much of the run. Flow velocities determined from this are tabulated below:

Table F11.    Slopeflow velocities - sloperun #6

| dist (cm) | video time-interval (h:min:sec) | dt (s) | t[prt] (min) | velocity (mm/s) |
|---|---|---|---|---|
| 2 | 1:36:49 - 1:37:21 = 32 | | 120.5 | 0.63 |
| 5 | 1:54:15 - 1:54:55 = 40 | | 138 | 1.25 |
| 5 | 2:00:12 - 2:01:02 = 50 | | 144 | 1.10 |
| 5 | 2:01:02 - 2:01:42 = 40 | | 145 | 1.25 |
| 5 | 2:01:42 - 2:02:21 = 39 | | 145.5 | 1.28 |
| 5 | 2:02:21 - 2:03:00 = 39 | | 146 | 1.28 |
| 5 | 3:08:13 - 3:09:08 = 55 | | 212 | 0.91 |
| 5 | 3:15:32 - 3:16:17 = 45 | | 219 | 1.11 |

A third order polynomial fit was done to data from the tray
fluid and from cell #1 to determine the salinity values at the
times that flow velocities were measured, which were used to
obtain saltflux estimates.

Table F12.    Salinities in tray and tank - sloperun #6

| t(prt) | S-C#3 | t(prt) | S-C#1 |
|--------|--------|--------|--------|
| 51 | 30.173 | 40 | 17.039 |
| 53 | 30.251 | 51 | 17.411 |
| 122 | 29.613 | 100 | 18.871 |
| 123 | 29.601 | 147 | 19.669 |
| 240 | 28.919 | 210 | 20.913 |
| 267 | 28.832 | 240 | 21.621 |
| 270 | 28.810 | 280 | 22.115 |
| 274 | 28.906 | 339 | 22.682 |
| 467 | 28.398 | 468 | 23.674 |
| 468 | 28.325 | 470 | 23.635 |
| 469 | 28.348 | | |

$$S2 = 30.779 + t(-0.1197 + t(2.3288E-5 - t*1.4454E-8))$$

(rms diff.= 0.0265)

$$S1 = 15.8225 + t(0.03325 + t(-4.4859E-5 + t*2.03725E-8))$$

(rms diff.= 0.0867)

Table F13. Flow velocities and saltfluxes - sloperun #6

| | | | | |
|---|---|---|---|---|
| video timer t(v) = | 1:54:35 | 2:01:30 | 3:11:30 | hr:min:sec |
| print-out   t(p) = | 138 | 145 | 216 | min |
| S-tray fluid  S2 = | 29.495 | 29.447 | 29.041 | PSS |
| S-mixed layer S1 = | 19.610 | 19.763 | 21.117 | PSS |
| tank temp  T-tnk = | 22.291 | 22.325 | 22.574 | °C |
| tray density  D2 = | 19.963 | 19.917 | 19.541 | sigma-t |
| tank density  D1 = | 12.494 | 12.601 | 13.556 | sigma-t |
| pressure       P = | 24.18 | 23.68 | 19.37 | g/cm/s² |
| volume flux   Vw = | 7.33e-5 | 6.50e-5 | 5.50e-5 | cm/s |
| membr.salt flux = | 2.205e-6 | 1.952e-6 | 1.628e-6 | gr/cm²/s |
| flow velocity  v = | 0.123 | 0.11-0.13 | 0.09-0.11 | cm/s |



Photo 10. Dye and shadowgraph.

Figure F-21.

MICRO-CELL TIMESERIES
8-5-86 SLOPERUN #6 d=20-57 h=34 K=1892, 1795, 1817

163
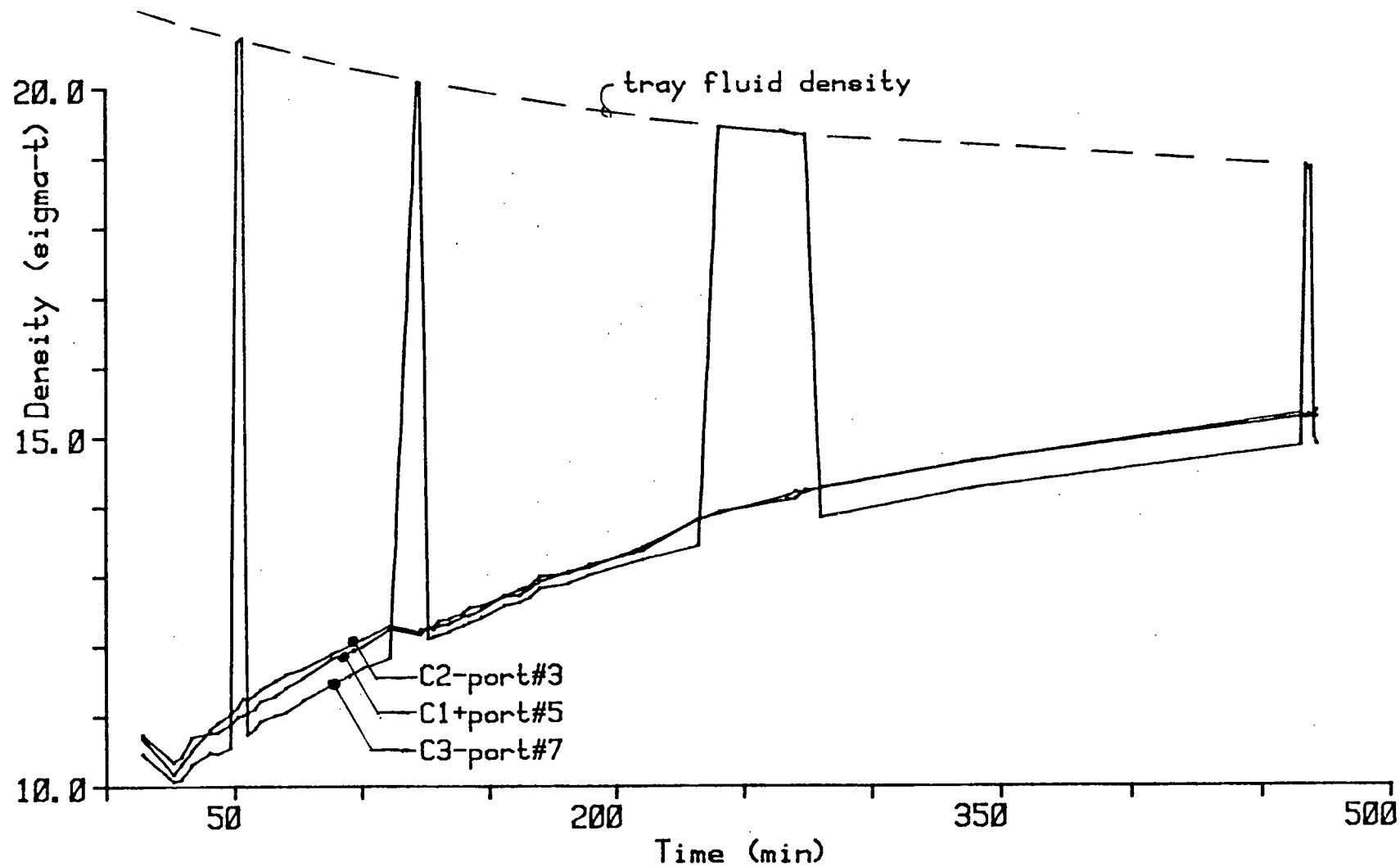
In this experiment the slope angle was 5.5 degrees. The tray rested on the bottom at the shallow end, the depth at the deep end was 78 mm. The starting salinities were 7 PSS in the tank and 28 PSS in the tray. The datalogger was again used with all three micro-cells.

Time-series of micro-cell data were taken with t=0 at 14:00. Salinity profiles from data taken at port #5 over t=40-59 (see figure F-23) and at port #4 over t=109-121 (figure F-24) show a typical mixed layer and the bottom slopeflow region with a rise in salinity of 0.2-0.4 PSS in the lowest 8 mm. As the salinity in both the mixed layer and the slope flow increases over time, the deep end of the tank becomes stably stratified. This can be seen in a profile at port #7 over t=87-100 (figure F-25).

The shadowgraph image shows that after one hour the mixed layer extends about 3 cm down from the tray and no convective penetration is seen below this depth. Dye in the slope flow was seen to split: one part continues along the bottom, the other flows along the interface where it is entrained into the mixed layer by the velocity shear .

Shadowgraph images of the onset of convection and the start-up of the slopeflow were recorded on videotape. The video timer was started at 13:48 so t[video]=t[prt]-12. The slope flow was seen to start up very close to the shallow end soon after the saltflux through the membrane became visible on the shadowgraph as a slowly descending curtain of lines. The descent was nearly even along the tank except slightly faster in the area where a

counter-rotating cell formed in previous experiments. No such cell was seen this time. A cloud of dye, injected in the stable layer near the deep end of the tank, slowly diffused below the sharp interface with the mixed layer. It was entrained above this and lifted into the return circulation. The slope flow velocity was determined from video footage of dye movement:

Table F14. **Flow velocity and saltflux - sloperun #7**

dye moved 5 cm in: dt(video)= 2:25:55-2:26:37 =42s

and: dt = 2:26:37-2:27:26 =49s

| | | |
|---|---|---|
| slope flow max. v= | 0.102-0.119 | cm/s |
| time 16:14 t[pr]= | 138 | minutes after start |
| S-tray fluid S2 = | 26.552 | PSS |
| S-mixed layer S1 = | 16.871 | PSS |
| tank temp T-tnk = | 24.179 | °C |
| tray density D2 = | 17.2106 | sigma-t |
| tank density D1 = | 9.930 | sigma-t |
| pressure P = | 23.569 | g/cm/s² |
| volume flux Vw = | 6.33e-5 | cm/s |
| membr.salt flux B= | 1.710e-6 | gr/cm²/s |

Figure F-22.

MICRO-CELL TIMESERIES
9-5-86 SLOPERUN #7 d=0-78mm h=34 K=1892, 1795, 1817

166
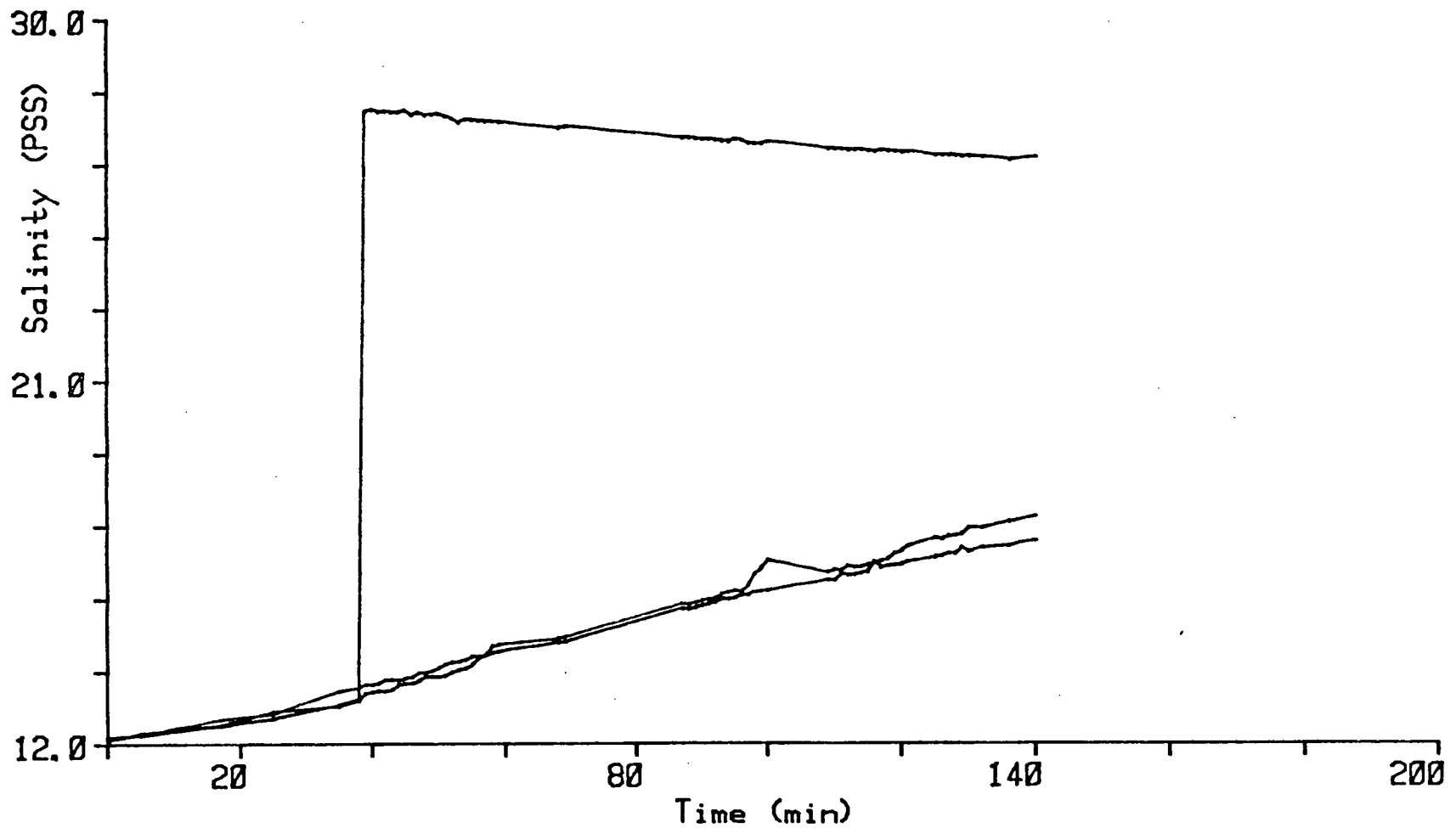
Figure F-23. SALINITY PROFILE
SLOPERUN #7 K=1892, 1795, 1817

Salinity (PSS)

PORT #5
t = 40-59 min
$\phi$ = profile data
x = bkgrnd
+ = corrected
(pointwise)

Depth (mm)
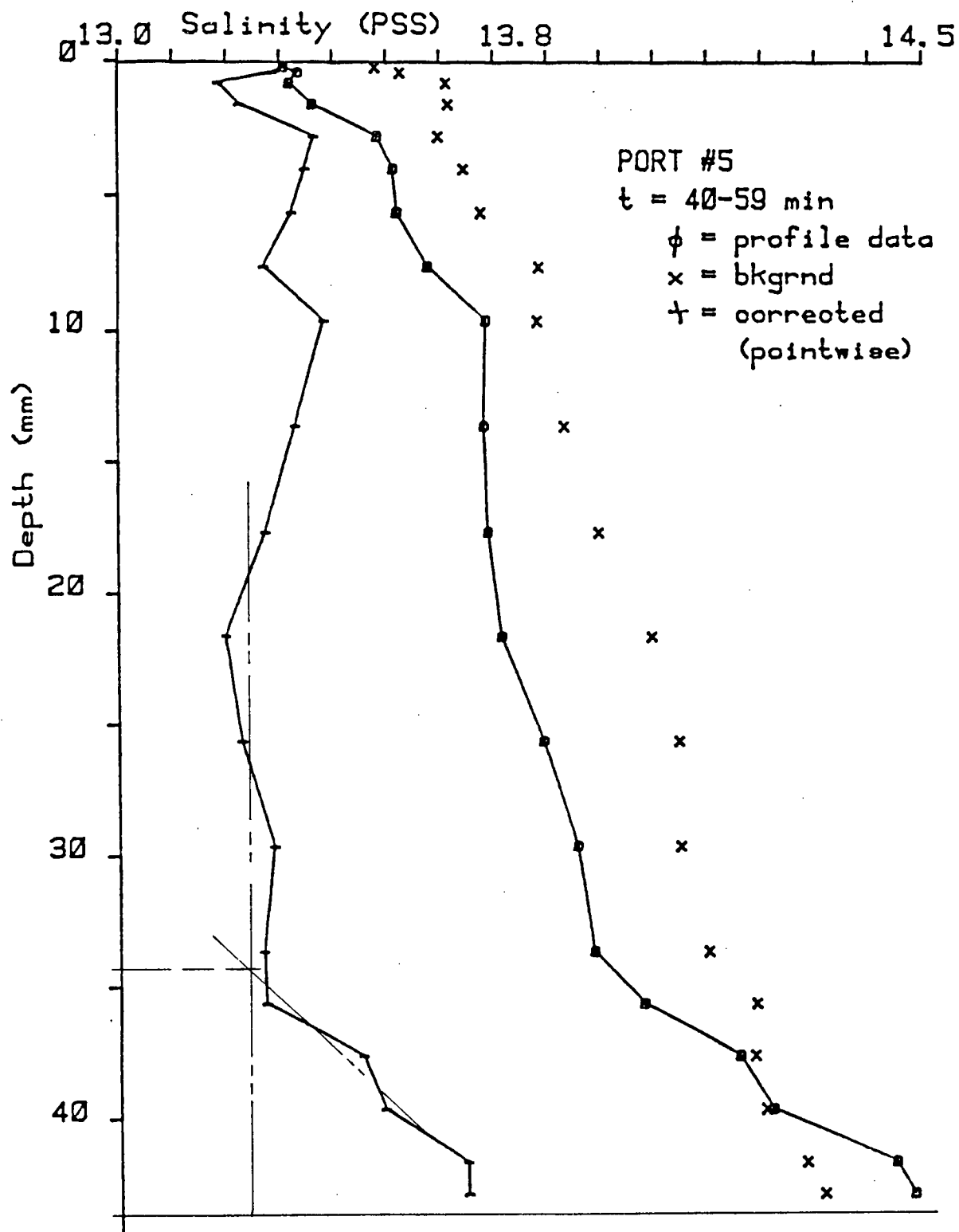
Figure F-24.  SALINITY PROFILE
SLOPERUN #7 K=1892, 1795, 1817

Salinity (PSS)

PORT #4  t= 109-121
&amp; = profile data
x = backgrnd
⅄ = corrected
    (pointwise)
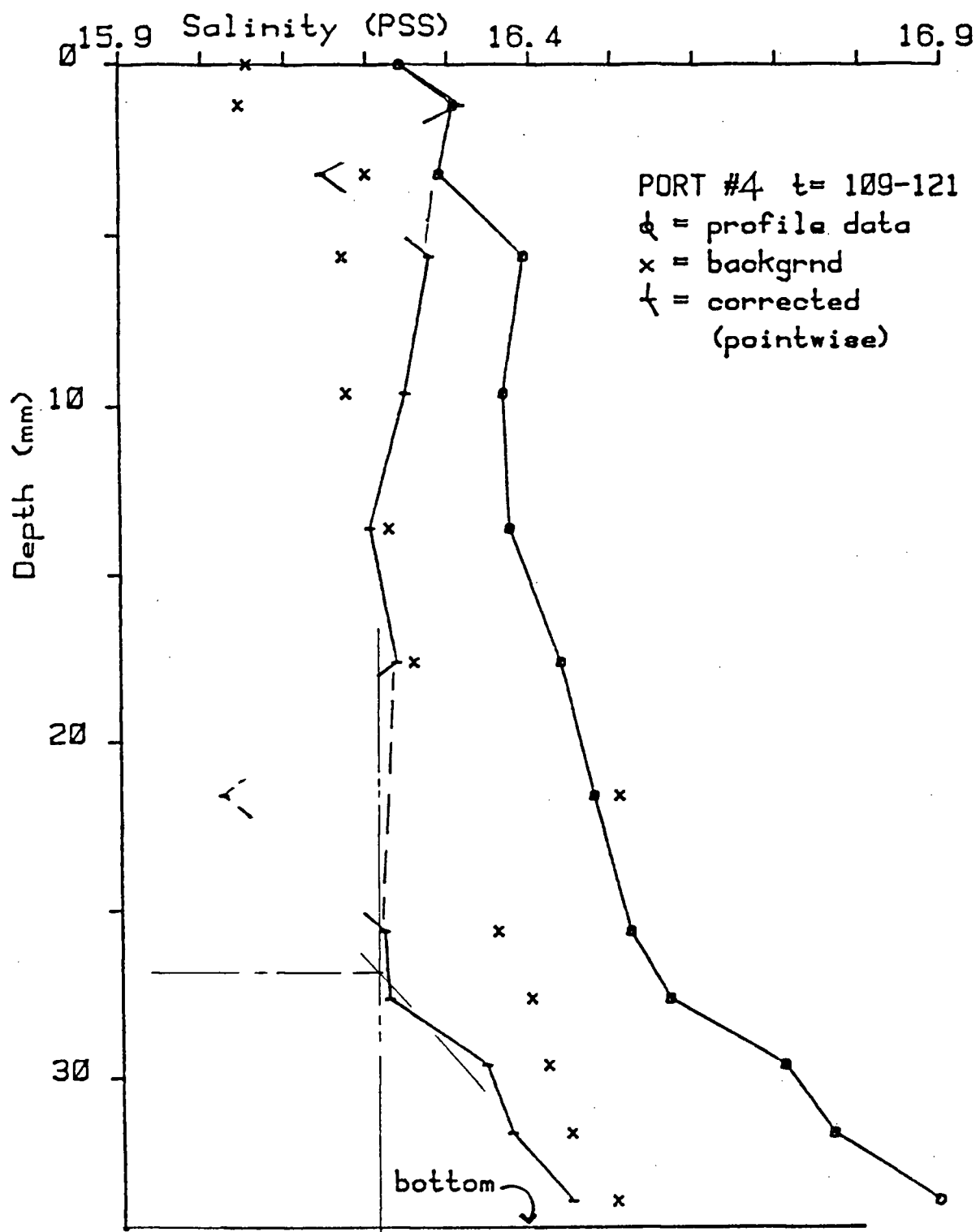
bottom

Figure F-25. SALINITY PROFILE
SLOPERUN #7 K=1892, 1795, 1817

PORT# 7  t =87-100 min
φ = profile data
x = backgrnd
† = corrected
    (pointwise)
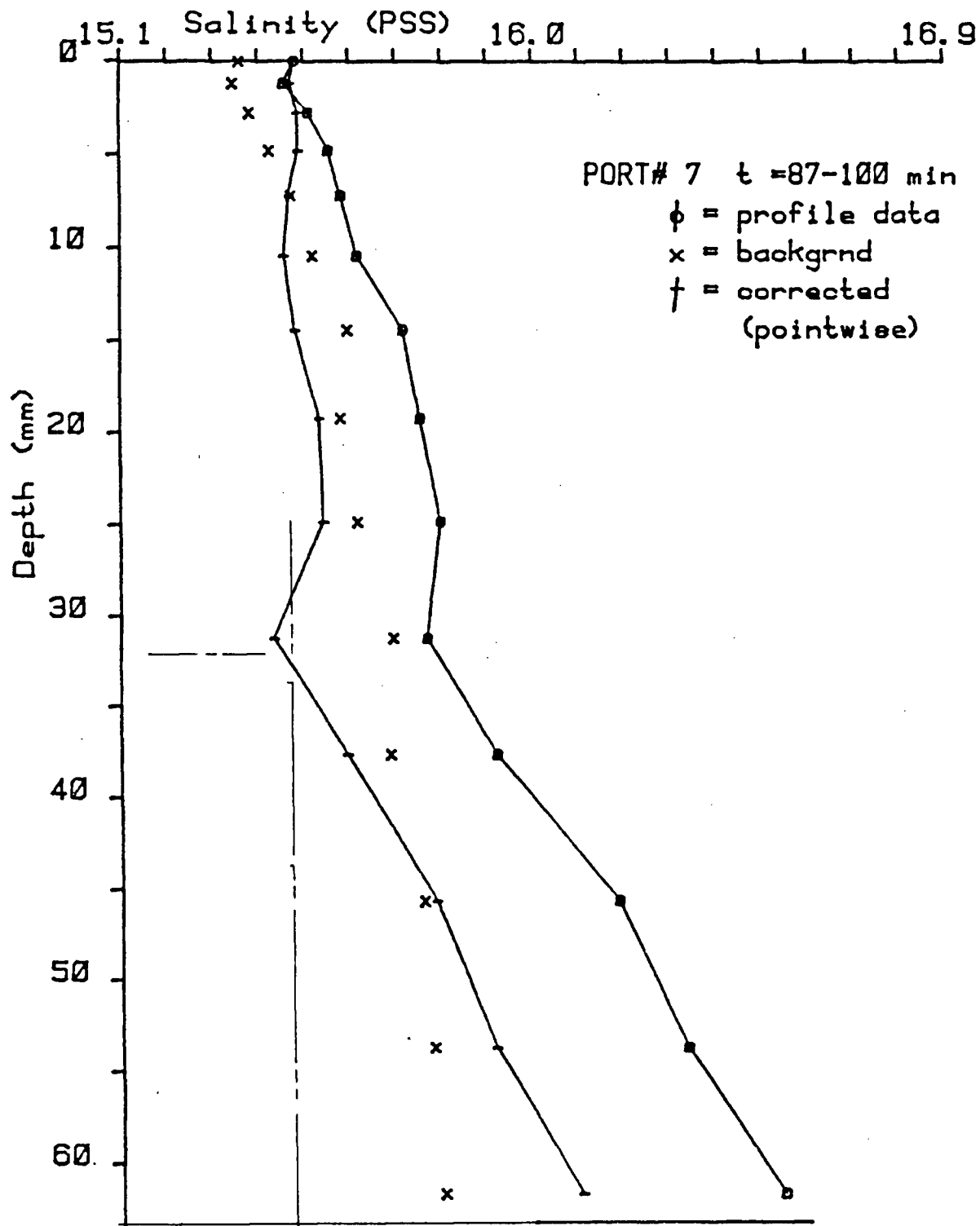
In experiment #8, the bottom slope angle was 5.1 degrees, and at the shallow end the depth under the tray was 12 mm. The HP-3497A Data Acquisition system was used for all thermistors and for the output from the individual conductivity circuits which powered the three micro-cells. The system was controlled with an HP-9825 computer which stored all data on tape, printed the calculated values from each sensor and plotted time-series data of calculated salinities.

Simultaneous salinity profiles were obtained from data taken near the middle of the tank and at 20 cm to either side. The intakes of micro-cells C#1, C#2 and C#3 were lowered through ports #7, #5 and #3 respectively, and set to touch the sloped bottom. Simultaneous data were taken at successive depths after raising the intakes of the micro-cell together to the same height above the bottom (see figure F-26).
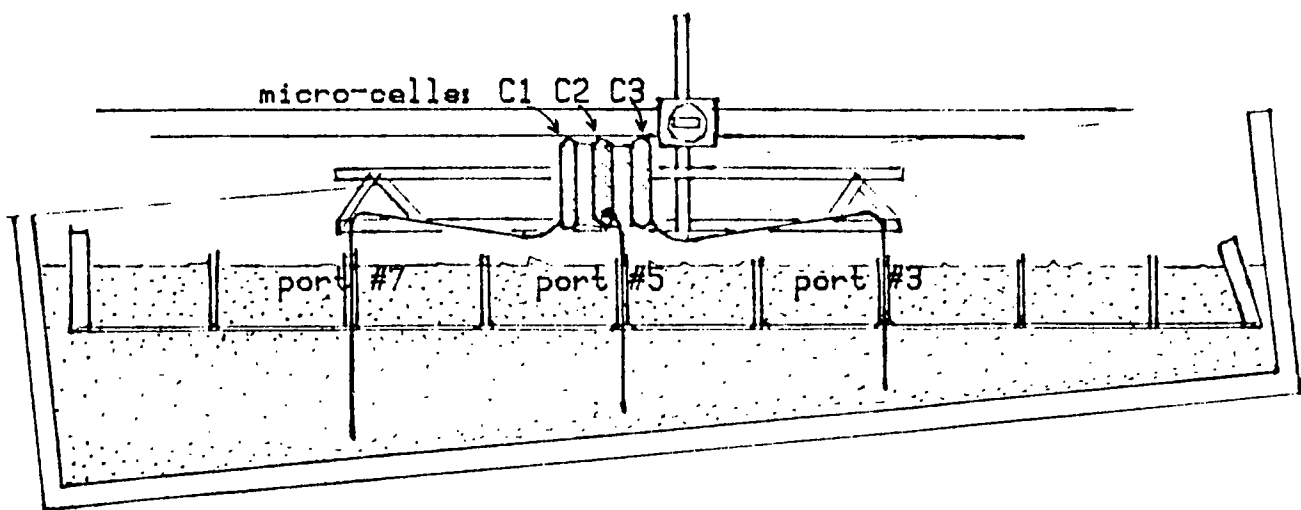


Figure F-26. Arrangement of micro-cells

In the first series of profile data, taken over a period of 20 minutes, the intakes were lowered through the convectively mixed layer and the slope flow region to the bottom and raised again. Second order curves were fit through those sequences of data from each cell which in an expanded time-series (figure F-28) appeared to be part of the mixed layer:
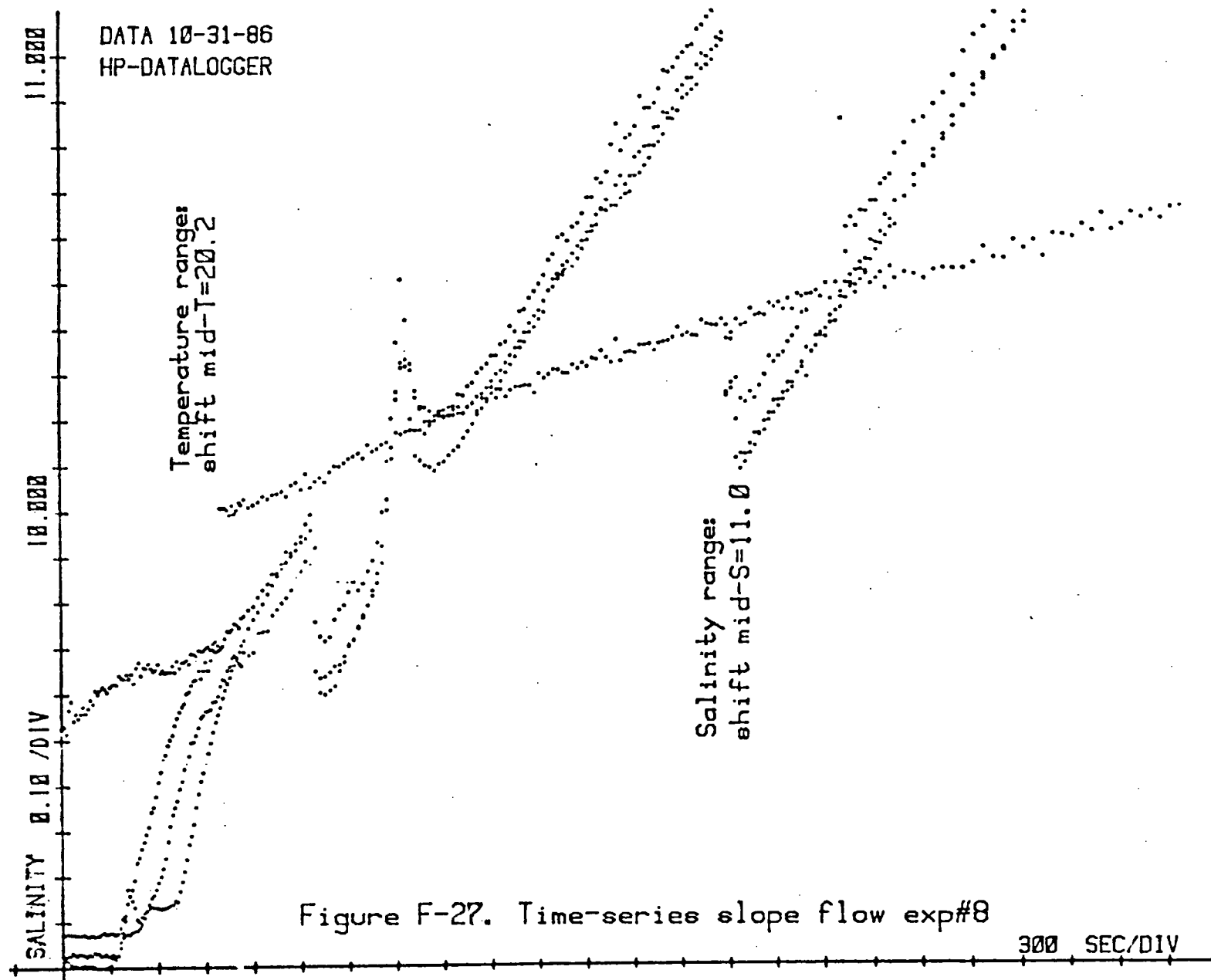
$$S(t) = A + Bt + Ct2$$

| Micro-cell | data-file number from to and to | | | | coefficients of 2nd order fit: | | |
|---|---|---|---|---|---|---|---|
| | F# | F# | F# | F# | A= | B= | C= |
| #1 | 95-104 | | 124-132 | | 9.564049 | 0.02755713 | -2.00482E-4 |
| #2 | 96-104 | | 119-132 | | 9.619223 | 0.02237656 | -1.101477-4 |
| #3 | 101-104 | | 121-132 | | 9.793305 | 0.02583053 | -2.490983-4 |

Simultaneous quasi-instantaneous profiles were obtained from:

S(corr) = S(actual) - S(fit) + S(fit at start)

and in the profiles so obtained, the mixed layer salinities of each individual station are the same at the start and end of the profile sequence (figures F-29,30).A second set of salinity profiles, from data taken about 85 minutes later, (figure F-31) shows that the salinity in the bottom current does not rise as much above that in the mixed layer as in the earlier set. The later profile from micro-cell #1 in port#7 near the deep end shows a nearly linear stratification from heavy fluid which collected in the bottom. Differences in the shape of profiles from micro-cells #2 and #3 did not change over that time. Tests done after this experiment show that a sudden shift in conductance may occur with a shift in relative position of the outlet tubes of those micro-cells which syphon into the same bottle.

Figure F-27. Time-series slope flow exp#8

DATA 10-31-86
HP-DATALOGGER

Temperature range:
shift mid-T=20.2

Salinity range:
shift mid-S=11.0

11.000

10.000

SALINITY    0.10 /DIV

300    SEC/DIV

172

# MICRO-CELL SALINITY TIME SERIES PLOT

0.05 /div   10.0   10.5

SLOPE FLOW EXP#8

F96
F101
F104
F119
F121
F124
F132
C1
C2
C3

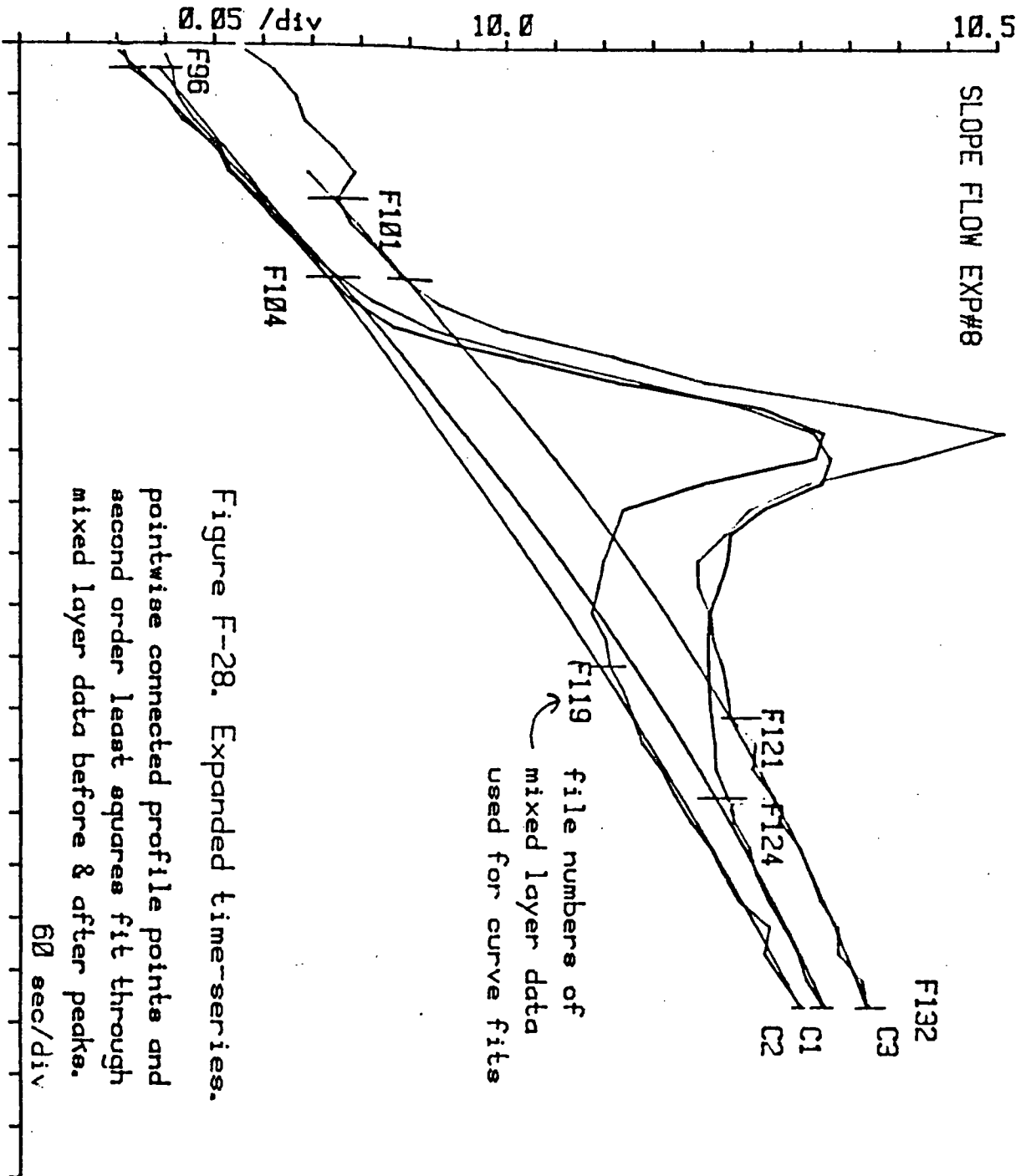file numbers of
mixed layer data
used for curve fits

Figure F-28. Expanded time-series.
pointwise connected profile points and
second order least squares fit through
mixed layer data before & after peaks.

60 sec/div

Figure F-29. SALINITY PROFILE
SLOPE RUN #8

Salinity (PSS)

9.55    9.85    10.15

Height above bottom (mm)

40

30

20

10

0

t=11:58-12:06
'quasi-instantaneous'
profiles, using 2nd
order fit.

C1 : port#7
C2 : port#5
C3 : port#3

h=17mm

ΔS=0.35-0.45

C2    C1

C3
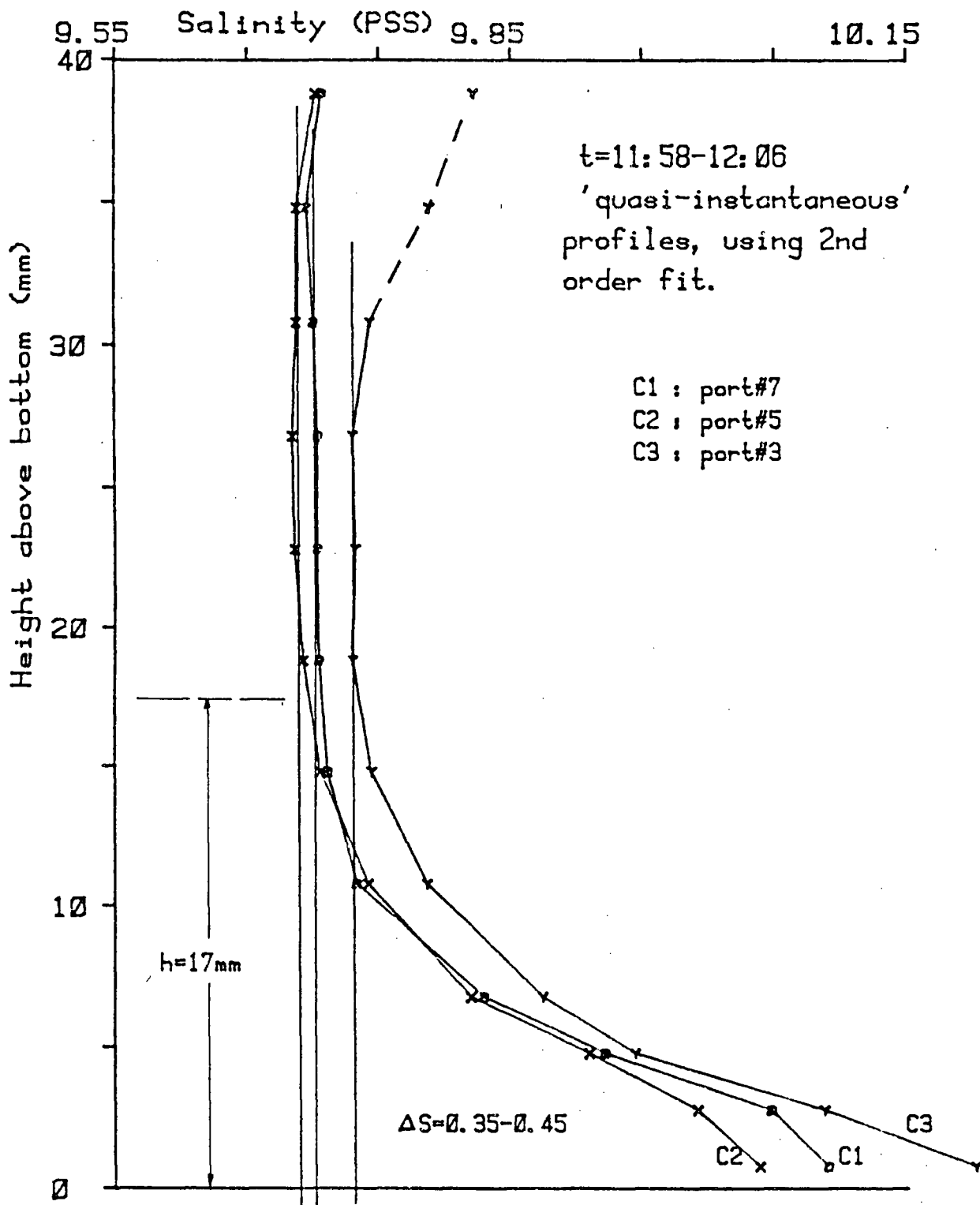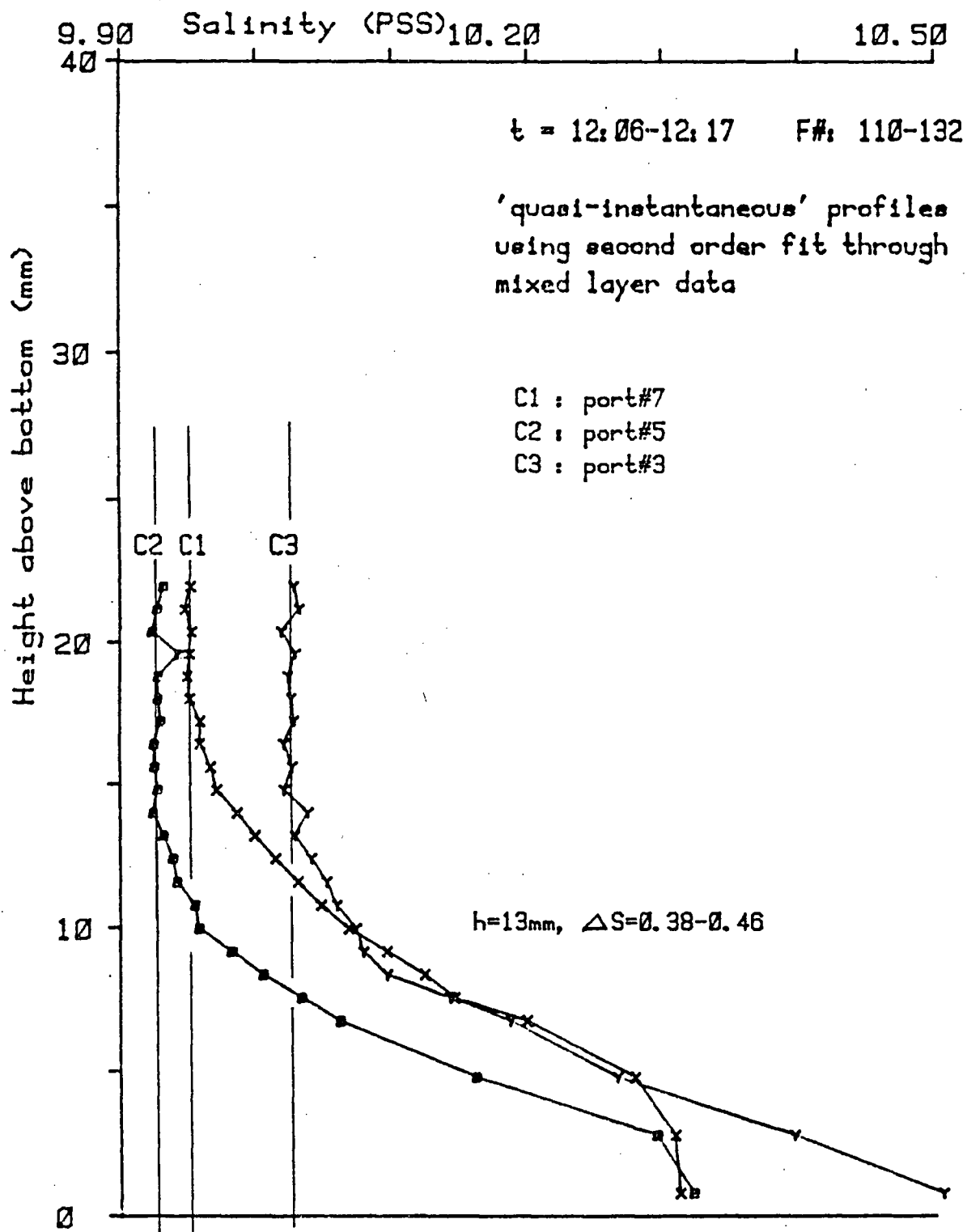
FIGURE F-30.  SALINITY PROFILE
SLOPE RUN #8

Salinity (PSS)

t = 12:06-12:17    F#: 110-132

'quasi-instantaneous' profiles
using second order fit through
mixed layer data

C1 : port#7
C2 : port#5
C3 : port#3

h=13mm,  $\triangle$S=0.38-0.46

# FIGURE F-31.   SALINITY PROFILE
## SLOPE RUN #8



Salinity (PSS)

13.0    13.3    13.6

quasi-instantaneous profiles (corrected for change in salinity in the mixed layer during profiling). Simultaneous points at equal heights above the sloping bottom, spaced 20 cm:

Cell#1 in port#7 (deep)
cell#2 in port#5 (middle)
cell#3 in port#3 (shallow)

t=13:42-13:56   (data F6-46)

Height above bottom (mm)

C#2    C#3    C#1

h=13mm   17mm

bottom

$\Delta S$ = 0.31-0.37